

**INVESTIGATION TO ENHANCE SOME CHARACTERISTICS OF
RECTANGULAR MICROSTRIP ANTENNAS**

**THIS THESIS IS SUBMITTED IN PARTIAL FULFILLMENT OF
THE REQUIREMENTS FOR THE DEGREE OF
DOCTOR OF PHILOSOPHY**

PAWAR UMESH ANKUSH

MZU REGN NO : 1702111

PH. D REGN NO : MZU/PH.D/1180 OF 23.04.2018



**DEPT. OF ELECTRONICS & COMMUNICATION ENGINEERING
SCHOOL OF ENGINEERING AND TECHNOLOGY**

MARCH 2021

**INVESTIGATION TO ENHANCE SOME CHARACTERISTICS
OF RECTANGULAR MICROSTRIP ANTENNAS**

BY

PAWAR UMESH ANKUSH

Department of Electronics & Communication Engineering

Name of Supervisor : Dr. Sudipta Chattopadhyay

Name of Co-Supervisor : Prof. (Dr.) L. Lolit Kumar Singh

Submitted

In partial fulfillment of the requirement of the Degree of Doctor of
Philosophy in Electronics & Communication Engineering of Mizoram
University, Aizawl



Department of Electronic And Communication Engineering
School of Engineering and Technology
MIZORAM UNIVERSITY
(A Central University)
Tanhril, Aizawl - 796 004, Mizoram

Dr. Sudipta Chattopadhyay

Phone: 9330422060 (M)

E-mail: sudipta_tutun@yahoo.co.in

CERTIFICATE

This is to certify that the thesis entitled **“INVESTIGATION TO ENHANCE SOME CHARACTERISTICS OF RECTANGULAR MICROSTRIP ANTENNAS”** submitted to Mizoram University for the award of the degree of **Doctor of Philosophy Electronics and Communication** by **PAWAR UMESH ANKUSH**, Ph.D Registration No. **MZU/Ph.d/1180 of 23.04.2018**, is Ph.D scholar in the Department of Electronics and Communication, under my guidance and supervision and has not been previously submitted for the award of any degree in any Indian or foreign University. He has fulfilled all criteria prescribed by the UGC (Minimum Standard and Procedure governing Ph.D. Regulations). He has fulfilled the mandatory publication (Publication enclosed) and completed Ph.D. course work. It is also certified that the scholar has been admitted in the Department through an entrance test, followed by an interview as per UGC Regulation of 2016.

Date: Mar 2021

Place: Aizawl

(Dr. Sudipta Chattopadhyay)

Supervisor

(Prof. (Dr.) L. Lolit Kumar Singh)

Co- Supervisor

MIZORAM UNIVERSITY
Aizawl - 796 004

(March 2021)

DECLARATION

I, **PAWAR UMESH ANKUSH**, hereby declare that the subject matter of this thesis entitled “**INVESTIGATION TO ENHANCE SOME CHARACTERISTICS OF RECTANGULAR MICROSTRIP ANTENNAS**” is the record of work done by me, that the contents of this thesis did not form basis of the award of any previous degree to me or to do the best of my knowledge to anybody else, and that the thesis has not been submitted by me for any research degree in any other University/Institute.

This is being submitted to the Mizoram University for the degree of Doctor of Philosophy in **ELECTRONICS AND COMMUNICATION ENGINEERING**.

Date: Mar 2021

(PAWAR UMESH ANKUSH)
Candidate

(Dr. Sudipta Chattopadhyay)
Supervisor

(Dr NP Maity)
Head

(Prof. (Dr.) L. Lolit Kumar Singh)
Co-Supervisor

Acknowledgement

At the outset, am grateful to the almighty God for his blessing that had lead me successfully to the end of my work. I wish to express my heartfelt gratitude to my supervisor and mentor **Dr. Sudipta Chattopadhyay** and my co-supervisor **Prof. (Dr.) L. Lolit Kumar Singh**, the Dean of School of Engineering and Technology, for their constant support, guidance, encouragement and patience throughout my research work. I am also thankful to **Dr. N. P. Maity**, the Head of Department of Electronic and Communication for extending all the facilities. Also, I am thankful to all the faculties and technical staff for their help, support and kind cooperation.

I would like to express my deepest gratitude to my senior, **Dr. Abhijyoti Ghosh** and all the staffs for their kind support, without whom, this work would not have been possible.

I owe my gratitude to **Corps of Electronic and Mechanical Engineers, Indian Army** for providing opportunity, constant support due to which I was able to manage service to nation and simultaneously completing my Ph.D. The primary reason for my interest in radars, antennas and communication systems is due to Corps of EME which has motivated me to pursue higher studies and research in antennas.

Also, I would like to thank my parents, my family, my beloved wife Jyoti and my daughter Mukti for their constant support, love and prayers. My father set the true example for me that educations can be persived at any age. Last but not the least; I place on record, my sense of gratitude to one and all who, directly or indirectly, have lent their helping hand in this venture.

PAWAR UMESH ANKUSH

Table of Contents

Acknowledgment	(i)
Table of Contents	(ii) – (iii)
List of Figures	(iv) – (ix)
List of Tables	(x)
Chapter 1 Introduction	1
Chapter 2 Defected Patch Surface approach for wide symmetrical radiation and low cross polarization	29
2.1 Introduction	29
2.2 Defected Patch Structure (DPS) with defects on non-radiating side	
2.2.1 Theoretical background of some ungrounded /grounded comb-shaped structures	32
2.2.2 Analysis of some ungrounded/ grounded comb-shaped structures	35
2.2.3 Proposed structure	40
2.2.4 Results	41
2.3 Defected Patch Structure (DPS) with defects on radiating side	
2.3.1 Background	47
2.3.2 Proposed structure	48
2.3.3 Results & physical insight	48
2.4 Comparison between both types of DPS RMAs	51
2.5 Conclusion	51
Reference	54
Chapter 3 Defected Ground Structure approach for gain and bandwidth improvement	56
3.1 Introduction	56
3.2 Hexagonal DGS (HDGS) integrated RMA	
3.2.1 Parametric study	58
3.2.2 Proposed structure	66
3.2.3 Experiments and Results	66
3.3 Performance evaluation of various DGS integrated RMAs (defects with increasing order of polygons)	
3.3.1 Requirement of various types of DGSS (polarimetric radar)	70
3.3.2 Selection criteria for comparison	71
3.3.3 Results of different structures	72
3.4 Conclusion	77
References	79
Chapter 4 Bracketed stub-loaded rectangular microstrip antenna: A novel approach to improve polarization purity	83
4.1 Introduction	83
4.2 Parametric study and design approach	

4.2.1	Effect of feed position	86
4.2.2	Effect of stub length	88
4.2.3	Influence of stub length on XP characteristics	92
4.2.4	Physical insight into XP suppression	93
4.2.5	Effect of stub width	95
4.3	Proposed structure	97
4.4	Results and analysis	
4.4.1	Single element - BSRMA	99
4.4.2	Two element array antenna – BSRMA	99
4.4.3	Comparative evaluation	102
4.5	Conclusion	102
	References	103
Chapter 5	Quasi planar composite rectangular microstrip antenna: An approach to achieve high gain, flat top radiation with low cross polarization	107
5.1	Introduction	107
5.2	Physical insight	
5.2.1	Effect of monopole height on improving co-polar (CP) radiation pattern of QPCMA	111
5.2.2	Effect of monopole length on suppressing cross-polar (XP) radiation from QPCMA	116
5.2.3	Effect of monopole spacing on CP and XP radiation patterns of QPCMA	116
5.3	Theory	
5.3.1	Theoretical look into flat-top radiation	120
5.3.2	Theoretical look into wide angle gain	122
5.3.3	Performance analysis of QPCMA with low loss substrate	125
5.4	Proposed structure	127
5.5	Results and analysis	127
5.6	Comparison between radiation properties of the QPCMA with various established designs of RMAs	130
5.7	Conclusion	132
	References	133
Chapter 6	Conclusions and scope for future studies	137
List of Publications		142
	Brief Bio-data of candidate	143
	Particulars of the candidate	144

List of Figures

Fig 1.1	Conventional RMA (a) Isometric View (b) Side View	5
Fig 1.2	(a) Fringing at radiating edges of probe fed rectangular microstrip patch antenna. (b) Cross-sectional view of rectangular microstrip patch antenna and fringing electric fields in quasi TEM mode	6
Fig 1.3	Schematic diagram of fringing fields of a classical probe fed RMA	9
Fig 1.4	A simulated 3D radiation pattern of a RMA with length of 8 mm and width of 12 mm.	10
Fig. 1.5	A simulated CP and XP radiation pattern of a RMA	11
Fig. 1.6	Electric field distribution with respect to modes. (a) Radiated electric field from edges due to TM_{10} mode, (b) Radiated electric field from edges due to TM_{02} mode, (c) Electric field orientation due to TM_{10} mode (d) Electric field orientation due to TM_{02} mode	12
Fig 2.1	Proposed DPS with defects on non-radiating side (a) Top view (b) 3D image and DPS with defects on radiating side (c) Top view (d) 3D image	30
Fig 2.2	Simulated substrate field distributions for conventional and proposed microstrip patch (a) Conventional structure, (b) Proposed structure.	33
Fig 2.3	Top view of different comb-shaped patches. (a) single slot with ungrounded single tooth, (b) two slots with ungrounded two teeth, (c) three slots with ungrounded four teeth, (d) single slot with grounded single tooth, (e) two slots with grounded two teeth, (f) three slots with grounded four thin teeth	35
Fig 2.4	Simulated and measured reflection coefficient (S_{11}) profile of different comb-shaped patch antennas	36
Fig 2.5	Variation of electric field magnitude over patch surfaces where the teeth of the comb is not grounded (a) conventional patch, (b) structure of fig 2.3a, (c) structure of fig 2.3c	38
Fig 2.6	Simulated substrate field distributions for single and double slotted	39

List of Figures

	grounded comb-shaped microstrip patch (a) structure as in Fig 2.3(d), (b) structure as in Fig 2.3(e). (<i>The distribution for proposed structure of Fig 2.3(f) is in Fig. 2.2(b)</i>)	
Fig 2.7	Variation of electric field magnitude over patch surfaces where the teeth of the comb is grounded with metallic strips (a) structure of figure 2.3d, (c) structure of figure 2.3f (proposed structure)	39
Fig 2.8	Schematic representation of proposed grounded comb-shaped microstrip antenna (a) Top view, (b) fabricated prototype; $L= 8.5$ mm, $W= 12.75$ mm.	41
Fig 2.9	Simulated and measured reflection coefficient (S_{11}) profile of the proposed antenna	42
Fig 2.10	Simulated and measured radiation pattern at $f=8.05$ GHz (a) E-plane, (b) H-plane	42
Fig 2.11	Beam width characteristics of proposed antenna near broadside region (-125^0 to $+125^0$) at $f=8.05$ GHz in the principal planes	43
Fig 2.12	Simulated Beam width characteristics of proposed antenna near broadside region (-150^0 to $+150^0$) at $f=8.05$ GHz in the diagonal planes	44
Fig 2.13	Simulated relative XP performance of proposed and conventional patch at diagonal skew ($\varphi =45^0$ and 60^0) planes.	45
Fig 2.14	Measured variation of front-to-back radiation isolation and beam width of the proposed patch as a function of ground plane dimension in terms of wavelength	46
Fig 2.15	Simulated radiation pattern of the present structure in both principal E and H-planes at $f=2.6$ GHz	47
Fig 2.16	Reflection coefficient profile (S_{11}) for conventional RMA, antenna 1 and antenna 2	49
Fig 2.17	Radiation patterns of conventional RMA and antenna 1 at the centre frequency at: (a) H- plane, (b) E-plane.	50

List of Figures

Fig 2.18	Radiation patterns of antenna 2 at: (a) $f=6.61$ GHz and (b) $f=7.72$ GHz	50
Fig 3.1	Proposed HDGS integrated RMA (a) Schematic diagram (b) 3D image	57
Fig 3.2	Reflection coefficient profile for conventional RMA and HDGS integrated RMA of different side length a_h in mm.	59
Fig 3.3	Fractional impedance band width of conventional and HDGS integrated RMA of different side length a_h in mm.	59
Fig 3.4	Simulated distribution of electric current and electric field magnitude on patch surface at different frequencies.	61
Fig 3.5	Gain and F/B radiation isolation of conventional and HDGS integrated RMA for different side length (a_h) in mm.	63
Fig 3.6	Magnitude of electric field distribution over the substrate for (a) conventional and (b) HDGS integrated RMA with $a_h=2.9$ mm.	64
Fig 3.7	Simulated reflection coefficient profile of X band HDGS integrated RMA with and without back plate (metallic or dielectric).	65
Fig 3.8	Image of fabricated HDGS (a) patch side, (b) ground plane side, (c) multi layer image with help of neon light and (d) ground plane side with completely integrated with SMA connector.	66
Fig 3.9	Measured and simulated reflection coefficient profile of HDGS integrated RMA with $a_h=2.9$ mm.	67
Fig 3.10	Measured and simulated radiation pattern for E and H plane with proposed HDGS integrated RMA ($a_h=2.9$ mm) at different frequencies.	68
Fig 3.11	Variation of measured gain and CP-XP radiation isolation as a function of frequency for proposed HDGS integrated RMA with $a_h=2.9$ mm.	70
Fig 3.12	Conventional RMA (a) 3D view, (b) reflection coefficient profile	73

List of Figures

	(c) H-plane radiation pattern	
Fig 3.13	Equilateral triangular DGS integrated RMA (a) 3D view, (b) reflection coefficient profile (c) H-plane radiation pattern	74
Fig 3.14	Regular pentagon dumbbell shaped DGS integrated RMA (a) 3D view, (b) reflection coefficient profile (c) H-plane radiation pattern	75
Fig 3.15	Hexagon shaped DGS integrated RMA (a) 3D view, (b) reflection coefficient profile (c) H-plane radiation pattern	76
Fig 3.16	Ring shaped DGS integrated RMA (a) 3D view, (b) reflection coefficient profile (c) H-plane radiation pattern	76
Fig 4.1	Proposed Bracketed Stub Loaded single layer RMA (a) Schematic diagram (Top view), (b) 3D CAD image.	85
Fig 4.2	The simulated electric current vectors and reflection coefficient profiles for a bracketed stub loaded RMA.	87
Fig 4.3	The simulated reflection coefficient profiles for the bracketed stub loaded RMA for different stub length S_l	88
Fig 4.4	The simulated impedance locus on the smith chart for (a) conventional RMA, (b) bracketed stub loaded RMA with $S_l=4.8$ mm ($S_l<0.25\lambda_g$), (c) bracketed stub loaded RMA with $S_l=6.5$ mm ($S_l>0.25\lambda_g$)	89
Fig 4.5	Reflection coefficient of the bracketed stub loaded RMA with $S_l<5$ mm i.e $S_l = 4.8$ mm and input impedance of the same and conventional RMA.	90
Fig 4.6	Input impedance of conventional RMA and bracketed stub loaded RMA (with $S_l=5.5$ mm, 6.0 mm and 6.5 mm ($S_l>0.25\lambda_g$ in all the cases)	91
Fig 4.7	(a) The simulated H plane radiation pattern of a bracketed stub loaded RMA ($L = 8$ mm, $W = 12$ mm and $S_l= 5.5$ mm) at different frequencies, (b) The simulated H plane radiation pattern of a bracketed stub loaded RMA at different stub length S_l .	94

List of Figures

Fig 4.8	(a) E and H field distribution over the substrate for conventional RMA, corresponding (b) E field component at patch corners for conventional RMA, (c) E and H field distribution over the substrate for single bracketed stub loaded RMA, corresponding (d) E field component at patch corners for single bracketed stub loaded RMA.	95
Fig 4.9	Radiation characteristics of bracketed stub loaded RMA with different stub widths S_w (a) Reflection coefficients profiles and (b) the input impedance profiles of bracketed stub loaded RMA with different stub widths S_w , (c) Normalized H plane radiation pattern	96
Fig 4.10	Image of fabricated BSRMA prototypes (a) Single element, (b) array antenna of two elements.	97
Fig 4.11	(a) Simulated and measured reflection coefficient profile for the proposed bracketed stub loaded RMA, (b) Measured and simulated H plane radiation pattern for the conventional RMA ($L = 8$ mm, $W = 12$ mm) and (c) Measured and simulated H plane radiation pattern for the proposed bracketed stub loaded RMA ($L = 8$ mm, $W = 12$ mm and $S_l = 6.5$ mm) ($f = 10.2$ GHz).	98
Fig 4.12	(a) Simulated electric field distribution over the aperture of single element conventional RMA, (b) Simulated electric field distribution over the aperture proposed single element bracketed stub loaded RMA (c) Simulated and measured S parameters of 2 element array constituted by proposed bracketed stub loaded RMA, (d). Measured H plane radiation pattern of 2 element array constituted by proposed bracketed stub loaded RMA.	100
Fig 5.1	Proposed QPCMA RMA (a) Schematic Diagram (b) 3D image	110
Fig 5.2	E and H-plane radiation patterns of QPCMA for different monopole height (a) for $\lambda_g/4$ monopole, (b) for $2\lambda_g/4$ monopole,	113

List of Figures

	(c) for $3\lambda_g/4$ monopole.	
Fig 5.3	Normalized H-plane CP profile of conventional RMA with PTFE substrate ($\epsilon_r = 2.33$), conventional RMA with FR-4 substrate ($\epsilon_r = 4.4$) and the present QPCMA with FR-4 substrate ($\epsilon_r = 4.4$).	114
Fig 5.4	Field distribution over the substrate for (a) QPCMA with FR-4 substrate, (b) conventional RMA with FR-4 substrate.	115
Fig 5.5	Normalized radiation pattern of the QPCMA for different spacing (a values) between monopole and the radiating edges of RMA.	118
Fig 5.6	Field distribution over the substrate for QPCMA with (a) $a = 2.5$ mm, (b) $a = 4$ mm, (c) $a = 5.5$ mm.	119
Fig 5.7	Computed E-plane pattern for conventional and present QPCMA	122
Fig 5.8	Radiation pattern of QPCMA with $a = 1.75$ mm and monopole length $l = 2\lambda_g/4$.	123
Fig 5.9	Simulated radiation pattern of QPCMA with different substrate (a) low loss substrate (RT-Duroid, $\epsilon_r = 2.33$), (b) same as (a) to depict the flat-top region, (c) low loss substrate (FR-4, $\epsilon_r = 4.4$).	126
Fig 5.10	Fabricated prototype (a) (Top view), (b) back-view, CAD based (c) isometric view and (d) side view depicting monopoles.	128
Fig 5.11	Measured reflection coefficient profile of the proposed QPCMA.	129
Fig 5.12	Measured E and H-plane radiation patterns for QPCMA at different frequency	129
Fig 5.13	Measured gain and minimum CP-XP isolation as a function of frequency for QPCMA.	130

List of Tables

Table 2.1	Comparison of simulated 3 dB beam widths and CP-XP isolation for some ungrounded and grounded comb-shaped patch.	37
Table 2.2	Tabulation of radiation parameters for performance analysis for both types of DPS integrated antennas.	51
Table 3.1	Parameters of the RMAs used for investigations (substrate thickness $h = 1.575$ mm)	73
Table 3.2	Comparison between input and radiation properties of different antenna structures	77
Table 4.1	Comparison of BSRMA with other recently reported results	101
Table 5.1	Radiation properties of the QPCMA with different monopole heights	117
Table 5.2	Comparison between radiation properties of the QPCMA with conventional RMA and earlier reported works	131
Table 6.1	Tabulated form of all the investigated structures for objective assessment and selection	140

CHAPTER

1

Introduction

1.1 Introduction

Antennas are metal based structures or transducer that radiates electromagnetic energy into space. Since year 1886, when Heinrich R. Hertz proved and proposed existence of electromagnetic waves, a momentous advancement has been done by scientists in the fields of wireless communications. Over the years antennas have acquired extensive range of configurations, to mention a few aperture antenna, wire antenna, loop antenna, patch antenna, slot antenna etc. As the requirement for wireless systems like 5G communication, IOT (Internet of Things), etc shifts towards the higher spectrum operations, requirements of small antenna increases. At the same time the mobility of the wireless device has become imperative and so an essential constraint to develop the antennas conformable and compatible with miniaturized/ handheld communication devices.

In this context, microstrip antenna emerges as the best candidate to address all the requirements of latest personal/ handheld wireless communication equipment. In year 1952, Greig and Engleman [1] introduced microstrip antenna as a new transmission technology in the range of kilomegacycle. However, microstrip antenna as a radiator was first perceived and proposed by Deschamps [2] in year 1953. In year 1955, Gutton and Bassinot [3] brought forward and patented the concept of the microstrip antenna and its application. With effect from year 1955 to almost 1969, various researchers explored and registered radiation from discontinuities of stripline and also brought forward its different perspectives [4]-[7]. Parallely various aspects of other basic types of antennas were getting developed and advanced concepts like

phased array antennas were implemented in slotted waveguides and reflectors. However, in fields of printed antennas or microstrip antennas for next five years till 1975, the research was pioneered by researchers like Byron, Howell, Munson, etc who analysed the radiation of a conducting stripline like copper clads with dielectric substrate of few wavelengths in between [8]-[15]. Due to its conformal nature, low profile and light weight it soon became popular in defense and space industry particularly in missiles and satellites [16]. In the same field further developments and analysis still being carried out for advances airborne systems [17]-[21]

Over last few decades of research and development of microstrip antenna, the primary phase of developments up to late 1970's was theoretical analysis of basic and different patch geometries. These developments and studies were well documented by Bahl and Bhartia [22] in a book published in 1980. The analysis and designs to include parametric studies were addressed in another book published in 1981 by James, Hall and Wood [23]. Also a well reviewed article by Carver and Mink [24] brought out the fundamental facets and aspects of microstrip antennas which is still referred. The basic and important expressions of input impedance, radiation resistance, and radiation fields were well expressed [12], [25] but were applicable specifically of center fed patch, and hence could not find proper application in many practical antenna structures. Lo et. al [26]-[29] provided more generalised expression based on modal-expansion techniques for varied geometry like rectangular, triangular, circular, semicircular, etc. Advanced analysis and techniques were also presented by Shen [30], Carver and Coffey [31]-[34] and it focused on calculating the mutual and self impedance and limitations of microstrip antenna when integrated to form array antenna. Different techniques of analysis, like aperture field model [35], vector potential approach [36], wire grid model [37], DGF techniques [38] etc to express the radiation characteristics were reported by various authors and researchers.

The second phase where in major developments took place and its applications stabilised by year 2000. Wherein basic mechanism of radiation was analysed and implemented by means of cavity model analysis, which is well documented in [39]-[40]. The ever increasing interests in printed antennas focused on antennas with compact configuration and wide bandwidth designs for new

developments in wireless applications, as reflected from the recently published titles like [41]-[42]. Recently published handbooks and well compiled reports [43]-[45] have well covered recent developments and CAD based antenna designs which is forming base for today's research and development both in commercial and academic fields.

Coming on to the latest and 3rd phase, advancements in material technology and manufacturing of exotic materials have facilitated the advanced microstrip antennas. Few significant ones are (a) antennas with metamaterials [46]-[52], (b) Defected ground structures for printed antenna [53]-[60], (c) Defected patch structures with help of Artificial Intelligence generated shapes (d) Electrically miniaturized antennas for mobile communication [61]-[69], and (e) printed antenna for RFID systems [70]-[77] with or without active power.

The above mentioned advances have been possible due to new analysis methods and CAD software. Due to high-speed computational methods incorporated in software and high speed memory in modern computers, full wave models to analysis of microstrip antennas can be done quickly. Some of the commercially available popular software use Method of Moment (MoM), Finite Element Method (FEM) and the Finite-Difference Time Domain (FDTD) technique. The MoM analysis can be used for accurate and versatile solutions by means of both spatial and spectral domain [78]-[79] respectively. Another technique is FEM, which takes volumetric approach and can easily handle in-homogeneous structures. Also, the FDTD technique has become popular being suitable for microstrip antenna analysis as the same can handle varied geometries, to mention a few, parasitically coupled patches [80], multilayered patches [81], arrays and phased arrays [82], and active antenna [83]-[84]. The FDTD analysis requiring more processing time even with latest computers hence such a problem being partially handled by using commercial full wave codes like HFSS, IE3D, CST Microwave Studio etc. Thereby assisting researchers get closed form expression readily to determine basic testing parameters like operating frequency and input impedance which can be further used for lab testing of prototypes.

This chapter deals with the basic historical background of the microstrip antennas in section 1.1. Section 1.2 deals with basic structures and limitations of the

rectangular microstrip antenna. Section 1.3, describes the feeding techniques of microstrip antennas. Section 1.4, describes the radiation characteristics of microstrip antennas. Section 1.5, gives an overview on to cross polarization and polarization purity. In section 1.6, a survey on improving polarization purity has been documented. Section 1.7, discusses the enhancement techniques for bandwidth and gain which are and paramount radiation characteristics. Section 1.8, discusses the preface to the thesis (other chapters) to include conclusion.

1.2 Rectangular Microstrip Antenna: Structure and Limitations.

The basic characteristics of RMAs have been discussed in the succeeding sub sections. Initially the basic structural geometry has been presented and its limitations have been discussed in brief. Followed by the same the limitations due to feeding techniques have been methodically documented.

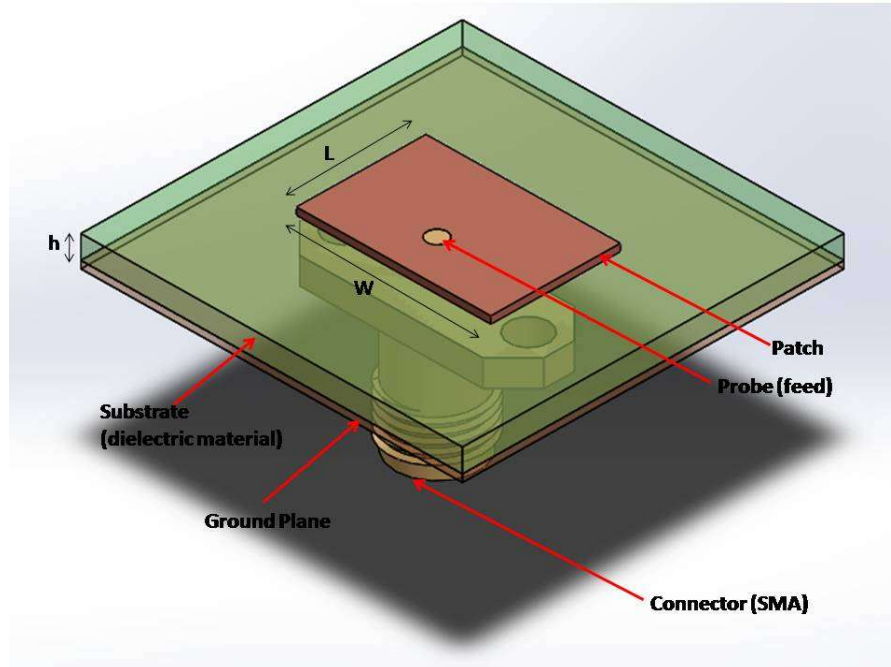
1.2.1 Structure of Rectangular Microstrip Antenna

Fig. 1.1(a) below depicts configuration of a conventional rectangular microstrip patch antenna of length (L) and width (W) claded on to a substrate of height (h). The co-ordinate are selected such that, the length of the patch is along the x axis, the width of patch is along the y axis and the height of patch is along the z axis. In **Fig. 1.1(b)** shows the side view of typical probe fed rectangular microstrip patch.

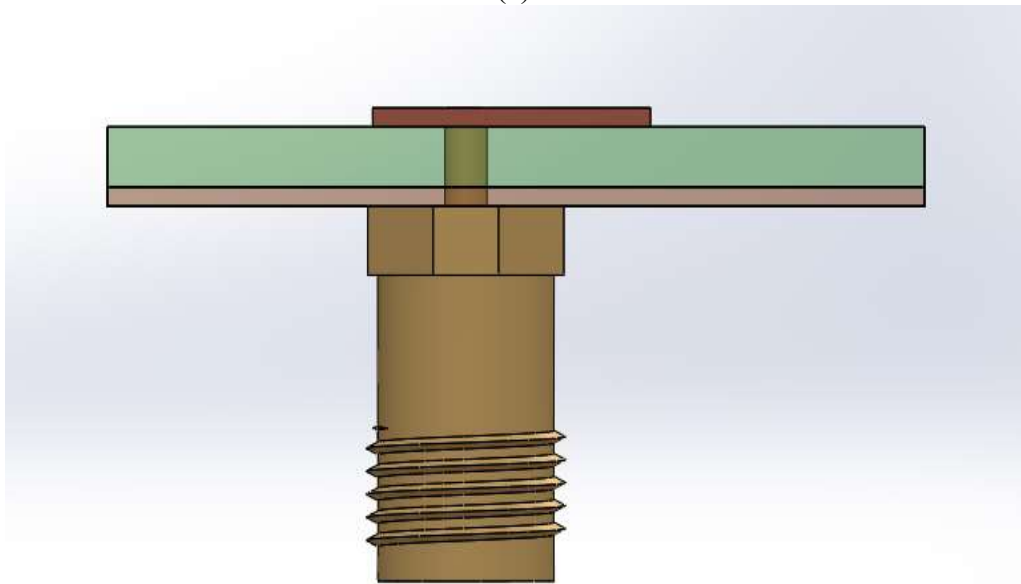
In order to excite the patch in the fundamental TM_{10} mode, the length of the patch should be a little less than $\lambda/2$ (λ : wavelength in the dielectric medium) and is equal to $\lambda_0/\epsilon_{reff}$ (λ_0 is the free space wavelength). In the fundamental mode, the field varies half cycle along the length, and there is no deviation in wave front along the patch width. In **Fig. 1.2(a)** depicted below, the microstrip patch antenna is represented by two conductors, separated by a transmission line of length L and terminated by open circuited at the ends. The voltage is at maximum and current is at minimum due to the open ends along the width of the patch. The fields at the edges can be further resolved into normal and tangential components.

It can be seen from **Fig. 1.2(b)** that along the width the normal components of the electric field at the two edges are out of phase by 180° since the patch is $\lambda/2$ long and hence they nullify each other in the broadside direction. However, the

tangential components (**Fig. 1.2(b)**), which are in phase, unite to give maximum radiated field normal to the surface of the structure.



(a)



(b)

FIGURE 1.1. Conventional RMA (a) Isometric View (b) Side View

Hence, the edges at the width of the patch can be represented as two radiating strips, which are half wavelength apart and excited in phase and thereby radiating in the

half space above the ground plane. It has also been observed that the fringing fields along the width exist and electrically the patch size appears greater than its physical dimensions. The extended dimensions of the patch are represented as ΔL and ΔW as shown in **Fig. 1.2(a)**

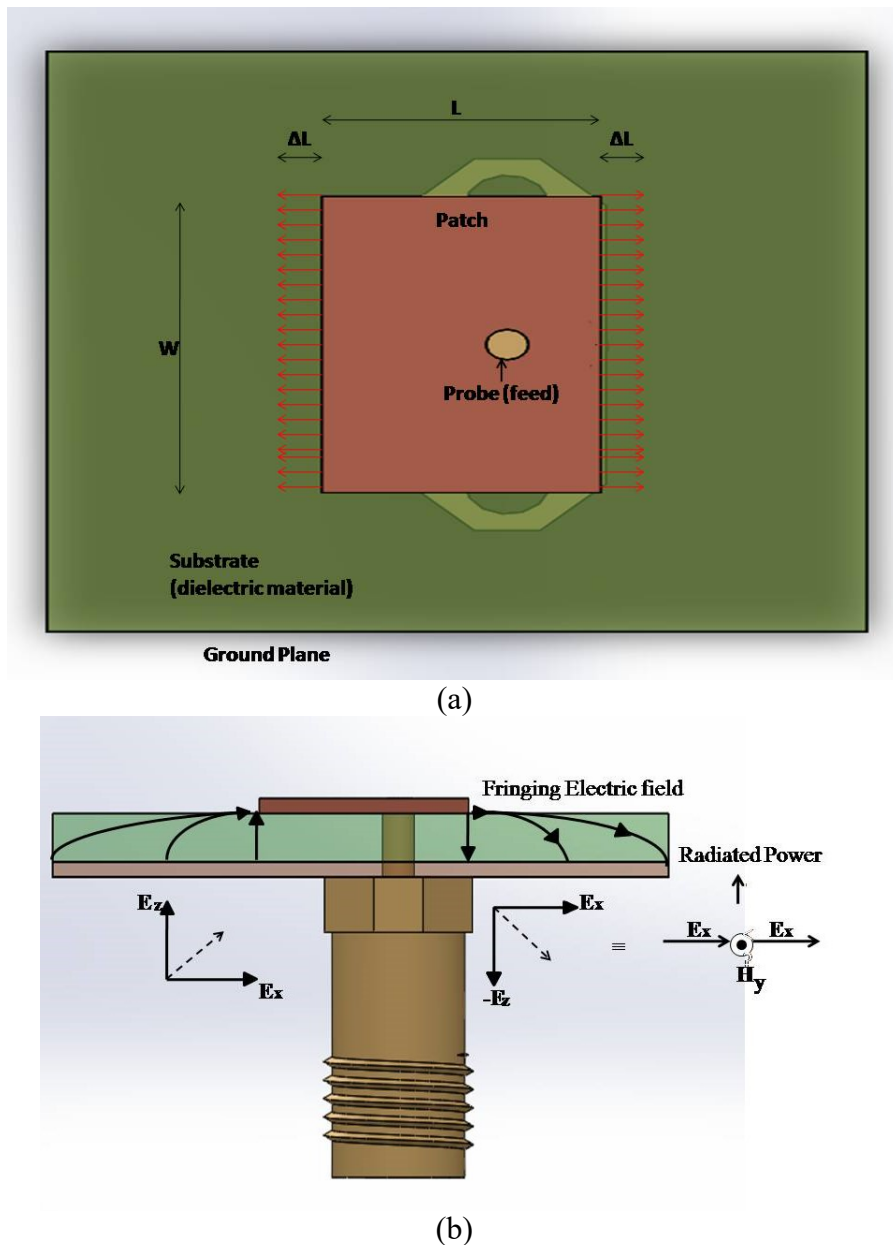


FIGURE 1.2. (a) Fringing at radiating edges of probe fed rectangular microstrip patch antenna. (b) Cross-sectional view of rectangular microstrip patch antenna and fringing electric fields in quasi TEM mode

1.2.2 Limitations of Rectangular Microstrip Antenna

Although rectangular microstrip (so called the printed antennas) antennas have certain essential advantages over conventional microwave antennas like, light weight, conformable, small volume, low profile or planar, easy to fabricate, low-cost fabrication, etc. However, conventional rectangular microstrip antenna suffers from some limitation as enumerated in [39]-[45]. The gain is poor and is around 3 to 4 dBi. The bandwidth is limited and is up to 5% for conventional microstrip antenna. The efficiency of the antenna is limited too due to the dielectric and conductor losses. The radiation efficiency is around -3.8 dB and total efficiency of is around -8.8 dB. The polarization purity is around 10 to 15 dB which is also not so promising. The power handling capacity is mW to few W which is suitable for home applications but not suitable for industry and military applications. Due to surface waves, the antenna suffers with reduced radiation efficiency and directivity. Also due to feeds, sharp edges, joints of solder and junctions there are spurious radiations too. The fabrication is quite simple but only for small size antennas the production complexity increases.

The above mentioned challenges are few important research subject in microstrip antenna field. For example, array configuration is used to address the issue of low gain and low power handling capacity [43] – [44]. For improving bandwidth, using thick substrate with low dielectric permittivity [86], slot, defect or slit loading on patch surface [85]-[86], stacking of patch elements [87], attachment of parasitic elements [88] are few ways. Surface wave issues can be handled with Photonic Band Gap structures (PBG), etc.

1.3 Feeding Techniques of Microstrip Antenna

As like any antenna, feed should be proper to achieve the efficient radiation. The classical techniques can be classified into two, namely direct contacting and non-contacting methods. Both the feeding techniques are well documented and researched. Coaxial probe feeding as shown in **Fig. 1.1(b)** and microstrip line feeding are the common direct method of feeding. Whereas, proximity coupled feed and aperture coupled feed are the two extensively used noncontact type of feeding.

Coaxial probe feed is easy to integrate to patch and also its suitability for

impedance matching at the desired contact point on the patch is a well known fact. Spurious radiation is very less from the probe since it is in direct contact with the patch if properly soldered, which makes this configuration more versatile and most efficient. However, coaxial feeding leads to narrow bandwidth, it is also difficult to analyse, and difficult to implement in high density array structures. Also, for thicker substrates the feed becomes more inductive due to length of probe. The strip line feed is also easy to fabricate since it form the part of the patch etching process and does not requires additional efforts. Also the fine tuning by means of modification of the width of the strip line is easy and has been extensively used.

The primary advantage of proximity coupled feed and aperture coupled feed is that, it eradicates spurious feed radiation and coupling, and also suitable to achieve wide bandwidth. Also, optimaziation for networking of the feeds for array configuration is feasible and has been well exploited by many researchers and industries. However, this technique is difficult in fabrication and the power coupled is restricted to the apparture size which is a dominating drawback of this technique.

Hence, due to the advantages and wide accepatability of probe feed technique, along with the versatility of rectangular microstrip patch antenna, this thesis concentrates to investigate to enhance some characteristics of rectangular microstrip antenna.

1.4 Rectangular Microstrip Antenna: Radiation Characteristics

For effective radiation from RMA, patch length ($L \sim \lambda_0/2$) and width ($W = 1.5L$) are preferred with substrate material of low dielectric constant in the range of $2.2 \leq \epsilon_r \leq 12$ and substrate height in the range of $0.003\lambda_0 \leq h \leq 0.05\lambda_0$ (where λ_0 denotes free space wavelength). **Fig. 1.3** shows fringing fields on a basic RMA on the radiating and non-raditing edges. The transmission line and the cavity model analysis are few of the models used for analysis of a microstrip patch antenna. Also, both the analysis model do consider fringing effects.

Due to the fringing fields, the effective patch size i.e. the length and width becomes higher than actual. The same can be expressed as in [89], Since the electric fields are not confined only within the substrate, the effective dielectric constant (ϵ_{reff}) would also be different from the actual dielectric constant of the substrate used.

$$L_{eff} = (L + 2\Delta L) \quad (1.1)$$

$$W_{eff} = (W + 2\Delta W) \quad (1.2)$$

note: ΔL and ΔW are as shown in **Fig. 1.3**

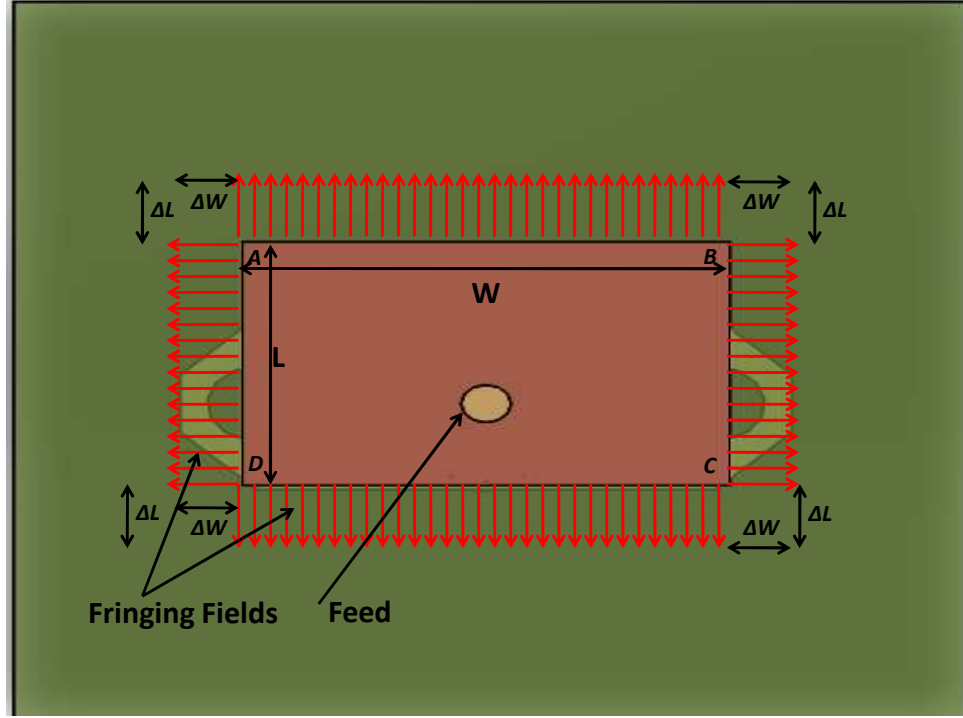


FIGURE 1.3 Schematic diagram of fringing fields of a classical probe fed RMA.

Hence, ϵ_{reff} would be slightly less than exact dielectric constant due to environment in close vicinity of the antenna and can be expressed as,

$$\epsilon_{reff} = \frac{\epsilon_r + 1}{2} + \frac{\epsilon_r - 1}{2} \left[1 + 12 \frac{h}{W} \right]^{-\frac{1}{2}} \quad (1.3)$$

The dominant mode excitation of a RMA is TM_{10} mode. In the dominant mode, effective radiation emits from AB and CD edges of the patch (**Fig. 1.3**) and they meet in-phase along the broadside of the patch. Therefore, RMA can be recognized as a broadside radiating antenna where in the sides AB and CD are the radiating edges and other two sides are the non radiating edges. An example of complete radiation pattern in 3D form is shown in **Fig. 1.4**. As it can be observed, E plane beam width is broader than the H plane beam width. Where in the E plane beamwidth is generally 90° while the H plane is generally 70° .

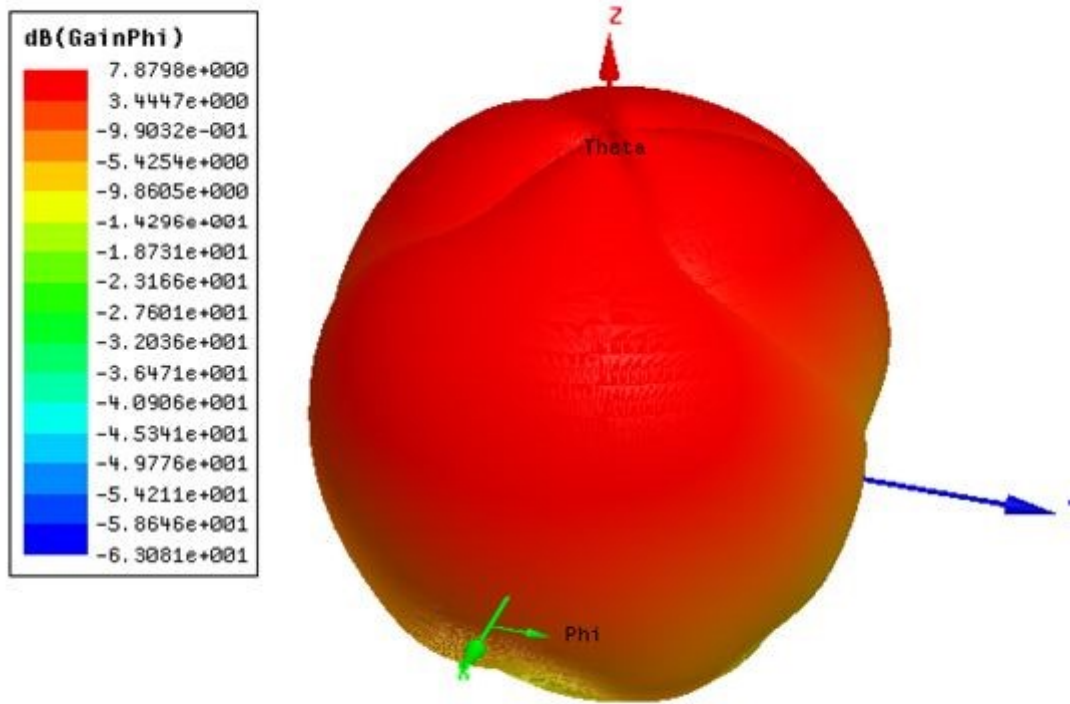


FIGURE 1.4 A simulated 3D radiation pattern of a RMA with length of 8 mm and width of 12 mm.

1.5 Overview of Cross Polarization and Polarization Purity of RMA

It may be noted that the XP level for RMA is quite high at off-boresight angle and is very much prominent in H-plane [40],[52]. As this XP radiation is unwanted radiation for purely linear polarized antenna the same need to be suppressed with respect to CP radiation. The isolation between this wanted CP radiation and unwanted XP radiation commonly referred as CP-XP isolation. Therefore, the enhancement of CP-XP isolation, is a major challenge to the researchers to develop an efficient RMA with pure linear polarization, particularly for H plane.

Rectangular microstrip antenna in its dominant TM_{10} mode radiated linear polarized radiation (CP radiation) in its broadside direction and cross polarized radiation (XP radiation) in the orthogonal direction as shown in **Fig. 1.5**. The unwanted XP radiation in E plane is not that much significant as it is always lower than -30 dB whereas, in H plane, XP radiation is quite significant and limiting the

RMA relevance in modern wireless communication system such as adaptive antenna arrays for cellular, mobile communications, RADAR and microwave communication which demands higher CP-XP isolation over wide range of frequencies.

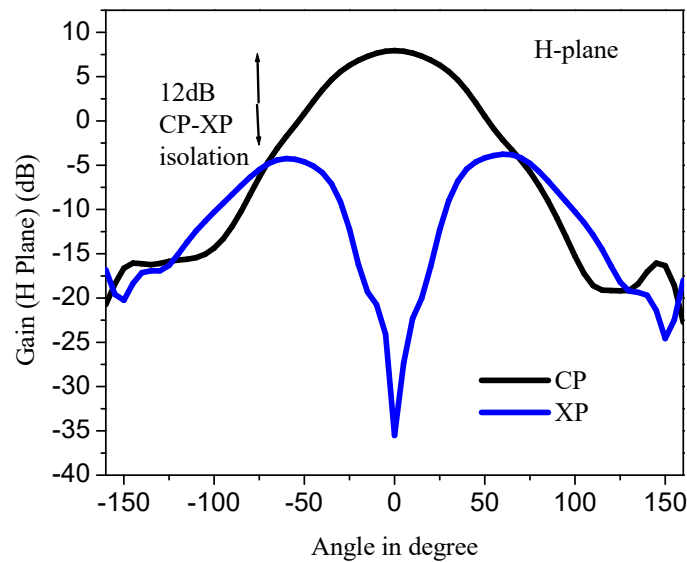


FIGURE 1.5 A simulated CP and XP radiation pattern of a RMA.

The primary sources of the H plane XP radiation are due to probe feeding, where in matching is an important issue. Improper matching causes XP radiation. Also, the XP radiation of RMA with thicker and lower dielectric constant substrate fed with co-axial probe is more significant [90]-[92]. Also, unwanted radiation from probe contributes in cross polarized radiation XP. Another source of XP is the fringing field along the non-radiating edges (**Fig. 1.6**) generated due to higher order orthogonal mode (mainly in TM_{02} mode) [22]. Moreover, orthogonal components of dominant TM_{10} radiation from the corner of the patch [52] and [93]-[95] is also an undesirable radiation and is termed under XP radiation and loss to the polarization purity.

1.6 Survey of Techniques to Improve Polarization Purity

The enhancement of CP-XP isolation is of paramount importance in almost all applications and excellent level of polarization purity is required in specific applications like polametric radars. Various scientests and industrial researchers have devised ways and means to enhance polarization purity. The survey on the

same is extracted in this section based on the techniques used. However, it is imperative that the polarization purity should be achieved keeping other parameters under control and the trade off should not be deranged type. Hence, the key challenge is to achieve polarization purity along with enhanced gain, broad banding, stable and symmetrical radiation.

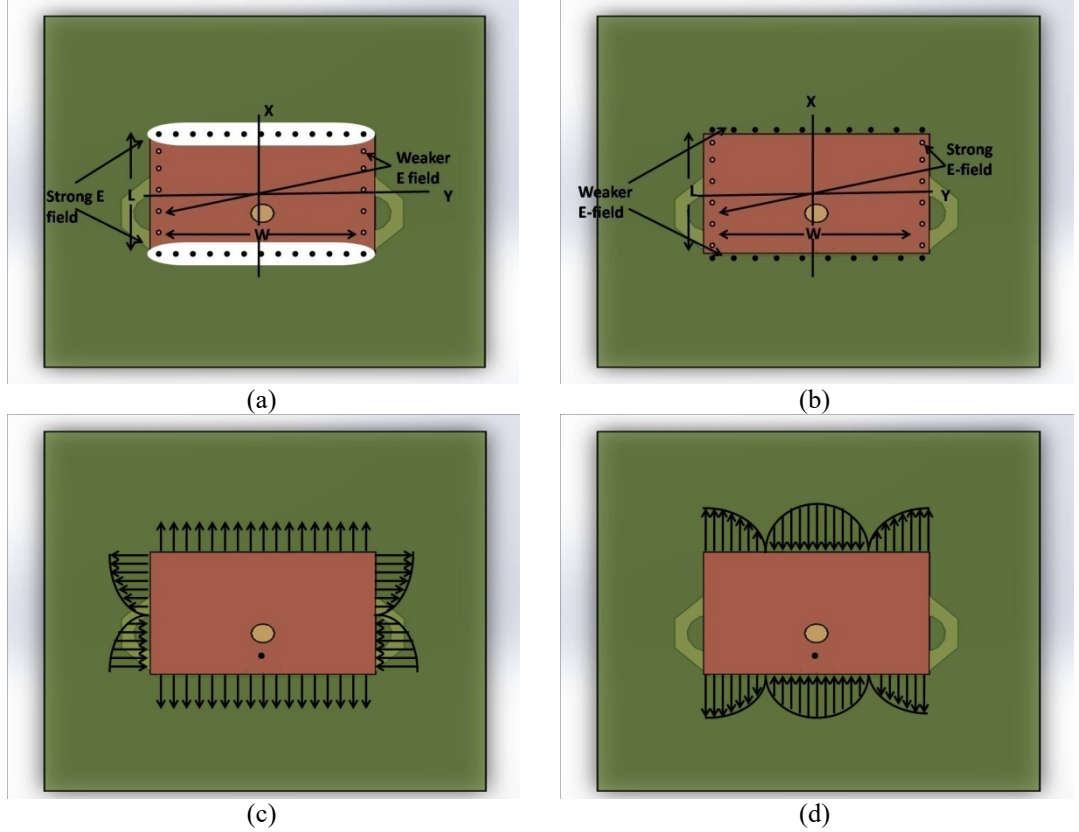


FIGURE 1.6 Electric field distribution with respect to modes. (a) Radiated electric field from edges due to TM_{10} mode, (b) Radiated electric field from edges due to TM_{02} mode, (c) Electric field orientation due to TM_{10} mode (d) Electric field orientation due to TM_{02} mode

(a) Non-contact form of feeding: Improvement in CP-XP isolation at H plane using this concept has been well documented in [96]-[98]. CP-XP isolation of 30 dB has been reported in [96] by means of dual polarized aperture coupled stacked MPA. CP-XP isolation of 23 dB has been reported in [97] by implementing aperture coupled T-shaped feed line along with annular ring integrated ground plane. CP-XP isolation of 22.5 dB has been reported in [98] by means of rat race feeding techniques with differential feed system.

(b) Modification of feed structure: Improvement in CP-XP isolation at H

plane using this concept has been well documented in [99]-[102]. Dual feed structure with customised modification to the feed structure in proportion to half wavelength is proposed in [99] to manage 20 dB CP-XP isolation. Complex meander line feeding [100] technique has been implemented to achieve XP level around -20 dB. In [101] another very complex feeding mechanism has been reported, where in a square patch having two in-phase aperture coupling and two out-of-phase gaps coupling of probe feeds to reach -20dB of XP level. A differentially fed patch is proposed in [102] to achieve around 20 dB to 40 dB suppression of cross polarized radiation with respect to peak co-polarized radiation gain in a dual polarized patch antenna.

(c) Stacked patches, meander line feeding and mirror pair feeding: Improvement in CP-XP isolation at H plane using this concept has been well documented in [103]-[105]. The XP radiation level of around -16.5 dB at over all angles in principal planes has been proposed in [103] by means of stacked patch structure. Also, similar kind of stacking of patch structure and mirrored pair feeding technique has been proposed for L band to achieve around 15-20 dB of CP-XP isolation in [104]. In [105], the authors proposed the stacked offset microstrip antenna arrangement to accomplish 15 dB improvement in CP-XP isolation. However, these configurations are either complex or bulky manufacturing processes.

(d) Modification to ground plane: A “W” shaped ground plane has been well investigated in [106] to attain around 14 dB CP-XP isolation. Also, a “U” shaped ground plane has been reported in [107] for 10-15 dB isolation in CP to XP. However, these configurations are complex in manufacturing processes.

(e) Defected Ground Structure (DGS) : The DGS concept is a new facet of research associated with the planar antennas for improving various radiation characteristics. In these structures defects of different forms and dimensions are created on the ground plane to achieve desired level of performance. The DGS integrated planar structures harnesses the concept of electromagnetic band gap (EBG) or so called photonic band gap (PBG). It

was first reported in [110], [111] where in a dumbbell shaped defect has been incorporated. Surely its an easy and compact implementation as compared to the above mentioned structures. Initially, the DGS integrated conventional patches were utilized for low-pass, band-stop, band-pass, and harmonics suppressor. Apart from the above mentioned applications, DGS has been mainly implemented for impedance matching [112] and to improve isolation between adjacent components also as documented in [113]. The first reported [54] of application of DGS for suppression of XP radiation in a microstrip antenna was made and is now a well established practise. In [54], around 5-8 dB XP suppression by incorporating a circular defect in ground plane specifically located near non-radiating edges has been reported. The employment of DGS to improve polarization purity is comparatively easier. However, DGS integrated antennas suffer from back radiation. Therefore, another technique, of defecting the patch surface has also been researched in subsequent years [114]-[116] to address the issue of XP radiation and improvement in other characteristics of radiation of microstrip antenna.

1.7 Gain and Bandwidth Enhancement

Bandwidth enhancement is an important requirement for and antenna to be useful. As in [52], bandwidth of an antenna is considered in which the magnitude of reflection coefficient is greater than -10 dB. As brought out earlier, it's in the range of 2 to 3 % and broad banding of an antenna is achieved by making the antenna perform with reflection coefficient greater than -10 dB at least for 10% of the band. Classically, methods to achieve the same are by altering the substrate characteristics and by coupling a resonator. Since standardized substrates are available, modifications with it is difficult. However, in the later methods the same can be achieved by DGS, DPS and slot concept [93], [94] and [109]. In a recent paper [117], in which technique to improve the impedance bandwidth is discussed by DGS configuration where in a planar air-gap-loaded rectangular shaped microstrip antenna was explored. The antenna had a single shorting post and two rectangular shaped DGS loading. Application of these configurations helped to wider the impedance

bandwidth than conventional one along with good co-polarization to cross-polarization isolation level.

Gain enhancement is of paramount importance and also it is a never-ending process. Higher gain generally would mean that the radiation is concentrated over smaller beam width. This is desirable and appropriate for some of the linear applications, such as those, which need to track and locate in terms of spatial resolution of azimuth and elevation. Classically, gain enhancement has been achieved by array forming. However, just enhancing the array cluster does not enhance the gain due to various reasons. In a recent and good research [118], 2 x 2 configuration, line feed U-slot rectangular array has been implemented to get antenna gain over 10 dBi however had limited bandwidth of 18%. Optimized array formation along with patch dimensions modifications, modifications to feeding has been used extensively to enhance gain [119]-[121].

1.8 Preface to the Thesis

In this dissertation, the most useful and versatile patch antenna geometry i.e. Rectangular Microstrip Antenna (RMA), has been investigated theoretically and experimentally for the improvement of bandwidth and radiation characteristics. Rectangular microstrip antenna (RMA) is the most useful antenna structure for its wide variety of applications, due to its simple design, ease of implementation, manufacturing and even production. Modification of RMA due to its basic structure of just copper clad and dielectrics is very easy and hence tweaking it as per requirement is relatively easy. Because of these features, RMA is a best choice to address all the requirements of latest personal or handheld wireless communication equipment. Notwithstanding the above, the RMA is also suitable for certain aerial applications like satellite and missiles due to its conformability and lightweight. Nevertheless, the parameters of an RMA viz-z-viz its versatility are not so promising. Hence, investigation to enhance some characteristics of rectangular microstrip antennas is imperative.

In **Chapter 2**, has been investigated the Microstrip patch antenna with defected patch surface (DPS). The chapter has been mainly divided in two parts

wherein detailed investigations have been shown in antennas having DPS at radiating and non-radiating side.

In **Chapter 3**, the employment of defected ground structure (DGS) of hexagonal geometry has been methodically investigated. Here, the employment of DGS has been considered mainly to improve the gain and bandwidth of RMA. As such, the classical report on implementation of DGS in RMA is prominently considered for lowering cross-polarized radiation.

In **Chapter 4** a single layer and planar bracketed stub loaded RMA has been investigated for high gain and low XP radiation in the entire elevation angle. The structure is simple being a single layered and easy to fabricate. In this concept, the magnetic field locus generated by attachment of coaxial probe is modulated in a desired manner and discussed in detail in Chapter 4.

In **Chapter 5**, a compact Quasi-planar Composite Microstrip Antenna (QPCMA) has been investigated thoroughly for concurrent improvement of all the radiation properties of a rectangular microstrip antenna.

And finally, along with the conclusion and future scope the performance comparison for all the investigated structures is tabulated, which may be helpful for practicing engineers to choose the antenna structure for their specific applications.

References

- [1] D. D. Greig and H. F. Engleman, "Microstrip-a new transmission technology for the kilomegacycle range," *Proc. IRE*, vol. 40, pp. 1644-1650, 1952.
- [2] G. A. Deschamps, "Microstrip Microwave Antennas", *3rd USAF Symposium on Antennas*, 1953.
- [3] H. Gutton, and G. Baissinot, "Flat Aerial for Ultra High Frequencies", French Patent No. 703113, 1955.
- [4] E. G. Fubini, "Stripline radiators," *IRE Transac. on Microwave Theory and Tech.*, vol.3, no. 2, pp. 149-156, 1955.
- [5] J.A. McDonough, R. G. Malech, and J. Kowalsky, "Recent developments in the study of printed antennas," *IRE Int. Conv. Rec.*, pp. 173-176, New York, 1957.
- [6] L. Lewin, "Radiation from discontinuities in strip lines," *Proc. IEE-Part C*, vol. 107, no. 12, pp 163-170, 1960.
- [7] E. J. Denlinger, "radiation from microstrip resonators," *IEEE Transac. on Microwave Theory and Tech.*, vol.17, no. 4, pp. 235-236, 1969.
- [8] E.V. Byron, "A new flush mounted antenna element for phased array applications", *Proc. Phased Array Antenna Symp.*, pp.187-192, 1970.
- [9] J. Q. Howell, "Microstrip antennas," *Dig. IEEE Int. Symp. Antennas Propagat.*, pp.177-180, 1972.
- [10] H. D. Weinschel, "Progress report on development of microstrip cylindrical arrays for sounding rockets", *Physical & Science. Lab.*, New Mexico State University, Las-Cruces, 1973.
- [11] G. G. Sanford, "Conformal microstrip phased array for aircraft tests with ATS-6", *Proc. National. Electronic Conference*, vol.29, pp. 252-257, 1974.
- [12] R. E. Munson, "Conformal microstrip antennas and microstrip phased arrays," *IEEE Trans. Antennas Propagat.*, Vol. 22, pp. 74-78, 1974.
- [13] R. E. Munson, "Dual slot microstrip antenna device," U.S. patent No. RE29296, 1975.
- [14] J. Q. Howell, "Microstrip antennas," *IEEE Trans. Antennas Propag.* vol. AP-23, no. 1, pp. 90-93, 1975.

- [15] J. R. James, and G.J Wilson, “New design technique for microstrip antenna arrays”, *Proc. 5th European Microwave Conf.*, pp-102-106, Hamburg, 1975.
- [16] G. W. Garvin, R. E. Munson, L. T. Ostwald, and K. G. Schroeder, “Low profile electrically small missile base mounted microstrip antennas”, *Dig. Int. Symp. Antennas Propag. Soc.*, Urbana, IL, pp-244-247, 1975.
- [17] J. P. Seaux, A. Reineix, B. Jecko, and J. H. Hamelin, “Transient analysis of a space-borne microstrip patch antenna illuminated by an electromagnetic pulse,” *IEEE Trans. Electromagnetic Compatibility*, Vol.33, pp. 224-233,1991.
- [18] P. K. Bondyopadhyay, “Spherical microstrip arrays for mobile satellite communication,” *Dig. IEEE Int. Symp. Antennas Propagat.*, Vol. 3, pp.1438–1441, 1995.
- [19] R. E. Thomas and J. Huang, “Ultra-wideband UHF microstrip array for Geo SAR application,” *Dig. IEEE Int. Symp. Antennas Propagat.*, Vol. 4, pp.2096-2099, 1998.
- [20] J. Huang, “Miniaturized UHF microstrip antenna for a Mars mission,” *IEEE Int. Symp. Antennas Propag.*, Vol. 4 , pp. 486 –489, 2001.
- [21] J. T. Bernhard, R. Wang, R. Clark, and P. Mayes, “Stacked reconfigurable antenna elements for space-based radar applications,” *Dig. IEEE Int. Symp. Antennas Propagat.*, Vol.1, pp. 158 -161, 2001.
- [22] I. J. Bahl and P. Bhartia, *Microstrip Antennas*, Artech House, Dedham, MA, 1980.
- [23] J. R. James, P. S. Hall, and C. Wood, *Microstrip Antennas: Theory and Design*, London, UK, Peter Peregrinus, 1981.
- [24] K. Carver and J. Mink, “ Microstrip antenna technology,” *IEEE Trans. Antennas Propagat.*, Vol. 29, pp. 2-24, 1981.
- [25] A. G. Derneryd, “Linear microstrip array antennas,” *Chalmer Univ. Technol.*, Goteborg, Sweden, Tech. Rep. TR 7505, 1975.
- [26] Y. T. Lo, D. D. Harrison, D. Solomon, G. A. Deschamps, and F. R. Ore, “Study of microstrip antennas, microstrip phased arrays, and microstrip feed networks,” *Rome Air Development Center, Tech. Rep.* TR-77-406, 1977.

- [27] Y. T. Lo, D.Solomon, and W. F. Richards, "Theory and experiment on microstrip antennas," *IEEE AP-S Symposium*, Japan, pp.53-55, 1978.
- [28] W.F Richards, Y.T Lo, and D.D Harrison, "Improved theory for microstrip antennas," *Electron. Lett.*, vol.15, no. 2, pp.42-44, 1979.
- [29] Y.T Lo, D. Solomon, and W.F Richards, "Theory and experiment on microstrip antennas," *IEEE Trans. Antennas Propagat.*, vol.27, no. 2, pp.137-145, 1979.
- [30] L. C. Shen and S. A. Long, "Low profile printed circuit antennas," *Dept. Elec. Eng., Univ. Houston*, Houston, TX, Contract DAAG-29-75-0187, Final Rep., 1977.
- [31] K. R. Carver and E. L. Coffey, "Theoretical investigation of the microstrip antenna," *Physic. and Sci. Lab.*, New Mexico State Univ., Las Cruces, Tech. Rep. PT-00929, 1979.
- [32] K.R Carver, "A modal expansion theory for the microstrip antenna", *Dig. Int. Symp. Antennas Propaga. Soc.*, Seattle, WA, pp.101-104, 1979.
- [33] K.R Carver and E.L Coffey, "Theoretical investigations of the microstrip antenna", *Tech. Rept. PT 00929, Physical Science Lab.*, New Mexico Science Univ., Las Cruces, 1979.
- [34] E.L Coffey and T.H Lehman, "A new analysis technique for calculating the self and mutual impedance of microstrip antennas", *Proc. Workshop on Printed Circuit Antennas*, New Mexico State Univ., pp.31/1-21, 1979.
- [35] J.R James and C.J Wilson, "Microstrip antennas and arrays part i fundamental action and limitations", *IEE Proc. Microwaves, Opt. & Antennas*, vol.1, pp. 165-174, 1977.
- [36] J.R Mosig and F.E Gardiol, "The near field of an open microstrip structure", *IEEE AP-S, Int.Symp. Digest*, pp.379-381, 1979.
- [37] P.K Agarwal and M.C Bailey, "An analysis technique for microstrip antennas", *IEEE Trans. Antennas Propagat.*, vol. 25, no. 6, pp.756-759, 1977.
- [38] N.G. Alexopoulose, N.K Uzunoglu, and I. E. Rana, "Radiation by microstrip patches," *Dig. Int. Symp. Antennas Propagat.*, pp.722-727, 1979.

- [39] C. A. Balanis, *Antenna Theory: Analysis and Design*, John Wiley & Sons, NY, 1997.
- [40] R. Garg *et. al.*, *Microstrip Antenna Design Handbook*, Artech House, Boston, 2001.
- [41] G. Kumar and K. P. Ray, “*Broadband microstrip antennas*,” Boston, Artech House, 2002.
- [42] Kin-Lu Wong, *Planar Antennas for Wireless Communications*, Wiley, 2003.
- [43] Rod Waterhouse, *Microstrip Patch Antennas: A Designer's Guide*, Springer, 2003.
- [44] Randy Bancroft, *Microstrip and Printed Antenna Design*, Noble Publishing, 2004.
- [45] Z. N. Chen and M. Y. W. Chia, *Broadband Planar Antennas: Design and Applications*, Wiley, 2006.
- [46] I. Bulu, H. Caglayan, K. Aydin and E. Ozbay, “Compact size highly directive antennas based on the SRR metamaterial medium,” *New Journal of Physics*, Vol. 7, 2005.
- [47] C. A. Allen, K. Leong, C. Caloz,; T. Itoh, “A two-dimensional edge excited metamaterial-based leaky wave antenna,” *IEEE Antennas and Propagation Society International Symposium*, pp.320-323, 2005.
- [48] J. L. Volakis *et.al*, “Miniaturization methods for narrowband and ultra wideband antennas,” *IEEE International Workshop on Antenna Technology: Small Antennas and Novel Metamaterials*, 2005.
- [49] T. Kokkinos, C. D. Sarris, G. V. Eleftheriades, “Finite-difference time-domain analysis of metamaterial-based leaky-wave antennas,” *IEEE Antennas and Propagation Society International Symposium*, pp. 26-29, 2005.
- [50] Aycan Erentok, Richard W. Ziolkowski, “Metamaterial-Inspired Efficient Electrically Small Antennas” *IEEE Transactions on Antennas and Propagation*, Vol. 56, no.3, pp. 691 –707, 2008.
- [51] M. A Hui Feng, Chen Xi, Yang Xin Mi, X U Hong Sheng, Cheng Qiang and Cui Tie Jun, “A broadband metamaterial cylindrical lens antenna,” *Chinese Science Bulletin.*, Vol. 55, no.19, pp. 2066–2070, 2010.

- [52] D. Guha, Y. M. M. Antar (Eds.), *Microstrip and Printed Antennas: New Trends, Techniques and Applications*, Ch. 11, Wiley, 2011.
- [53] D. Guha, M. Biswas, and Y. M. M. Antar, "Microstrip patch antenna with defected ground structure for cross polarization suppression," *IEEE Antennas Wireless Propag. Lett.*, vol. 4, pp. 455–458, 2005.
- [54] D. Guha, S. Biswas, T. Joseph and M. T. Sebastian, "Defected ground structure to reduce mutual coupling between cylindrical dielectric resonator antennas", *Electronic Lett.*, vol. 44, no.14, pp. 836-837, 2008.
- [55] H. Moghadas, A. Tavakoli, M. Salehi, "Elimination of scan blindness in microstrip scanning array antennas using defected ground structure," *Int. J. Electron. Commun.*, Vol. 62, pp.155 – 158, 2008.
- [56] D. B. Hou, *et al.*, "Elimination of scan blindness with compact defected ground structures in microstrip phased array," *IET Microwave Antennas propag.*, Vol. 3, no. 2, pp. 269-275, 2009.
- [57] D. Guha, C. Kumar, and S. Pal, "Improved Cross-Polarization Characteristics of Circular Microstrip Antenna Employing Arc-Shaped Defected Ground Structure (DGS)," *IEEE Antennas Wireless Propag. Lett.*, Vol. 8, pp. 1367–1369, 2009.
- [58] D. Guha, S. Biswas, and C. Kumar, "Annular Ring Shaped DGS to Reduce Mutual Coupling Between Two Microstrip Patches," *IEEE Applied Electromagnetics Conf. AEMC 2009*, pp. 1-4, Kolkata, India, 2009.
- [59] C. Kumar, and D. Guha, "A New Look into the Cross-Polarized Radiation from a Circular Microstrip Antenna and Suppression Using Dot-Shaped DGS," *IEEE AP-S Symp.*, Toronto 2010.
- [60] F. Y. Zulkili, E. T. Rahardjo, and D. Hartanto, "Mutual coupling reduction using dumbbell defected ground structure for multiband microstrip antenna array," *Progress In Electromagnetics Research Letters*, Vol. 13, pp. 29-40, 2010.
- [61] Aaron K. Shackelford, Kai-Fong Lee, and K. M. Luk, "Design of Small-Size Wide-Bandwidth Microstrip Patch Antennas," *IEEE Antennas and Propagation Magazine*. Vol. 45, no. 1, 2003.

- [62] S.I. Latif, L. Shafai, and S. K. Sharma, "Bandwidth Enhancement and Size Reduction of Microstrip Slot Antennas," *IEEE Transaction on Antennas and Propagat.*, Vol. 53, no. 3, 2005.
- [63] R. Głogowski and C. Peixeiro, "Multiple Printed Antennas for Integration Into Small Multistandard Handsets," *IEEE Antennas and Wireless Propagation Letters*, Vol. 7, 2008.
- [64] L. Han, W. Zhang, G. Han, R. Ma and L. Li, "Differential Dual-Frequency Antenna for Wireless Communication," *ETRI journal*, Vol. 30, no. 6, pp. 877- 879, 2008.
- [65] Sunil Kumar Rajgopal and Satish Kumar Sharma, "Investigations on Ultrawideband Pentagon Shape Microstrip Slot Antenna for Wireless Communications," *IEEE Transaction on Antennas and Propagat.*, Vol. 57, no. 5, 2009.
- [66] P. Rakluea, N. Anantrasirichai, K. Janchitrapongvei, and T. Wakabayashi, "Multiband Microstrip-Fed Right Ange Slot Antenna Design for Wireless Communication Systems," *ETRI journal*, Vol. 31, no. 3, pp. 271-281, 2009.
- [67] A. Foroozesh and L. Shafai, "Performance Enhancement of the Compact Microstrip Antennas Using AMC Ground Planes," *IEEE International Symposium on Antennas and Propagation and the USNC/URSI National Radio Science Meeting*, 2009.
- [68] D. R. Jackson *et. al.*, Computer-Aided Design of Rectangular Microstrip Antennas, in *Advances in Microstrip and Printed Antennas*, K. F. Lee and W. Chen (*Eds.*), Wiley, NY, 1997.
- [69] Cheng-Tse Lee, and Kin-Lu Wong, "Uniplanar Printed Coupled-Fed PIFA With a Band-Notching Slit for WLAN / Wi MAX Operation in the Laptop Computer," *IEEE Transaction on Antennas and Propagat.*, Vol. 57, no. 4, 2009.
- [70] J. Siden, P. Jonsson, T. Olsson, and G. Wang, "Performance Degradation of RFID system due to the distortion in RFID tag antenna", *11th International Conference on Microwave and Telecommunications Technology (CriMiCo 2001)*, Sevastopol, Crimea, Ukraine, 2001.

- [71] P. Nikitin, S. Lam, and K. Rao, "Low cost silver ink RFID tag antennas," *IEEE Antennas and Propagation Society International Symposium*, Vol. 2B, p. 353, 2005.
- [72] K. Rao, P. Nikitin, and S. Lam, "Antenna design for UHF RFID tags: a review and a practical application," *IEEE Transactions on Antennas and Propagation*, Vol. 53, no. 12, p. 3870, 2005.
- [73] S. R. Aroor and D. D. Deavours, "Evaluation of the State of Passive UHF RFID: An Experimental Approach," *IEEE Systems Journal*, Vol. 1, no. 2, pp. 168-176, 2007.
- [74] Daniel M. Dobkin, *The RF in RFID*, Elsevier-News, Chapter 7, 2007.
- [75] M. Sivakumar and D. Deavours, "A Dual-Resonant Microstrip Antenna for Paper board in the Cold Chain," *IEEE Symposium*, 2008.
- [76] D. D. Deavours, "Analysis and Design of Wideband Passive UHF RFID Tags Using a Circuit Model," *IEEE RFID*, April 27–28, Orlando, FL, 2009.
- [77] N. A. Mohammed, M. Sivakumar, and D. D. Deavours, "An RFID Tag Capable of Free-Space and On-Metal Operation", *IEEE Radio and Wireless Symposium*, January 18-22, San Diego, CA, 2009.
- [78] E. H. Newman and P. Tulyathan, "Analysis of microstrip antennas using moment method," *IEEE Trans. Antennas Propagat.*, Vol. 29, no. 1, pp. 47-53, 1981.
- [79] J.T. Aberle and D.M. Pozar, "Accurate and versatile solutions for probe-fed microstrip patch antennas and arrays," *Electromagnetics*, Vol.11, no.1, pp. 1-19, 1991.
- [80] G. S. Hilton, C. J. Railton, and M. A. Beach, "Modeling parasitically-coupled patch antennas using the finite-difference time-domain technique," *IEE 8th Int. Conf. Antennas Propagat.*, Vol. 1, pp. 186-189, 1993.
- [81] C. Wu, K.L. Wu, Z. Bi, and J. Litva, "Accurate characterization of planar printed antennas using the finite-differences time-domain Method," *IEEE Trans. Antennas Propagat.*, Vol. 40, no. 5, 1992.
- [82] K. Uehara and K. Kagoshima, "Rigorous analysis of microstrip phased array antennas using a new FDTD method," *Electron. Lett.*, Vol. 30, no. 2, pp. 100-101, 1994.

- [83] B. Toland, J. Lin, B. Houshmand, and T. Itoh, "FDTD analysis of an active antenna," *IEEE Microwave Guided Wave Lett.*, Vol. 3, no. 11, 1993.
- [84] S. Chebolu, S. Dey, R. Mittra, and J. Svigelj, "Efficient modeling of microstrip antennas using the finite-difference time-domain method," in *Advances in Microstrip and Printed Antennas*, K. F. Lee and W. Chen (Eds.), Ch.10, Wiley, NY, 1997.
- [85] W. Menzel, "A 40 GHz Microstrip Array Antenna," *IEEE MTT-S Int. Symp. Digest*, pp.225-226, 1980.
- [86] A. G. Derneryd and A. G. Lind, "Extended analysis of rectangular microstrip resonator antennas," *IEEE Trans. Antennas Propagation*, vol. 27, no. 6, pp. 846–849, 1979.
- [87] L. Zaid, G. Kossiavas, J. Dauvignac, J. Cazajous, and A. Papiernik, "Dual-frequency and broadband antennas with stacked quarter wavelength elements," *IEEE Trans. Antennas Propag.*, vol. 47, no. 4, pp. 654-660, 1999.
- [88] C.K. Wu and K.L. Wong, "Broadband microstrip antenna with directly coupled and gap-coupled parasitic patches," *Microwave Opt. Technol. Lett.*, vol. 22, no. 5, pp. 348-349, 1999.
- [89] J. D. Kraus, R. J. Marhefka, and A. S. Khan," *Antennas and wave propagation*," 4th Ed., McGraw Hill Edu., New, Delhi, India, 2002.
- [90] T. Huynh, K. F. Lee, and R.Q. Lee, "Cross-polarization characteristics of rectangular patch antennas," *Electronics Letter*, vol. 24, no. 8, pp. 463–464, 1988.
- [91] A. Petosa, A. Ittipiboon, and N. Gagnon, "Suppression of unwanted probe radiation in wideband probe-fed microstrip patches," *Electronics Letter*, vol. 35, no. 5, pp. 355–357, 1999.
- [92] S. Bhardwaj, and Y. R. Rahmat-Samii, "Revisiting the generation of cross-polarization in rectangular patch antennas: a near-field approach," *IEEE Antennas Propag. Magazine*, vol. 56, no. 1, pp. 14-38, 2014.
- [93] S. Chakraborty and S. Chattopadhyay, "Substrate Fields Modulation with Defected Ground Structure: A Key to Realize High Gain, Wideband Microstrip Antenna with Improved Polarization Purity in Principal and

- Diagonal Planes, ” *International Journal of RF and Microwave Computer-Aided Engineering*, vol. 26, no.2, pp. 174 – 181, 2016.
- [94] S. Chakraborty and S. Chattopadhyay,” Arc-cornered microstrip antenna with defected ground structure for broad banding and improved cross-polarization suppression over whole skew planes, “ *Int. Journal of Microwave and Wireless Technologies*, vol. 9, no. 2, pp. 437-446, 2017.
 - [95] S. Chattopadhyay, and S. Chakraborty, “A physical insight into the influence of dominant mode of rectangular microstrip antenna on its cross-polarization characteristics and its improvement with T-shaped microstrip antenna”, *IEEE Access*, 6, pp. 3594-3602, 2018.
 - [96] S. Gao, L. W. Li, M. S. Leong, and T. S. Yeo, “A broad-band dual-polarized microstrip patch antenna with aperture coupling,” *IEEE Transaction Antennas Propag.*, vol. 51, no. 4, pp. 898–900, 2003.
 - [97] C. H. Lai, T. Y. Han, and T. R. Chen, “Broadband aperture coupled microstrip antennas with low cross polarization and back radiation,” *Progress In Electromagnetic Research Letter*, vol. 5, pp. 187–197, 2008.
 - [98] K. S. Chin, J. A. Liu, C. Chang, and J. C. Cheng, “LTCC differential fed patch antenna with ratrace feeding structures,” *Progress In Electromagnetics Research C*, vol. 32, pp. 95–108, 2012.
 - [99] P. Li, H. W. Lai, K. M. Luk, and K. L. Lau, “A Wideband Patch Antenna With Cross-Polarization Suppression,” *IEEE AWPL*, vol. 3, pp. 211-214, 2004
 - [100] Z. N. Chen and M. Y. W. Chia, “Broad-band suspended probe-fed plate antenna with low cross-polarization level,” *IEEE Transaction on Antennas Propagation*, vol. 51, no. 2, pp. 345-347, 2003.
 - [101] T. W. Chiou, and K. L. Wong, “Broad-Band Dual-Polarized Single Microstrip Patch Antenna with High Isolation and Low Cross Polarization,” *IEEE Transactions on Antennas and Propagation*, vol. 50, no. 3, pp. 399-401, 2002.
 - [102] C. D. Sim, C. Chang, and J. Row, “Dual-Feed Dual-Polarized Patch Antenna with Low Cross Polarization and High isolation,” *IEEE Transactions on Antennas and Propagation*, vol. 57, no. 10, pp. 3321-3324, 2009.

- [103] D. Loffler, and W. Wiesbeck, "Low-cost X-polarised broadband PCS antenna with low cross-polarisation level," *Electronics Letters*, vol. 35, no. 20, pp. 1689-1691, 1999.
- [104] J. Granholm, and K. Woelders, "Dual Polarization Stacked Microstrip Patch Antenna Array with Very Low Cross-Polarization," *IEEE Transactions on Antennas and Propagation*, vol. 49, no. 10, pp. 1393- 1402, 2001.
- [105] V. P. Sarin et. al., "A Wideband Stacked Offset Microstrip Antenna with Improved Gain and Low Crosspolarization," *IEEE Transactions on Antennas and Propagation*, vol. 59, no. 4, pp.1376-1379, 2011.
- [106] K. L. Wong, C. L. Tang, and J. Y. Chiou, "Broad-band probe-fed patch antenna with a W-shaped ground plane," *IEEE Transactions on Antennas and Propagation*, vol. 50, no. 6, pp. 827–831, 2002.
- [107] W. H. Hsu, and K. L. Wong, "Broad-band probe-fed patch antenna with a U-shaped ground plane for cross-polarization reduction," *IEEE Transactions on Antennas and Propagation*, vol. 50, no. 3, pp. 352–355, 2002.
- [108] D. Ghosh et al., "Physical and quantitative analysis of compact rectangular microstrip antenna with shorted non-radiating edges for reduced cross-polarized radiation using modified cavity model," *IEEE Antennas Propagation Magazine*, vol. 56, no. 4, pp. 61–72, 2014.
- [109] R. Poddar, S. Chakraborty, and S. Chattopadhyay, "Improved Cross Polarization and Broad Impedance Bandwidth from Simple Single Element Shorted Rectangular Microstrip Patch: Theory and Experiment," *Frequenz*, vol. 70, no.1-2, pp. 1-9, 2016.
- [110] J. I. Park et. al., "Modeling of a photonic bandgap and its application for the low-pass filter design," in *Proceedings of the Asia Pacific Microwave Conference (APMC '99)*, vol. 2, pp. 331–334, Singapore, 1999.
- [111] C. S. Kim, J. S. Park, D. Ahn, and J. B. Lim, "A novel 1-D periodic defected ground structure for planar circuits," *IEEE Microwave Wireless Components Letters*, vol. 10, no. 4, pp. 131-133, 2000.
- [112] J. P. Thakur, and J. Park, "An advanced design approach for circular polarization of microstrip antenna with unbalanced DGS feed line," *IEEE Antenna and Wireless Propagation. Letters*, vol. 5, pp. 101-103, 2006.

- [113] Y. Chung et. al., "Multifunctional microstrip transmission lines integrated with defected ground structure for RF frontend application," *IEEE Transaction on Microwave Theory Techniques*, vol. 52, no. 5, pp. 1425-1432, 2004.
- [114] A. Ghosh et. al., "Improved Cross Polarization Performance of Circular Microstrip Antenna with Arc Shaped Defected patch Surface," *Proceedings 1st International Science & Technology Congress*, vol. 1, pp.87-92, Kolkata, India, 2014.
- [115] A. Ghosh, S. K. Ghosh, D. Ghosh, and S. Chattopadhyay, "Improved polarization purity for circular microstrip antenna with defected patch surface," *International Journal of Microwave and Wireless Technologies*, vol. 8, no. 1, pp. 89- 94, 2016.
- [116] A. Ghosh et. al., "Rectangular microstrip antenna with defected patch surface for improved polarization purity," *Proceedings 3rd International Conference on Computer, Communication, Control and Information Technology (C3IT)*, pp. 1-5, Hooghly, India, 2015.
- [117] T. Sarkar, A. Ghosh, L. L. K. Singh, S. Chattopadhyay and C. Sim, "DGS-Integrated Air-Loaded Wideband Microstrip Antenna for X- and Ku-Band," in *IEEE Antennas and Wireless Propagation Letters*, vol. 19, no. 1, pp. 114-118, Jan. 2020.
- [118] H. Wang, X. B. Huang and D. G. Sang "A single layer wideband U-slot microstrip patch antenna array " *IEEE antennas and wireless propagation letters*, vol. 7, pp. 9-12, Feb 2008
- [119] N. T. Nguyen, R. Sauleau and L. Le Coq, "Reduced-size double-shell lens antenna with flat-top radiation pattern for indoor communications at millimeter waves", *IEEE Trans. Antennas Propag.*, vol. 59, pp. 2424-2429, 2011.
- [120] Z.-Y. Zhang, N.-W. Liu, S. Zuo, Y. Li and G. Fu, "Wideband circularly polarised array antenna with flat-top beam pattern", *Microw. Antennas Propag.*, vol. 9, no. 8, pp. 755-761, 2015.

- [121] C. Meng, J. Shi and J.-X. Chen, "Flat-gain dual-patch antenna with multi-radiation nulls and low cross-polarisation", *Electron. Lett.*, vol. 54, no. 3, pp. 114-116, 2018.

**Defected Patch Surface Approach
for Wide Symmetrical Radiation
and Low Cross Polarization****2.1 Introduction**

In the present era, with the expeditious development of modern wireless communication systems, antennas having low profile, low cross polarization, wide beam, symmetrical E and H-plane radiation patterns with stable gain are in the spotlight in current research on the subject. In this context, microstrip patch antennas are becoming increasingly popular as they have small volume and a profile planar configuration with low fabrication cost as discussed in Chapter 1. In general, these antennas radiate linearly polarized waves in broadside direction (i.e., co-polarized (CP) radiation). However, the E-plane beam of such a patch is always broader than the H-plane beam and hence causes asymmetry in the 3D radiation patterns. The E-plane beam width of such conventional patch antennas is around 80° , whereas the same in H-plane is only 67° . Moreover, such antennas suffer from high cross polarized (XP) radiation and it becomes worse in its H-plane. Therefore, such antennas suffer from poor polarization purity (co-polarized radiation to cross polarized radiation isolation or CP-XP isolation) which is a major restriction to various applications where improved polarization purity is required over a wide angular range [1].

In the current research on antennas, the wide-angle scanning phased array has also become the major challenge to researchers [2], [3]. To reduce the side lobe of the wide-angle scanning phased array, a broad beam antenna is required [4]. Although the microstrip antenna is a good candidate for the phased array, the narrow

H plane beam width with asymmetrical 3D radiation pattern of such antennas is a major drawback when it is used in a wide-angle scanning phased array. Symmetrical E and H-plane radiation beam along with wide beam width is always preferred for using such patch antennas as an efficient feed for a parabolic reflector or to cover a wide area, particularly for wireless communication.

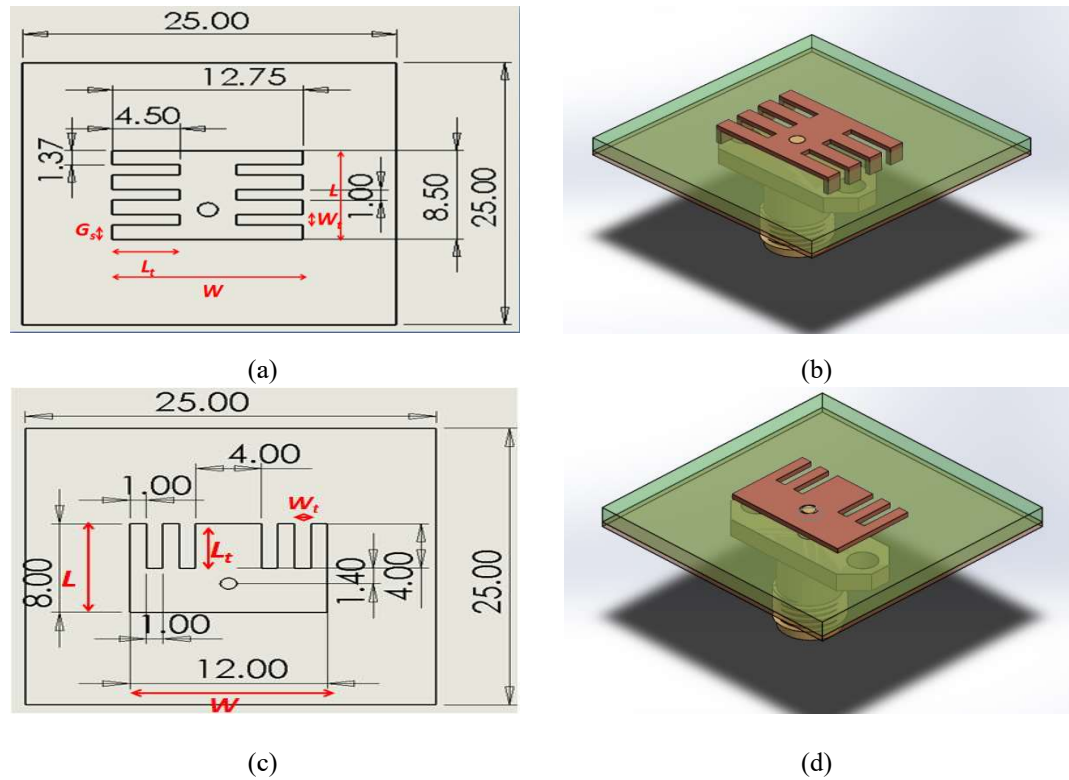


FIGURE 2.1. Proposed DPS with defects on non-radiating side (a) Top view (b) 3D image and DPS with defects on radiating side (c) Top view (d) 3D image.

Some significant research results were reported to broaden the beam width of microstrip antennas in [5]–[6]. Around 130° 3 dB axial ratio beam width was obtained from [5] with no evidence of XP performance improvement or symmetry in 3D radiation beam. Moreover, the structure was bulky and followed complex manufacturing process. Recently, the employment of composite substrate to obtain high gain wide beam characteristics in conventional rectangular patch has been studied in [6]. Around 8 dBi gain with wide E and H-plane beam widths of 88° and 64° , respectively, has been found from [6], with asymmetrical radiation pattern and poor polarization purity (CP-XP isolation of only 9 dB).

The microstrip patch for low XP radiation is an extensively investigated topic of research at present. The XP radiation from a patch becomes significant in probe-fed designs and particularly when the thickness as well as the dielectric constant of the substrate increase [7]. The XP fields are more significant in H-plane than in E-plane. The employment of defected ground structure (DGS) to improve XP radiation for microstrip patch is a widely accepted and recent technique for scientific community and those have been reported in [8]–[9]. Different geometries of DGS have been used in patch antennas to achieve 22–25 dB of CP-XP isolation. However, the DGS-integrated patch antennas suffer from difficulty in probe feeding because of the placement of slots at ground plane. Moreover, the enhanced back radiations, narrow beam and asymmetrical radiation pattern from such DGS-integrated microstrip antenna inevitably impose severe limitation in designing any wireless link.

To alleviate the lacunae of the earlier studies and to address improvements for complete radiation performance such as symmetry in radiation beam, 3 dB beam width, and XP performances, a simple single element grounded comb-shaped patch with defects on non-radiating side and other concept with defects on radiating side (though not grounded) has been proposed and as depicted in **Fig 2.1**. The investigation has been performed on a patch with width (W) to length (L) ratio 1.5 as it yields better performance in terms of XP radiation [10] and impedance band width [11]. As the microstrip radiator has poor impedance band width [1], a relatively electrically thicker substrate with high dielectric constant is utilized. The substrate with high dielectric constant is preferable for electrically thick antenna to remove unwanted radiation from the probe and hence produces undistorted CP profile and also minimizes XP radiation. Recently, a simple shorted conventional patch has been reported in [12] for improvement of the CP-XP isolation. Around 70° and 100° of E and H-plane 3 dB beam width has been obtained, respectively, from the structure. Still, it cannot be designated as wide beam antenna as its E-plane radiation beam is 13% narrower than that of a conventional patch. Moreover, the structure fails to bring symmetry in 3D radiation beam [12]. On the contrary, the proposed structure is envisaged to perform better than that reported in [12] with respect to the symmetry, E- and H-plane 3-dB bandwidth, with 34 dB of CP-XP isolation in the entire

elevation angular range. The proposed structures have been intuitively conceived with a view to modifying the field distribution beneath the patch and results in a wide symmetrical radiation beam along with excellent polarization purity. The proposed structures are simple, easy to manufacture, and surely a good candidate for array antenna with low side lobe level. Unlike DGS-integrated antennas, the present ones do not extend beyond the patch periphery and hence it is free from the problems related to inter-element spacing in array antenna design.

In subsequent sections, the proposed antenna structures and parameters have been discussed. In Section 2.2.1, qualitative analysis has been used to explain the radiation performance characteristics of the proposed structure. Also the effect of grounded strips in minimizing the XP radiations from the proposed structure has been discussed in the same section. In Section 2.2.2, radiation characteristics of grounded and ungrounded comb shaped microstrip patch antennas have been discussed in light of the aperture theory and electric field distribution within the substrate. In Section 2.2.3, proposed structure has been enumerated. In Section 2.2.4, results (simulated and measured) for the proposed structure have been presented. Later, the applicability of the proposed structure in relatively lower frequency band has been discussed which germinates a cross polar radiation free antenna. In Section 2.3.1, Defected Patch Structure (DPS) with defects on radiating side on RMA is discussed in detail. In Section 2.3.2, its results and physical insight has been brought out very deliberately. Section 2.4 gives the comparison between the proposed structures studied in details. Finally Section 2.5 contains the conclusions derived from the findings of the present work.

2.2 Defected Patch Structure (DPS) with Defects on Non-Radiating Side

Theoretical and parametric analysis of various grounded and ungrounded shaped structures are discussed in the succeeding sections.

2.2.1 Theoretical Background of Some Ungrounded/ Grounded Comb-Shaped Structures

Cavity model analysis of microstrip patch antennas is widely acceptable even today. The radiation characteristics of a rectangular patch antenna has been reported in [6] and [13] using the aperture antenna concept. The fringing fields along both the

radiating and non-radiating edges increase the effective dimensions of the patch aperture area. In this section, the aperture theory of antenna has been utilized to explain the obtained radiation performance of the present antenna. Use of such aperture theory to explain planar antenna beam is completely new. Along with the physics of aperture theory, an insightful visualization of the fact as been brought out. In that regard, the simulated field distribution has been portrayed using High Frequency Structure Simulator v. 14 [14].

The simulated [14] field distribution over the entire aperture area of the microstrip patch (conventional and comb-shaped patch) is depicted in **Fig. 2.2**. In general, the beam width of the microstrip patch ($W/L=1.5$) is different in two principal planes. The E-plane beam is always broader than the H-plane beam. The widening of beam from an aperture radiator is mainly because of two reasons:

- (i) The aperture dimension in the corresponding plane.
- (ii) The type of field variation that exists in that plane.

In a conventional patch, one cosine variation of the electric field distribution is observed along the E-plane, whereas, no such variation is present along the H-plane. Moreover, the effective dimension of the patch in the E-plane (i.e., $L+2\Delta L$) is smaller than the effective dimension of the patch in the H-plane (i.e., $W+2\Delta W$). These may be attributed for a broader E-plane beam width compared to the H-plane. The lateral slots symmetrically cut in the E-plane makes the proposed structure essentially a comb-shaped microstrip patch antenna (**Fig. 2.1(a)**).

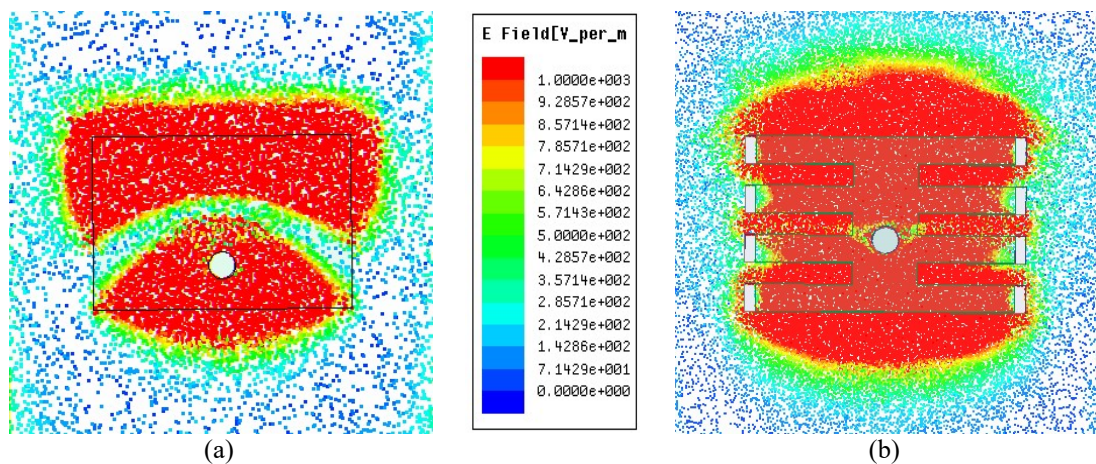


FIGURE 2.2 Simulated substrate field distributions for conventional and proposed microstrip patch (a) Conventional structure, (b) Proposed structure (scales are same in both figures).

With the introduction of the lateral slots on the patch surface, the top wall of the cavity boundary is perturbed. Therefore, the deviation of electric field comes into existence along the patch length and hence, it broadens the beam width in its E-plane.

Again, each tooth of the comb is grounded with metal strips to the ground plane at the non-radiating edges, and because of the shorting strips placed at the non-radiating edges; the electric fields are forced to disappear there to satisfy the vanishing electric field boundary condition. Hence, an electric field variation comes into existence along the width of the patch, which results in the broadening of the H-plane beam. The fringing along the non-radiating edges are minimized because of the shorting strips and, hence the fringing width ΔW decreases. This reduction in $W+2\Delta W$ also contributed for broadening the H-plane radiation beam. Therefore, in both E and H-planes, the radiation beam becomes broader compared to conventional microstrip antenna. However, as the fields are restricted within the physical width W of the patch because of the shorting strips, all the electric fields beneath the patch are clutched from the non-radiating sides of the patch. This, in turn, increases the fringing along the radiating edges and consequently the fringing length ΔL in the E-plane increases (**Fig. 2.2(b)**). Therefore, the E-plane dimension of the patch (i.e., the effective length of the patch $L+2\Delta L$) increases, which in turn, reduces the beam width in its E-plane. Therefore, the beam broadening is more prominent in the H-plane than in E-plane for the present structure. In the present investigation, the structure has been chosen judiciously to obtain symmetrical wide beam radiation in both the principal and diagonal planes. Here, the fields within the cavity beneath the patch have modified themselves in a particular manner to produce a wide and symmetrical radiation beam. Nevertheless, as the fringing fields near the radiating edges are not hampered because of modification of the patch structure, the CP radiation pattern remains unaltered.

The XP radiation from an optimally fed rectangular patch antenna mainly depends on the radiation from the non-radiating edges [8]. The higher order orthogonal resonating fields oscillating back and forth along the width of a patch leave significant amount of electric fields near the non-radiating edges which contribute in XP radiation from the patch. The asymmetry of the dominant mode

field distributions between the lower and upper half sections of a patch is also another cause of XP radiation from the microstrip patch [9]. In fact, this asymmetry in field distribution is basically because of the placement of the feeding probe and is unavoidable for a probe fed patch. This asymmetry in the field causes asymmetry in the electric field distributions between the lower and upper half sections of a patch. In the proposed structure, the fields near the non-radiating edges are minimal because of the placement of shorting strips as shown in **Fig 2.1(a)** and **(b)**. Therefore, the radiations from non-radiating edges caused by orthogonal resonances are minimized and, consequently, their contributions to the XP fields are minimized. Moreover, as the slots have been judiciously cut along the width of the patch, the cavity field beneath the patch gets reoriented and brings symmetry between the lower and upper half sections of a patch. These may be attributed for low XP radiation from the patch antenna.

2.2.2 ANALYSIS OF SOME UNGROUNDED AND GROUNDED COMB-SHAPED STRUCTURES

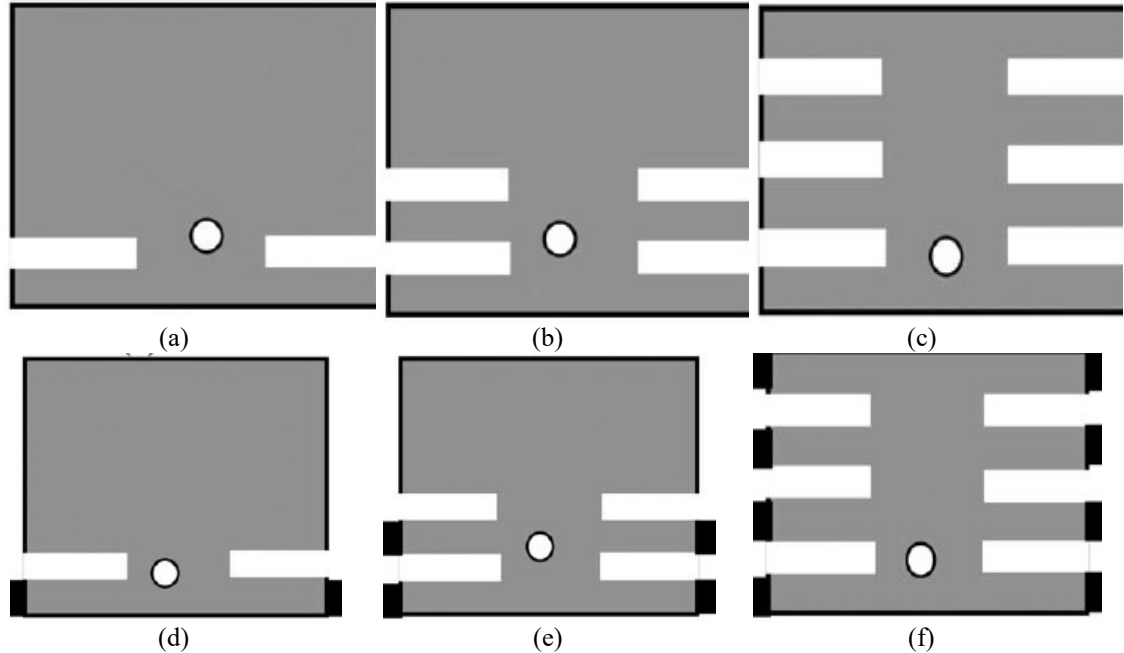


FIGURE 2.3. Top view of different comb-shaped patches. (a) single slot with ungrounded single tooth, (b) two slots with ungrounded two teeth, (c) three slots with ungrounded four teeth, (d) single slot with grounded single tooth, (e) two slots with grounded two teeth, (f) three slots with grounded four thin teeth.

In the initial effort, the investigations on the effect of lateral slots (in E-plane) over the patch surface are demonstrated with the six structures (**Fig. 2.3**). Before

going to radiation characteristics, the reflection coefficient profiles are analyzed as shown in **Fig. 2.4**.

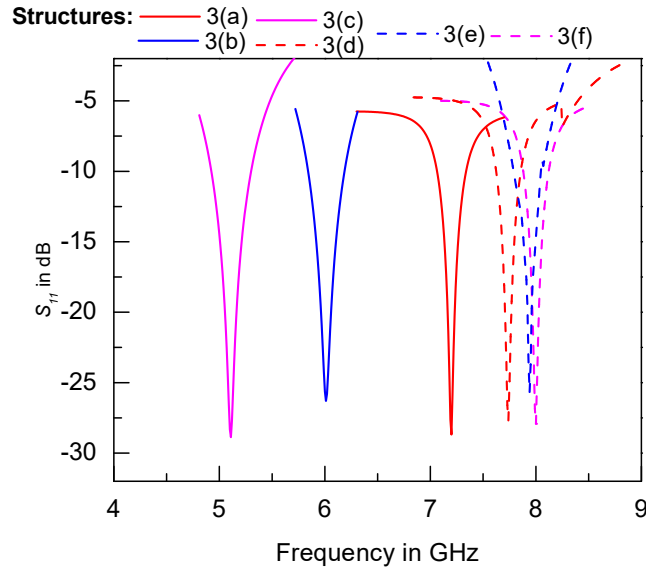


FIGURE 2.4. Simulated and measured reflection coefficient (S_{11}) profile of different comb-shaped patch antennas.

When a pair of lateral slots (near both the non-radiating edges; structure **Fig. 2.3(a)**), are cut the resonant frequency decreases from 8 GHz (for conventional patch with band width of 4.1%) to 7.2 GHz (4.6% band width). As the number of slots increases, this resonant frequency continuously decreases along with the slight enhancement in band width. It is found that the resonant frequency of structure **Fig. 2.3(b)** becomes 6.05 GHz with 5.1% band width, whereas, the same for structure **Fig. 2.3(c)** becomes 5.1 GHz with 6.8% fractional band width. In fact, the reason for such changes in resonant frequency can be obtained from one classic analysis [15].

When horizontal slots are added to a patch, the capacitance of the antenna is increased as the current distribution is dispersed by each horizontal slot. The current path is diverted through horizontal strips (teeth of the comb) and hence it is increased. Therefore, the impedance bandwidth is extended and the operating frequency is decreased [16].

With the introduction of the shorts as can be seen in **Fig. 2.3(d) and (e)** the current gets diverted through the horizontal strip and short-circuited to the ground plane. In this manner, when three slots are embedded on to the patch, the four horizontal strips (four teeth) develop and those teeth are shorted as in **Fig. 2.3(f)**.

Therefore, all the current dispersed through the horizontal strip/teeth gets shorted to ground plane. Therefore, a significant amount of dominant mode current flows through the central region of the patch instead of following a longer route (via each tooth/horizontal strip).

TABLE-2.1 Comparison of simulated 3 dB beam widths and CP-XP isolation for some ungrounded and grounded comb-shaped patch of Fig. 3

Structure Description	3 dB beam width in E-plane	3 dB beam width in H-plane	CP-XP isolation	Symmetry in radiation beam at E and H-planes
No slot/No short (conventional patch)	80 ⁰	67 ⁰	15 dB	50 ⁰
Configuration 3a	95 ⁰	69 ⁰	15.5 dB	52 ⁰
Configuration 3b	110 ⁰	70 ⁰	16 dB	51 ⁰
Configuration 3c	120 ⁰	72 ⁰	15 dB	53 ⁰
Configuration 3d	113 ⁰	95 ⁰	20 dB	90 ⁰
Configuration 3e	110 ⁰	102 ⁰	25 dB	100 ⁰
Configuration 3f	108 ⁰	110 ⁰	35 dB	125 ⁰
No slot/Full shorted non radiating edge [12]	70 ⁰	100 ⁰	34 dB	60 ⁰

In fact, the effective path length of the dominant mode current (structure **Fig. 2.3(f)**) is similar to conventional structure and is equal to the length of the patch. As a result, the resonant frequency of the said structure becomes similar to the conventional patch and it is around 8 GHz. The conventional microstrip patch without any slot and grounded strips produces broader beam in its E-plane (around 80⁰) compared to the H-plane (around 67⁰) (**Table 2.1**). The magnitude of the simulated [14] electric field distribution over the patch is shown in **Fig.2.5**. When a single lateral slot has been introduced on the patch surface (**Fig. 2.3(a)**), the variation in the electric field has come into existence along the patch length (**Fig. 2.5(b)**) and hence it significantly has broadened the beam width in its E-plane as discussed in section 4.2.1. This introduction of a single lateral slot over the patch surface has modified the field to a little extent along the H-plane. Hence, the beam width along the H-plane has increased by a small amount. **Table 2.1** and **Fig. 2.5** depict that, introduction of more number of lateral slots over the patch surface results in more perturbation along the E-plane of the patch and hence, cause more deviations of electric field along the length of the patch (i.e., along E-plane). The comparison of the variation of electric field magnitudes over the patch surface (along the length)

(Figs 2.5(a), (b), and (c)) undoubtedly illustrate the fact as discussed. **Table 2.1** shows that the 3 dB beam width of 120° and 72° is achieved in E and H-plane, respectively, with a patch with three lateral slots without shorting. Around 50% and 8% increment in the E-plane and H-plane 3 dB beamwidth, respectively are evident in comparison with the conventional patch. The introduction of a single lateral slot on the patch surface in its E-plane leaves a thin tooth that is shorted to the ground plane with a grounded metallic strip. In a similar manner, when more number of lateral slots are introduced, it creates more number of thin teeth that are shorted with grounded metallic strips.

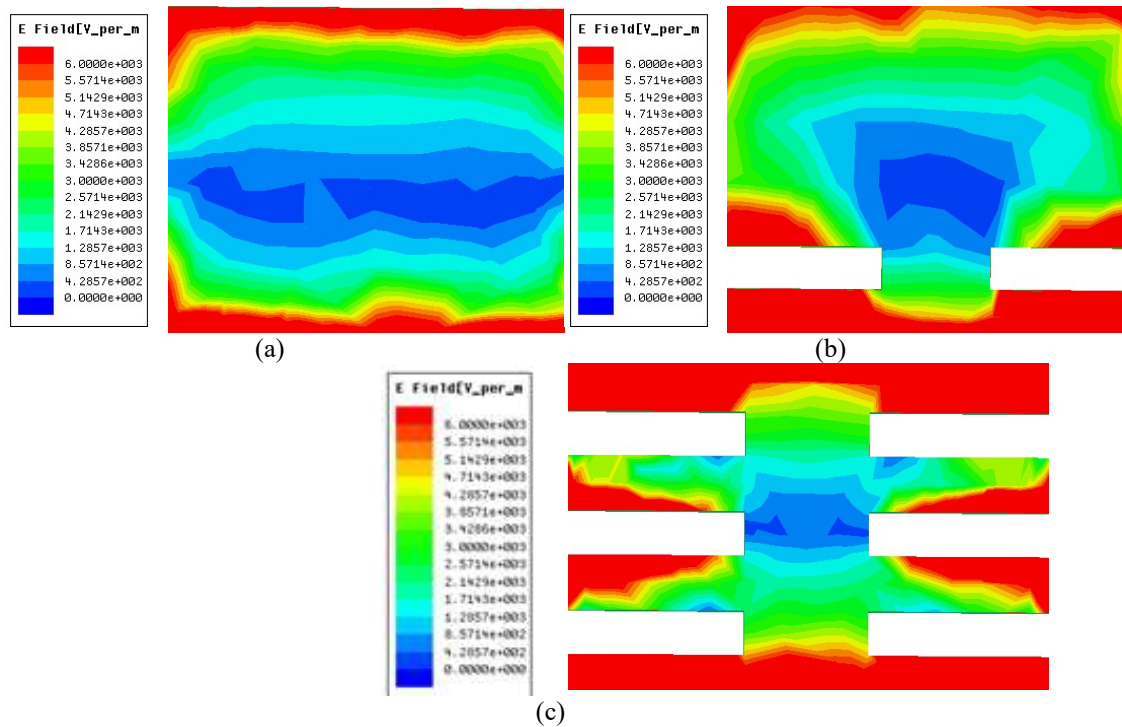


FIGURE 2.5. Variation of electric field magnitude over patch surfaces where the teeth of the comb is not grounded (a) conventional patch, (b) structure of fig 2.3a, (c) structure of fig 2.3c.

It is noted that, as the number of shorted teeth are increased, the E-plane beam width decreases gradually, whereas, the same in the H-plane increases significantly. Around 4.4% decrement in the E-plane beam width and 17% improvement in the H-plane beam width is revealed with four grounded teeth comb-shaped patch structure. In fact, as the numbers of slots are increased, it in turn increases the number of grounded teeth. Now, because of the shorts placed near non-radiating edges, the fields are trapped beneath the patch rather than being extended from non-radiating edges because of fringing. The comparison of **Figs. 2.6(a), (b),**

and Fig. 2.2(b) clearly depicts this observable fact. Therefore, the fringing width ΔW becomes zero, which in turn reduces the H-plane dimension of the patch (i.e., the effective width of the patch $W+2\Delta W$).

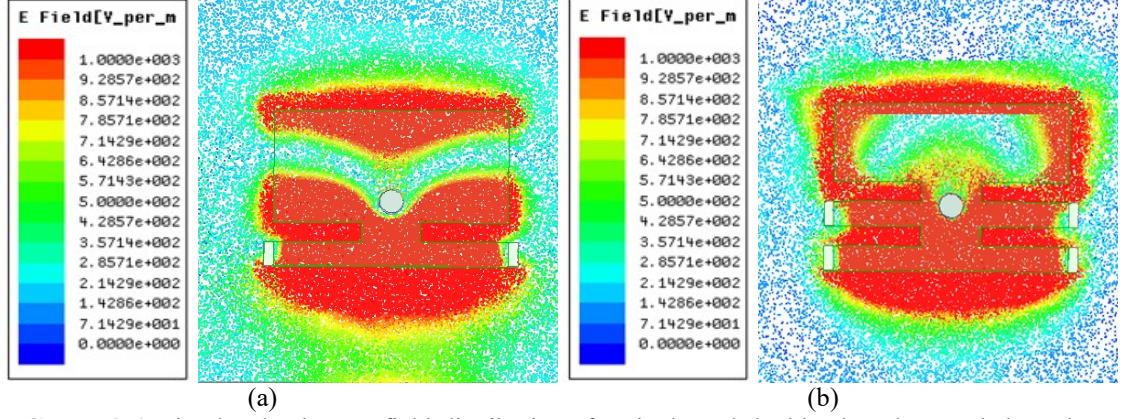


FIGURE 2.6. Simulated substrate field distributions for single and double slotted grounded comb-shaped microstrip patch (a) structure as in Fig 2.3(d), (b) structure as in Fig 2.3(e). (The distribution for proposed structure of Fig 2.3(f) is in Fig. 2.2(b)).

Moreover, the grounded strips minimize the fields near the non-radiating edges because of the disappearing electric field boundary condition. Therefore, certain field variations are exposed along the H-plane (Fig. 2.7), for single slot and three-slot grounded comb-shaped structures. These two factors result in broadening the H-plane beam width.

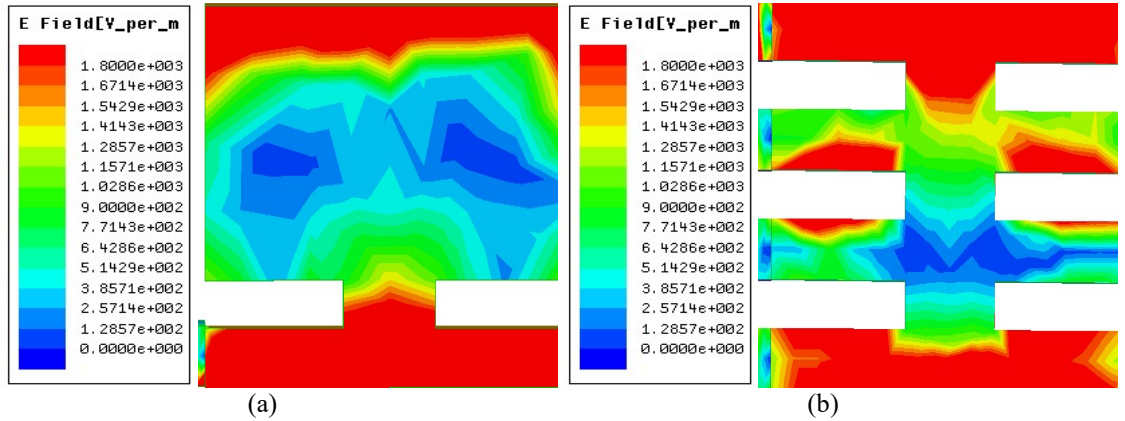


FIGURE 2.7. Variation of electric field magnitude over patch surfaces where the teeth of the comb is grounded with metallic strips (a) structure of figure 2.3d, (c) Structure of fig 2.3f (proposed structure).

On the contrary, when the fields are restricted within the physical width W of the patch because of the shorting strips, the entire electric fields beneath the patch is squeezed. This in turn increases the fringing at the radiating edges and consequently the fringing length ΔL in the E-plane increases as discussed in section 2.2.1.

Therefore, the E-plane dimension of the patch (i.e., $L+2\Delta L$) increases and beam width decreases. Around 108° and 112° of the E and H-planes, 3 dB beam widths are evident from the present three-slot four-tooth grounded comb-shaped patch structure (proposed structure). In the view of above discussions, if we compare the simple shorted patch (no slot but fully shorted non-radiating edges) with conventional microstrip patch (with no slot and no short), it shows a 13% decrement and in the E-plane beam widths. However, its H-plane beam is broader than the conventional patch.

The symmetry in 3dB beam width in the principal planes is depicted in **Table 2.1**. For conventional and ungrounded comb-shaped patch, the symmetry in radiation beam is similar and is around 50° . As soon as the teeth of the comb-shaped patch are grounded, symmetry increases gradually (**Table 2.1**). This symmetry of up to 125° in the radiation beam in the principal planes is achieved for the proposed structure as is apparent from the Table.

Also, **Table 2.1** corroborates that as the shorting strips are more at the non-radiating edges, the CP-XP performance improves because of the minimization of electric fields near the non-radiating edges caused by the shorting strips (as discussed in section 4.2.1).

2.2.3 Proposed Structure

A thin copper strip is utilized as patch (length $L=8.5$ mm and width $W=12.75$ mm) and it is fabricated on glass epoxy substrate with $\epsilon_r = 5.2$ and height $h = 1.58$ mm. Three pairs of slots are cut along the width of the patch symmetrically (**Fig. 2.8(a)**). The length of each tooth of the comb is $L_t = 4.5$ mm and the width is $G_s = 1.375$ mm. The gap between two thin teeth is $W_t = 1$ mm. The entire structure is fabricated on $30 \times 30 \text{ mm}^2$ ($2 \lambda_g \times 2 \lambda_g$) copper ground plane of thickness 0.5 mm. Each tooth of the comb-shaped patch is grounded by a metal strip of height equal to substrate height $h = 1.58$ mm. The proposed patch is fed at 1.2 mm from the center. The fabricated prototype is shown in **Fig. 2.8(b)**.

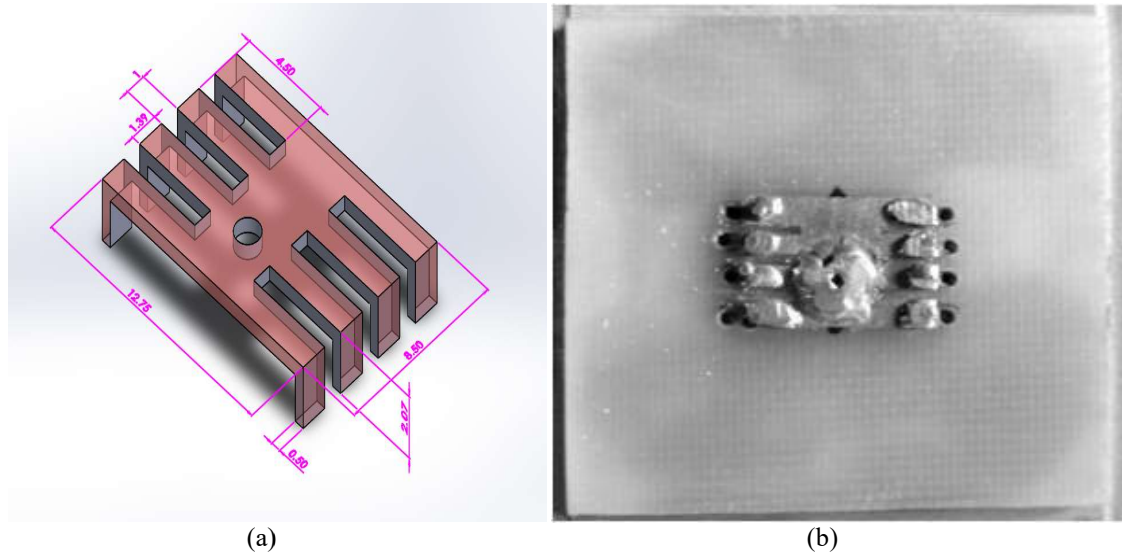


FIGURE 2.8. Schematic representation of proposed grounded comb-shaped microstrip antenna (a) Top view, (b) fabricated prototype; $L = 8.5$ mm, $W = 12.75$ mm.

2.2.4 Results

The simulated [14] and measured results obtained for the proposed grounded comb-shaped patch antenna (with length $L = 8.5$ mm and width $W = 12.75$ mm, $\epsilon_r = 5.2$ and height $h = 1.58$ mm as defined in Section-2.2.2) are presented in this section. The radiation pattern has been measured in an automated anechoic chamber using Agilent's E8363B network analyzer, Agilent's E4413A CW power sensor. A correct measure is taken to avoid improper soldering during experiment as it may degrade the S_{11} characteristics. Too poor soldering cannot feed the antenna efficiently and hence the optimum input and radiation performances cannot be achieved. A small air gap introduced because of improper soldering can cause an increase in the resonant frequency of the structure. The measured resonant frequency of the proposed structure (8.05 GHz) is shifted by 0.62% toward the higher side of the spectrum compared to simulation result (**Fig. 2.9**). This little up-shift of resonant frequency may be because of the fabrication error as discussed. The structure exhibits narrowband width of 4.5% as the structure has been fabricated on a substrate with higher ϵ_r . **Figs. 2.10(a)** and **(b)** depict the radiation pattern of the proposed antenna in the E and H-planes, respectively. Both the simulation and measured results show that the E-plane radiation beam is quite broad and the 3 dB beam width becomes around 108° . The XP level of the proposed structure is also below -35 dB in all the elevation angular ranges.

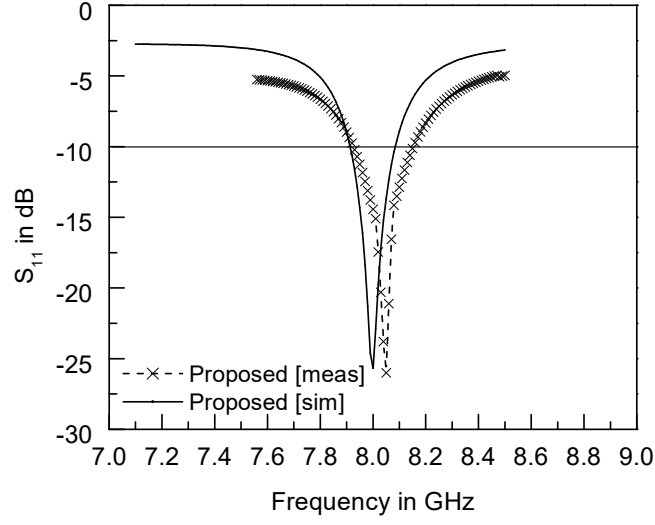


FIGURE 2.9. Simulated and measured reflection coefficient (S_{11}) profile of the proposed antenna.

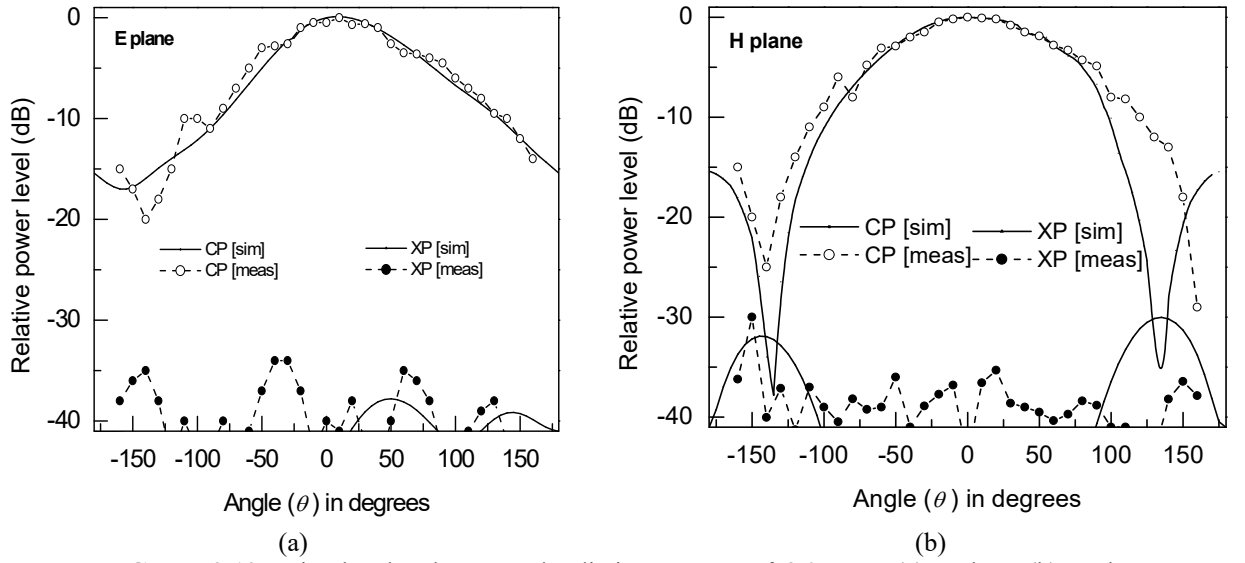


FIGURE 2.10. Simulated and measured radiation pattern at $f=8.05$ GHz (a) E-plane, (b) H-plane.

In the H-plane, the proposed structure exhibits around 110° of 3 dB beam width along with more than 35 dB CP-XP isolation in the entire angular range. The measured gain of the proposed antenna is 4.89 dBi. The measured gain of the conventional patch of same dimension and frequency is 5.6 dBi (**Fig. 2.11**). Therefore, a decrement in gain by 0.71 dB in the proposed structure is observed. The shorts at the non-radiating edges impose restrictions to the fringing fields at the non-radiating edges. This restricts the fields to be bound within the physical width of the

patch only and reduces effectively the width ' W ' of the patch. It in turn reduces the effective aperture of the patch.

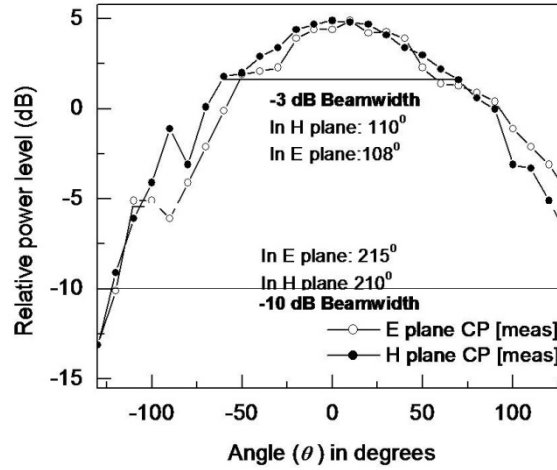


FIGURE 2.11. Beam width characteristics of proposed antenna near broadside region (-125° to $+125^{\circ}$) at $f=8.05$ GHz in the principal planes.

Therefore, this decrement in effective aperture may be attributed for the decrement in gain in the present structure by 0.71 dB. The measured gain of the conventional and proposed structure is around 0.9–0.98 dB below the simulated gain. This may be because of the losses in cables and connectors during measurement and presence of some ohmic loss in the structure. The simulated radiation efficiency of the proposed structure is around 95% and the rest may be considered as the ohmic loss. The measured CP radiation profiles in E and H-plane are presented in **Fig. 2.11**. In both the principal planes, broad beam widths (108° and 110° of 3 dB beam width and 215° and 210° of 10 dB beam width in E and H-planes, respectively) are found (**Fig. 2.11**). The measured radiation pattern in E and H-planes are remarkably symmetrical in the entire broadside region from -125° to $+125^{\circ}$. For further corroboration of the symmetrical radiation beam in other diagonal planes ($\varphi = 30^{\circ}$, 45° and 60°), the simulated CP pattern is presented in **Fig. 2.12**. Around 107° of simulated 3 dB beam widths in $\varphi = 30^{\circ}$, 45° and 60° diagonal planes are clear from the figure. Similar to the principal planes, the uniformity of CP radiation profiles in the other skew planes ($\varphi = 45^{\circ}$ and 60°) persist in the entire broadside region from -125° to $+125^{\circ}$. It further confirms the wide symmetry in 3D radiation beam from the present structure that can be surely beneficial as feed of reflector antennas. There are some ripples in the measured radiation pattern (**Figs.**

2.10 and 2.11). This is mainly because of the finiteness of the ground plane and substrate dimensions. The surface waves propagate through the substrate until they reach the truncated edge of the dielectric substrate or the edge of a finite (substrate-covered) ground plane where they are either diffracted or reflected. The diffracted signals then interact with the primary space wave radiation from the patch antenna and can cause ripples in the far field radiation pattern. This ripple effect in the radiation pattern becomes more for electrically thicker substrate. Nevertheless, in actual usage, a finite size ground plane can only be implemented.

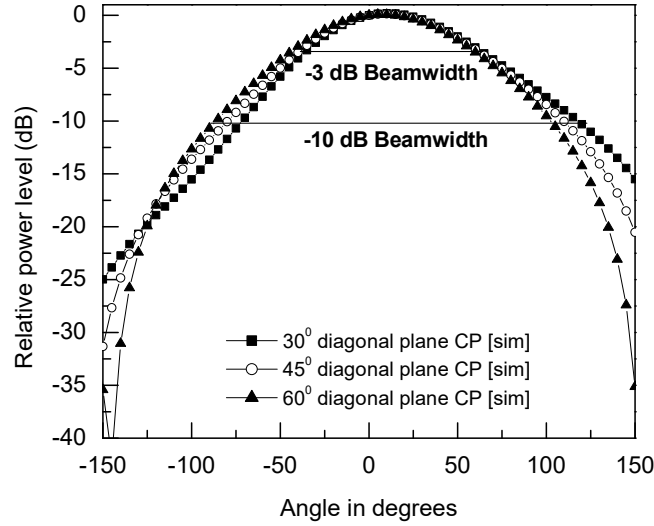


FIGURE 2.12. Simulated beam width characteristics of proposed antenna near broadside region (-150° to $+150^\circ$) at $f=8.05$ GHz in the diagonal planes.

In some applications, for instance, in hand held receivers, space is at a premium. Moreover, for the use of microstrip antenna as a reflector feed (which is the focus of the present study), the ground plane size should be limited. The goal is to reduce the antenna size and the ground plane extension beyond the patch dimensions to a minimum [1].

The CP-XP isolation of the present structure is around 35 dB, whereas the same for conventional patch is only 9 dB in other diagonal/skew planes ($\varphi = 30^\circ$, 45° and 60°) (Fig. 2.13). In the diagonal planes, XP radiation depends on the ratio of fringing fields at radiating to non-radiating edges (i.e., E_r/E_{nr}) [9]. The reduction of E_{nr} and increment of E_r causes reduction of XP in diagonal planes. There is a significant asymmetry in XP fields along the off-broadside direction in case of conventional patch (Fig. 2.13). The asymmetric distribution of fringing fields at non-

radiating edges (E_{nr}) between lower and upper half section of the patch (**Fig. 2.2(a)**) causes significant asymmetry in E_r/E_{nr} , which may be attributed to the asymmetric XP at off-broadside direction of conventional patch. This asymmetry is reduced in the proposed structure (**Fig. 2.2(b)**) and therefore, the XP fields are nearly symmetrical along the broadside direction (**Fig. 2.13**).

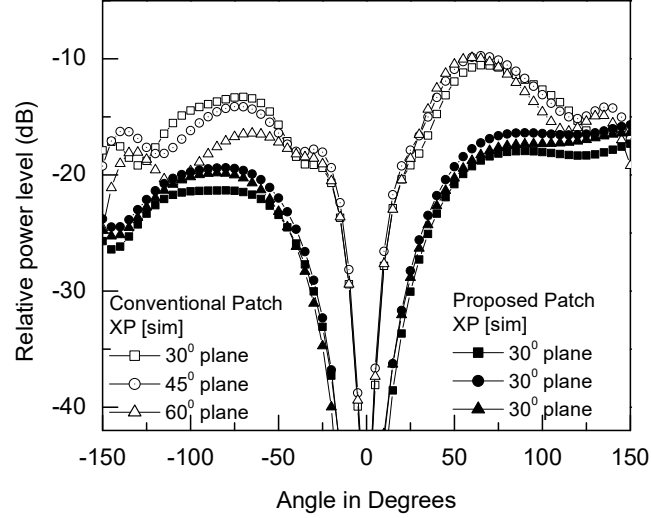


FIGURE 2.13. Simulated relative XP performance of proposed and conventional patch at diagonal skew ($\phi = 45^\circ$ and 60°) planes.

It is found that front-to-back radiation isolation increases with ground plane dimension ($D/\lambda_g = D/\lambda_g$) but has a tendency to saturate beyond $D/\lambda_g = 1.5$ to 3. The 3 dB beam width in the E-plane increases and that for H-plane decreases with D/λ_g when D/λ_g varies from 0.5 to 3. The beam widths in both E and H-planes become similar nearly when $D/\lambda_g = 2$. However, it is interesting to note that, for conventional patch antenna, the beam widths in both principal planes are similar when D/λ_g is small and the same happen to be different when D/λ_g becomes greater than 1.5. On the contrary, the proposed structure can produce wide symmetrical radiation in the entire range of D/λ_g and it varies within a limited range from 105° to 111° in both the principal planes (**Fig. 2.14**).

In [17] an antenna has been reported with a grounded E shaped patch for improved polarization purity (around 30-40 dB) in the both principal planes and wide 3 dB beam width of 94° in the H-plane only. The structure is purely intuitive and simulation based. Therefore, the investigation fails to exploit the structure for the improve radiation performance in terms of symmetry in radiation patterns and beam width enhancement in different diagonal planes.

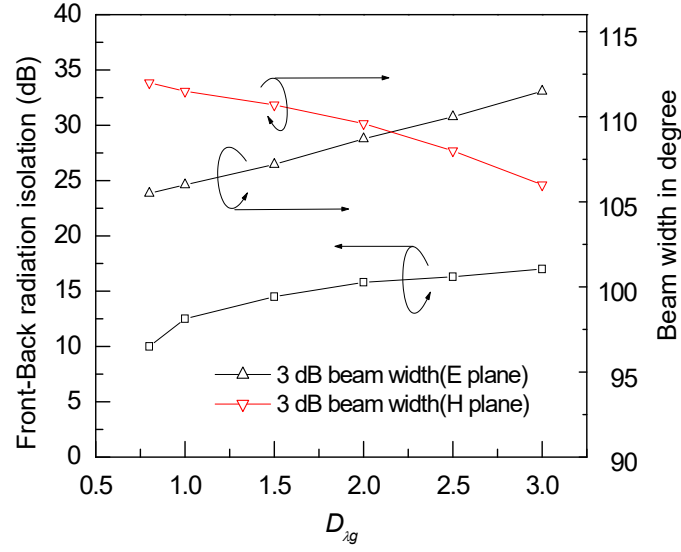


FIGURE 2.14. Measured variation of front-to-back radiation isolation and beam width of the proposed patch as a function of ground plane dimension in terms of wavelength.

Hence, we believe that the researchers should carry out more rigorous investigation with the similar structure. The issue of antenna cross-polarization isolation is very much crucial for the design of fully polarimetric synthetic aperture radars (P-SARs) [18]. Dual-polarized antennas with cross-polarization isolation that is better than -25 dB are desirable for more convenient polarimetric data calibration and in maritime surveillance applications [18]. The polarization purity is significantly required for dual-polarized hybrid antenna array operating in the 2.6-GHz band (2550-2650 MHz) for 5G communication multi-input multi-output (MIMO) operation [19]. Therefore, for further corroboration of the applicability of the present configuration in relatively lower frequency (S band-2.6 GHz), the simulated radiation pattern of a 30×45 mm patch with $D/\lambda_g=2.1$ have been examined and presented in **Fig. 2.15**. The simulated gain is around 5.3 dBi. Around 107° of 3 dB beam width in both the principal E and H-plane is evident from the fig. 14. The radiation beams in principal planes are really symmetrical in the entire broadside region from -100° to $+100^\circ$. It may be noted that the said antenna exhibits excellent polarization purity (CP-XP isolation around 50 dB) in the entire elevation angular range and hence gives birth to a 2.6 GHz “cross polarization free planar antenna” with 6.5% bandwidth.

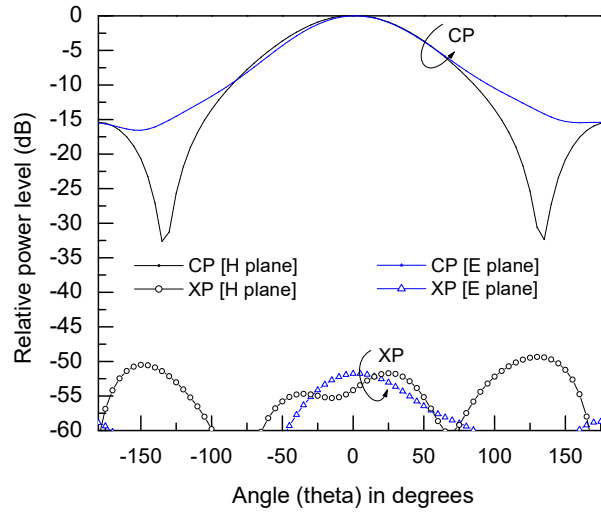


FIGURE 2.15. Simulated radiation pattern of the present structure in both principal E and H-planes at $f=2.6$ GHz

2.3 Defected Patch Structure (DPS) with Defects on Radiating Side

Parametric and physical insight has been given in succeeding sections for DPS integrated RMA with defecting at radiating sides of the patch which is a rare practice however the pros and cons have also been enumerated.

2.3.1 Background

Compared to DGS integrated antennas, which have its own established benefits, defected patch structure (DPS) is a newer technique to suppress XP radiation [20] and as is discussed in preceding sections. This technique reduces back radiation level from a RMA in comparison to DGS integrated antennas. Around 25-30 dB of CP-XP ratio is revealed from [20] while the same is 35dB in case of proposed structure. In these structures, the defects have been judiciously placed at the non-radiating edges of the patch so that, the electric field distributions of spurious higher order modes particularly that of TM_{02} can be nullified with same variation in the electric field distribution of dominant TM_{10} mode.

In this work, single layer, simple and compact RMA, with corrugation like defects at the radiating edge, is studied thoroughly to reduce XP radiation from the patch. Unlike the earlier works on DGS and DPS integrated RMAs, the defects have been judiciously placed at the radiating edge of the RMA (**Fig 2.1(d)**). Earlier, different research groups reported application of corrugated circular patch for

miniaturization and corrugated ground plane for improving CP-XP isolation at $\varphi=45^\circ$ plane.

On the contrary, from the present work and proposed structure (**Fig 2.1(d)**) around 40dB, 30 dB CP-XP isolation have been revealed at principal E and H plane, respectively, over whole elevation angle ($\pm 180^\circ$), whereas, for a RMA the same is around 8-10 dB in the H-plane. The structure resonates around $f=7.72$ GHz with 7% impedance bandwidth when defect length $L_t=4$ mm. However, it has also been observed that with a slight increase in the defect length ($L_t=5$ mm), the structure exhibits dual resonance at $f=6.61$ GHz and $f=7.72$ GHz. In the latter case, CP-XP isolation are around 11 dB, 30 dB in the principal H plane at $f=6.61$ GHz and $f=7.72$ GHz, respectively. The antenna has been designed on FR-4 substrate ($\epsilon_r=4.4$) of dimensions 25×25 mm². The peak CP gain from the proposed structure is around 5 dBi.

2.3.2 Proposed Structures

A thin copper strip of length (L) = 8 mm and width (W) = 12 mm, is utilized as patch and it is fabricated on FR-4 substrate with height (h) = 1.575 mm and $\epsilon_r=4.4$ of dimensions 25×25 mm² (**Fig. 2.1(d)**). Two antenna structures are studied and analyzed in the following sections.

- (a) In antenna 1, four defects of dimensions $(L_t \times W_t) = 4 \times 1$ mm² have been cut on the patch surface at the radiating edge.
- (b) In antenna 2, the length of each defect has been increased to $L_t=5$ mm but, the width of the slot W_t is kept unaltered.

The ground plane dimensions are $(L_G \times W_G) = 25 \times 25$ mm². The antenna 1 and antenna 2 are fed at $p_c=1.4$ and 1.6 mm from the center of the patch, respectively, through a co-axial probe.

2.3.3 Results and Physical Insight

In this section, the simulated [14] results of a conventional RMA and RMAs with corrugated edge with slot dimensions $(L_t \times W_t) = 4 \times 1$ mm² and 5×1 mm² have been presented.

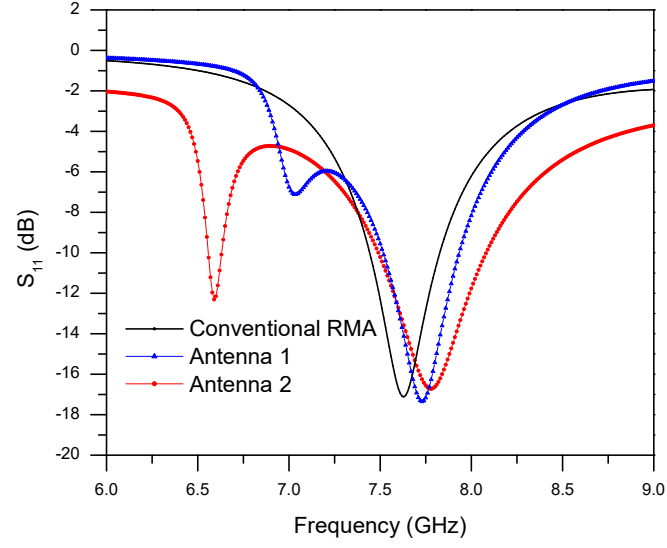


FIGURE 2.16 Reflection coefficient profile (S_{11}) for conventional RMA, antenna 1 and antenna 2.

Conventional RMA:

Fig. 2.16 and **Fig. 2.17** shows the simulated reflection coefficient (S_{11}) and radiation patterns for a conventional RMA. The conventional RMA resonates at $f = 7.61$ GHz with 4% impedance bandwidth (**Fig. 2.16**). It can be noted that for the conventional patch, peak CP-XP isolation is nearly 12 dB at around $\pm 50^\circ$ in H-plane whereas, in E plane, CP-XP isolation is around 40 dB (**Fig. 2.17**).

Antenna 1: RMA with corrugated radiating edge with slot dimensions ($L_t \times W_t$) = $4 \times 1 \text{ mm}^2$

The antenna 1 resonates at $f = 7.72$ GHz with 4.2% impedance bandwidth (**Fig. 2.16**). It can be noted that for antenna 1, peak CP-XP isolation is nearly 30 dB at around $\pm 50^\circ$ in H-plane whereas, in E plane, CP-XP isolation is around 50 dB (**Fig. 2.17**). It is evident that, 30-40 dB of XP suppression is achieved over whole elevation angle ($+180^\circ$ to -180°) than that of a conventional RMA (**Fig. 2.17**).

Antenna 2: RMA with corrugated radiating edge with slot dimensions ($L_t \times W_t$) = $5 \times 1 \text{ mm}^2$

The antenna 2 exhibits dual resonances at $f = 6.61$ GHz and $f = 7.72$ GHz with 6% impedance bandwidth (**Fig. 2.16**). It can be noted that for antenna 2, at $f = 6.61$ GHz, peak CP-XP isolation is nearly 12 dB at around $\pm 50^\circ$ in H-plane whereas, in E plane, CP-XP isolation is around 55 dB (**Fig. 2.18**). At $f = 7.72$ GHz, peak CP-

XP isolation is nearly 30 dB at around $\pm 50^\circ$ in H-plane whereas, in E plane, CP-XP isolation is around 55 dB (**Fig. 2.18**). At, $f = 7.72$ GHz, 30-40 dB of XP suppression is achieved over whole elevation angle ($+180^\circ$ to -180°) than that of a conventional RMA. It is also observed that the CP radiation patterns are nearly same at $f = 6.61$ GHz and $f = 7.72$ GHz which indicate excitation of dominant modes at both the frequencies.

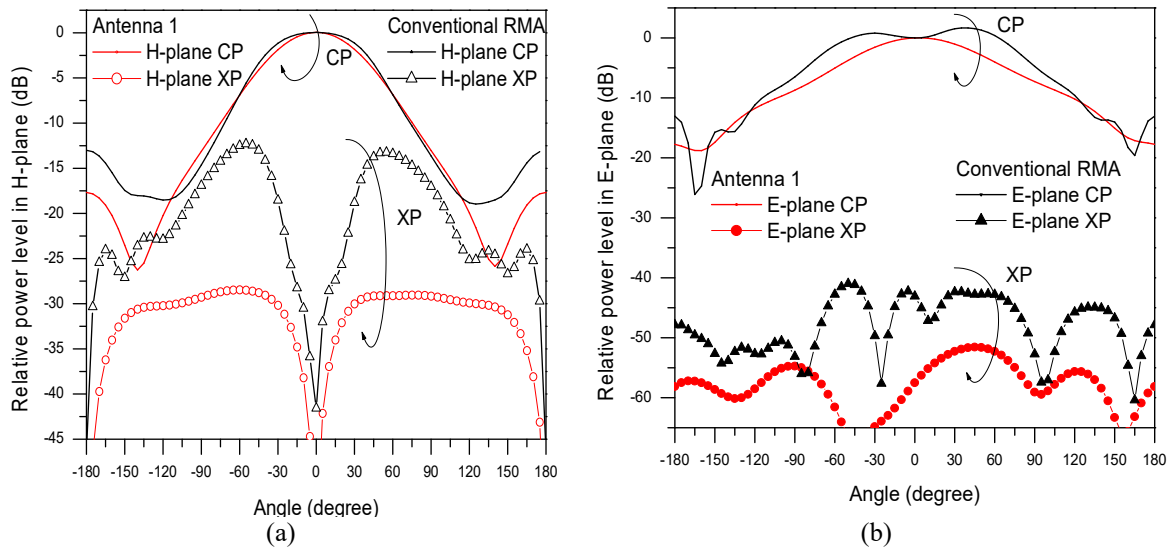


FIGURE 2.17 Radiation patterns of conventional RMA and antenna 1 at the centre frequency at: (a) H-plane, (b) E-plane.

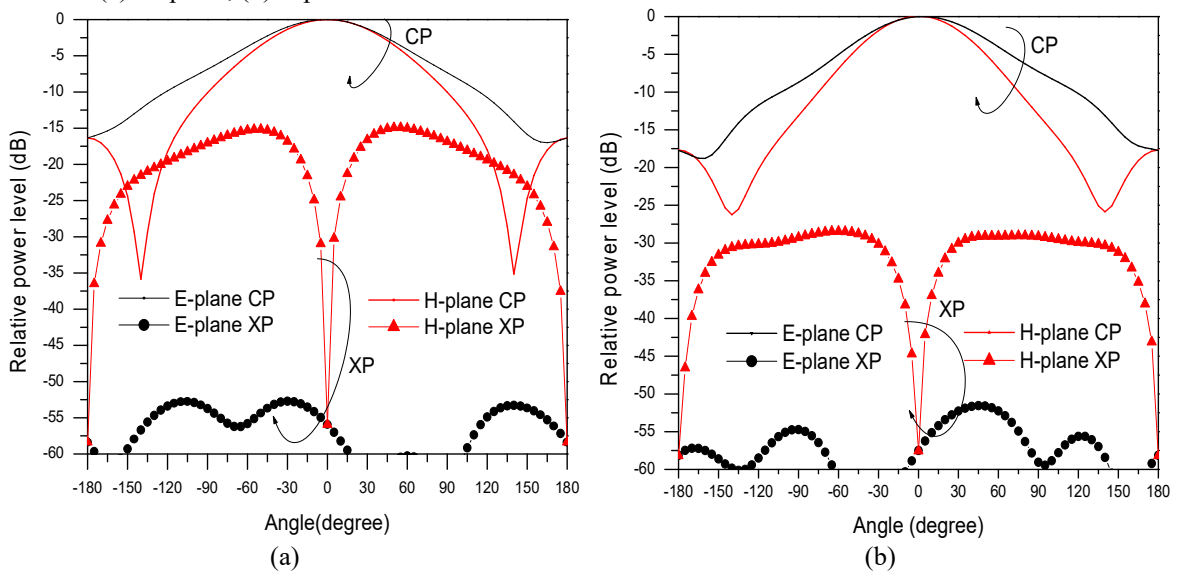


FIGURE 2.18 Radiation patterns of antenna 2 at: (a) $f = 6.61$ GHz and (b) $f = 7.72$ GHz.

2.4 Comparison between Both Types of DPS RMA

Table 2.2 tabulates various radiation parameters for performance analysis for both types of DPS integrated antennas.

TABLE 2.2 Tabulation of radiation parameters for performance analysis for both types of DPS integrated antennas.

Type of DPS	Name	Antenna Structure	L (mm)	W (mm)	Feed position (offset from centre) (mm)	Symmetry in radiation beam at E and H-planes	Resonating Freq (GHz)	Gain (dBi)	Impedance BW (%)	Polarization purity (dB)
No Defecting	CRMA	Conventional RMA	8.5	12.75	1.2	5°	8	5.6	4.1	15
DPS at non-radiating Side	Grounded Comb-Shaped Patch Antenna	length of tooth 4.5 mm and width is 1.375 mm, gap between teeth is 1 mm. Ground 30x30mm	8.5	12.75	1.2	125°	8.05	4.89	4.5	35 (measured)
No Defecting	CRMA	Conventional RMA	8	12	1.2	5°	7.61	5.6	4	12
DPS at radiating Side ##	Antenna 1	Lt = 4 mm. Gap of 1mm and Ground 25x25mm	8	12	1.4		7.72	5	4.2	30-40 (simulated)
	Antenna 2	Lt = 5 mm. Gap of 1mm and Ground 25x25mm	8	12	1.6		6.61 & 7.72	5	6	30dB-H plane 55dB-E Plane (simulated)

aiming to find wide symmetrical radiation beam with defects in radiating edge fails to address the same.

2.5 Conclusion

The chapter deals mainly with the Microstrip patch antenna with defected patch surface. The chapter has been mainly divided in two parts wherein detailed investigations have been shown in antennas having DPS at radiating and non-radiating side. The independent conclusions are as enumerated below and the final or holistic conclusion has been drawn based on the section 2.4 above and the benefits as described in preceding sections:-

- DPS integrated RMA (with defects on non-radiating side): A simple and compact grounded comb-shaped microstrip patch antenna has been proposed for significantly improved radiation performance. The experimental investigation has been carried out for two different frequencies in X and S

bands. In both the cases, the present structure show consistently improved radiation performances such as wide symmetrical radiation beam with very low XP radiation. In fact, these characteristics are very much positive for modern 5G communication, fully polarimetric synthetic aperture RADARs and some other applications in modern wireless communication links. Around 105^0 - 110^0 of 3 dB beam width is evident with more than 35 dB CP-XP isolation from the structure while the same for a conventional patch is only 15 dB. Around 15 dB of front-to-back radiation isolation is found from the proposed patch. Most importantly, the proposed antenna produces 65% and 35% broader beam in H and E-planes respectively than that of a classical microstrip antenna. The structure is surely helpful for the scientists, researchers and practicing engineers looking for such simple low profile single element antenna with symmetrical beam and low XP radiation pattern mainly for polarimetric radars or as feed to reflector antennas like parabolic reflector antennas.

(b) DPS integrated RMA (with defects on radiating side): Single layer, simple and compact RMA, with corrugation like defects at the radiating edge, is recommended herewith to achieve improved polarization purity over whole elevation angle. Linear defects have been placed at the radiating edges of the patch to reduce cross polarization radiation. Around 30-40 dB of CP-XP isolation is observed in H plane with 7% impedance bandwidth in case of antenna 1 and in E plane also, more than 55 dB CP-XP isolation is found. Also, in case of antenna 2, dual resonances have been found due to an increase in defect length. The proposed structure is simple and easy to fabricate. It will surely find applications in array antenna design and establishing wireless links where, improved polarization purity is required. However, placing defects on radiating edges are not reliable as it may hamper radiating edge fields of TM_{10} mode specifically for smaller patches. The selection of above mentioned DPSs for particular applications to be based mainly on the level of requirement of polarization purity and the scope of implementation of array. The employment of array is must since the individual gain is limited here as observed but the polarization purity is

extremely high which makes it one of the most suitable candidates for array and for polarimetric radars or as feed to reflector antennas like parabolic reflector antennas. The bandwidths are limited too however the design and fabrication is extremely easy and would be fast and simple for automated factory level production chain. If a scope of slight investment of time and soldering efforts is available then DPS integrated RMA (with grounded defects on non-radiating side) should be preferred, else the easiest and fastest concept proposed herewith is DPS integrated RMA (with defects on radiating side) for second best results.

With the above discussed facets in mind of a limited short coming of marginal gain and restriction of bandwidth. Some other techniques must be explored to enhance the gain and bandwidth of RMA.

References

- [1] R. Garg, P. Bhartia, I. Bahl and A. Ittipiboon, *Microstrip Antenna Design Handbook*, Norwood, MA, USA:Artech House, 2001.
- [2] Y.-Y. Bai, S. Xiao, M.-C. Tang, Z.-F. Ding and B.-Z. Wang, "Wide-angle scanning phased array with pattern reconfigurable elements", *IEEE Trans. Antennas Propag.*, vol. 59, no. 11, pp. 4071-4076, 2011.
- [3] A.G. Toshev, "Multipanel concept for wide-angle scanning of phased array antennas", *IEEE Trans. Antennas Propag.*, vol. 56, pp. 3330–3333, 2008
- [4] C. Wu, L. Han, F. Yang, L. Wang and P. Yang, "Broad beamwidth circular polarisation antenna: Microstrip-monopole antenna", *Electron. Lett.*, vol. 48, no. 19, pp. 1176-1178, 2012.
- [5] C.W. Su, S.K. Huang, and C.H. Lee, "CP microstrip antenna with wide beam width for GPS band application", *Electron. Lett.*, vol. 43, pp. 1062–1063, 2007
- [6] S. Chattopadhyay, J.Y. Siddiqui and D. Guha, "Rectangular microstrip patch on a composite dielectric substrate for high gain wide-beam radiation patterns", *IEEE Trans Antennas Propag*, vol. 57, pp. 3324–3327, 2009
- [7] A. Petosa, A. Ittipiboon, and N. Gagnon, "Suppression of unwanted probe radiation in wide band probe probe-fed microstrip patches", *Electron. Lett.*, vol. 35, pp. 355–357, 1999.
- [8] A. Ghosh, D. Ghosh, S. Chattopadhyay, L. L. K. Singh, "Rectangular microstrip antenna on slot type defected ground for reduced cross polarized radiation", *IEEE Antennas Wireless Propag Lett*, vol. 14, pp. 321–324, 2015.
- [9] S. Chakraborty and S. Chattopadhyay, "Substrate Fields Modulation with Defected Ground Structure: A Key to Realize High Gain, Wideband Microstrip Antenna with Improved Polarization Purity in Principal and Diagonal Planes", *Int. Journal of RF, Microwave and Computer Aided Engineering (Wiley)*, vol. 26, pp. 174-181, 2016.
- [10] M. L. Oberhart, R. Q. H. Lee, "New Simple feed network for an array module of four microstrip elements", *Electron. Lett.*, vol. 23, 1987.

- [11] D. R. Jackson, N. G. Alexopoulos, "Simple approximate formulas for input resistance, bandwidth, and efficiency of a resonant rectangular patch", *IEEE Trans. Antennas Propag*, vol. 39, pp. 407-410, 1991.
- [12] D. Ghosh, S.K. Ghosh and S. Chattopadhyay, "Physical and quantitative analysis of compact rectangular microstrip antenna with shorted non-radiating edges for reduced cross-polarized radiation using modified cavity model", *IEEE Antennas Propag. Mag.*, vol. 56, pp. 61-72, 2014.
- [13] D. Guha, S. Chattopadhyay and J. Y. Siddiqui, "Estimation of gain enhancement replacing PTFE by air substrate in a microstrip patch antenna", *IEEE Antennas Propag Mag.*, vol. 52, pp. 92–95, 2010.
- [14] HFSS, "High Frequency Structure Simulator, Version 14," Ansoft Corp.
- [15] J. Jung, H. Lee, Y. Lim, "Broadband flexible comb-shaped monopole antenna", *IET Micro., Antennas Propagation*. Vol. 3, pp. 325-332, 2009.
- [16] D. M. Pozar, "Considerations for Millimeter Wave Printed Antennas," *IEEE Trans. Antennas Propagat.* Vol. 31, 1983.
- [17] S. Chakraborty, R. Poddar, S. Chattopadhyay, R. Guha, "Wide beam microstrip patches with grounded E-shaped edges to improve the polarization purity", *Proceedings' in Frontiers in Computer, Communication and Electrical Engineering*, Mankundu, India, 2016.
- [18] A. R. Touzi, P. W. Vachon, J. Wolfe, "Requirement on Antenna Cross-Polarization Isolation for the Operational Use of C-Band SAR Constellations in Maritime Surveillance", *IEEE Geoscience and Remote Sensing Letters*, vol. 7, pp. 861-865, 2010.
- [19] M. Y. Li, Y. L. Ban, Z. Q. Xu, G. Wu, C. Y. D. Sim, K. Kai, Z. F. Yu, "Eight-Port Orthogonally Dual-Polarized Antenna Array for 5G Smartphone Applications", *IEEE Transactions on Antennas and Propagation*, vol. 64, pp. 3820-3830, 2016.
- [20] A. Ghosh, S. K. Ghosh, D. Ghosh and S. Chattopadhyay. "Improved Polarization Purity for circular microstrip antenna with defected patch surface," *Int. J. of Microwave and Wireless Technologies*, Vol.8, No.1, pp.89-94, 2016.

**Defected Ground Structure Approach
for Gain and Bandwidth Improvement****3.1 Introduction**

Rectangular microstrip antenna (RMA) is the most useful antenna structure for its wide variety of applications, due to its simple design, ease of implementation, low profile, thin and conformal properties. Apart from these desirable properties, a simple RMA suffers from some severe disadvantages like low gain (around 5-7 dBi) and narrow impedance bandwidth (around 5%). RMA radiates linearly polarized wave along its broadside called, co-polarized (CP) radiation with poor CP gain which is not suitable for some specific applications where a little higher gain is required. Notably a few degree of cross-polarized (XP) radiation is also accompanied with CP radiation. Therefore, enhancement of CP gain without affecting the XP performance of RMA is a crucial assignment for research community. Further, the improved gain along with wider bandwidth specifically ultra wide bandwidth (UWB) is always preferred for using such antenna as an efficient radiator, particularly for satellite communications. There has been considerable research effort put into UWB radio technology worldwide. However, the non digital component of UWB system i.e transmitting/ receiving antennas remains a particularly challenging topic.

Larger CP gain is always a positive requirement for a RMA and that using an air and air dielectric composite substrate has been achieved earlier [1]-[3]. Although, around 8.5 dB of peak CP gain is achieved, they fail to keep satisfactory level of XP

and bandwidth performances of RMA. Polarization purity (CP-XP radiation isolation) in those cases are around 7-8 dB in X band RMA and nevertheless, it will worsen at the higher frequency as the XP radiation increases with frequency [4], [5]. Also, the bandwidth in those cases was only 5-7%. Defected ground structure (DGS) is a well established technique for RMA to improve its polarization purity [6]-[10]. It is observed that, the polarization purity of 20-25 dB can be achieved from slot DGS [7], [8] and circular headed dumbbell DGS [6], non proximal [10] and asymmetric [9] DGS integrated RMA. However, in all these reports except [6] neither the gain nor the bandwidth of RMA is improved. Around 6-7 dBi peak gain with maximum 11% bandwidth is revealed from those. On the contrary, the structure [6] offers the best result where, 9 dBi peak CP gain along with 22% bandwidth and a polarization purity of around 19-20 dB is achieved.

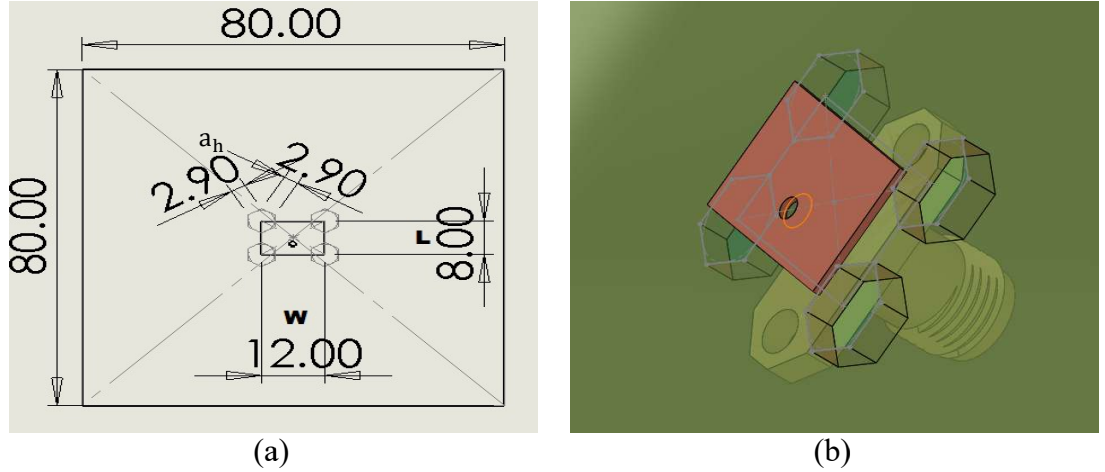


FIGURE 3.1. Proposed HDGS integrated RMA (a) Schematic diagram (b) 3D image

In order to overcome the above mentioned shortcomings of RMA, in this Chapter, a hexagonal DGS (HDGS) integrated RMA (**Fig. 3.1**) has been thoroughly studied for high gain UWB operation at X, Ku and Ka band. Efforts have been given to achieve stable radiation pattern with high stable gain in the entire operating band. Unlike other structures, in the present structure the defect has been shaped in such a way that it modulates the field structure beneath the patch which in turn, improves both the gain and the bandwidth simultaneously without hampering its XP performance. Around 9 dBi stable peak CP gain, ultra wide bandwidth (UWB) of 58% with stable radiation pattern is revealed from present single layer RMA.

Therefore, the present work happens to be the first work where, DGS technology has been adopted to achieve high gain with UWB performance from single element RMA. In section 3.2, parametric study of the proposed Hexagonal DGS integrated RMA has been done followed with the structural details, experiments and results. In section 3.3, performance evaluation of various DGS integrated RMAs with defects in increasing order of polygons has been done. Also, the parameters have been compared and tabulated for better analysis and to selection by research and industry community. Section 3.2 concludes the chapter to curl out advantages and limitations.

3.2 Hexagonal DGS (HDGS) integrated RMA

Parametric and physical insight based on results by simulation and measurements has been given in succeeding sections for HDGS integrated RMA.

3.2.1 Parametric Studies

The rectangular microstrip antenna (RMA) is an open resonator where top and bottom walls are electric walls (PEC) and the four side walls are considered magnetic walls (PMC). Now, if the defect is placed on the ground plane, it perturbs the cavity boundary conditions and hence modulates the field beneath the patch. Therefore, the near field distribution becomes altered, which in turn, influence the input and radiation property of the RMA. The modulation of the cavity fields depends critically on the geometrical shape of the defect. Therefore, the judicious choice of the defect geometry is critical to obtain the optimum performance of the antenna. With this in view, four hexagonal defects have been incorporated at the ground plane in such a way that, the centre of the hexagon becomes coincident with the patch corners as shown in **Fig. 3.1**

Initially a RMA with length $L = 7.1$ mm and width $W = 10.8$ mm has been fabricated on RT Duroid/ 5870 substrate with thickness of $h = 1.575$ mm and with dielectric substrate of permittivity $\epsilon_r = 2.33$. In the next, a hexagon defect of side length 1 mm ($a_h = 1$ mm) is incorporated at four corners of the patch. The reflection coefficient profile and the impedance band width (**Fig. 3.2 and 3.3**) of such HDGS integrated RMA with $a_h = 1$ mm shows sudden improvement in impedance band width compared to the conventional RMA. The input impedance band width of conventional patch with no DGS ($a_h = 0$) shows around 5.35% impedance band

width while the same for HDGS integrated RMA with $a_h = 1\text{mm}$ is around 11% at its lowest order dominant TM_{10} mode. It is also interesting to note that, as soon there is introduction of defect at the ground plane, the resonant frequency of lowest order dominant mode shifts around 2% in the higher side of the spectrum (Fig. 3.2).

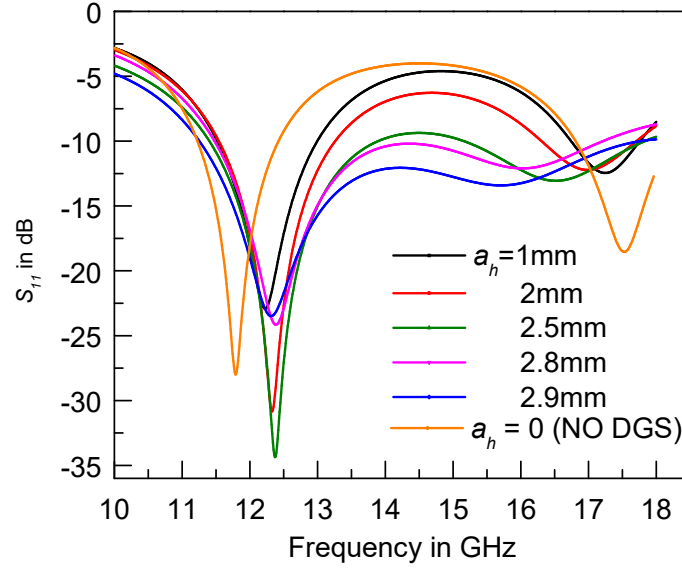


FIGURE 3.2 Reflection coefficient profile for conventional RMA and HDGS integrated RMA of different side length a_h in mm.

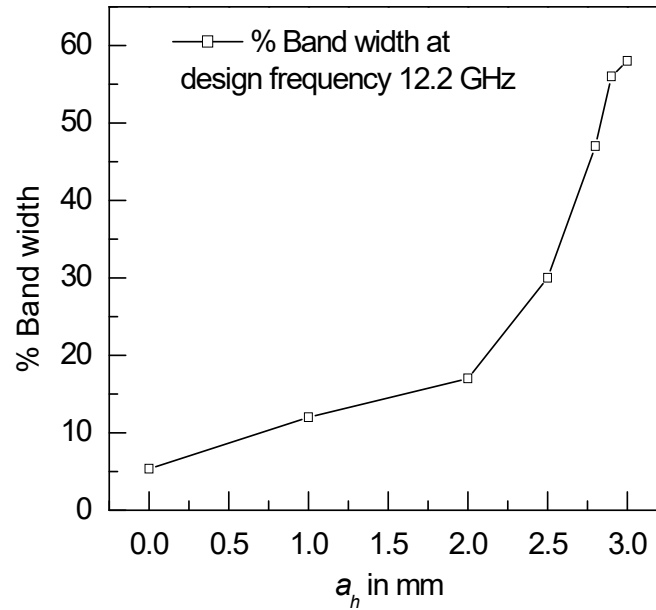


FIGURE 3.3. Fractional impedance band width of conventional and HDGS integrated RMA of different side length a_h in mm

This may be due to slight decrement of effective permittivity of substrate due to hexagonal defect for present RMA as is indicated in [8]. Now, as the value of a_h increases, fractional bandwidth increases monotonically up to $a_h = 2.8$ mm. In fact, the defect beneath the patch increases loss and lowers the cavity Q factor and that can be obtained from cavity model as indicated in [6]. Therefore, as the defect dimension increases, it increases the bandwidth of proposed RMA. Indeed, the fringing fields near radiating edges follow the defect periphery because the fields always try to be terminated at the sharp edges of the defect. As a result, the fringing fields increase in such structures instead of being confined under the patch. Consequently, stored energy under the patch i.e microstrip cavity resonator decreases. Moreover, the radiation leaked through the defect into the back side increases the radiation loss and hence lowers the Q factor due to radiation loss. Therefore, the decrease in stored energy and increase of radiation loss may be attributed for lowering the total Q factor of the microstrip resonator which in turn increases the bandwidth of HDGS integrated RMA. The fractional band width of HDGS integrated RMA with $a_h = 2.5$ mm becomes around 30%. Now, further increment of the value of a_h shows more improvement in fractional band width of HDGS integrated RMA. Around 58% impedance bandwidth is evident from proposed HDGS integrated RMA with $a_h = 2.9$ mm at its design frequency ($f = 12.2$ GHz).

It may be noted from **Fig. 3.2** that, the 2nd higher order orthogonal TM_{02} mode for conventional RMA lies at 17.6 GHz. The simulated current distribution and magnitude of electric field distribution on the patch surface at $f = 17.6$ GHz is shown in **Fig. 3.4(a)** and **3.4(c)**. This confirms that, the above said frequency is corresponding to TM_{02} mode for the conventional RMA. Now, as the value of a_h increases, the reflection coefficient profile become more and more flat and the 2nd dip of the S_{11} profile of HDGS integrated RMA gradually comes closure towards the 1st dip of S_{11} profile (primary TM_{10} mode frequency at which the antenna is designed). Therefore, it may be apparent that, the 2nd higher order orthogonal mode merges with the primary mode resulting in broader bandwidth of the proposed structure. However, the simulated current distribution and magnitude of electric field distribution on the patch surface at $f = 16$ GHz (2nd dip of S_{11} profile of HDGS

integrated RMA with $a_h = 2.9$ mm), depicted in **Figs. 3.4(b)** and **3.4(d)**, confirms that the conjecture is not true. It is evident from **Figs. 3.4(b)** and **3.4(d)** that, both the distributions of electric surface current and electric field magnitude on the patch surface of HDGS integrated RMA with $a_h = 2.9$ mm at $f = 16$ GHz is exactly similar to that of the dominant mode. Hence, it corroborates that, there is no such influence of TM_{02} mode at the higher frequency region in the operating band of proposed HDGS integrated RMA with $a_h = 2.9$ mm.

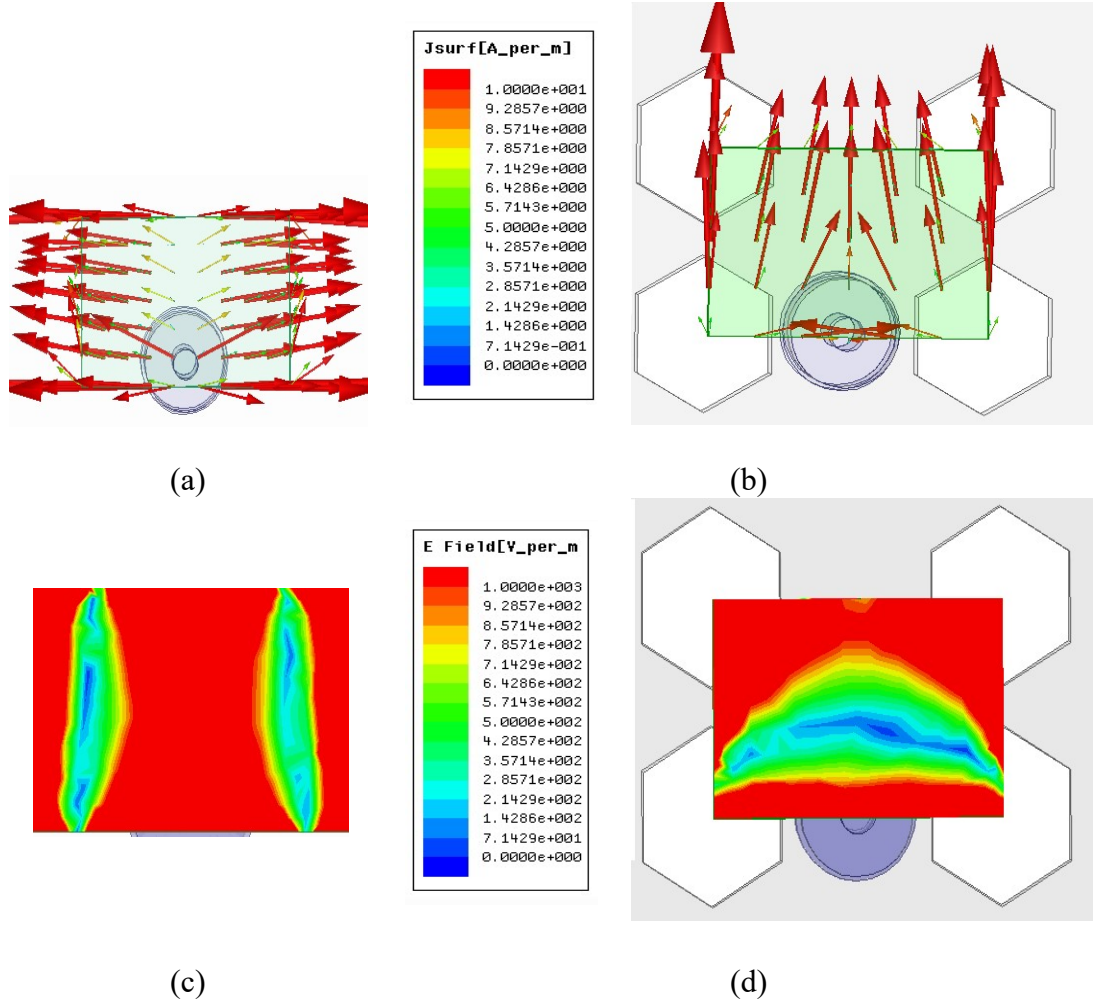


FIGURE 3.4. Simulated distribution of electric current and electric field magnitude on patch surface (a) electric surface current on conventional patch at $f = 17.6$ GHz, (b) electric surface current on present structure with $a_h = 2.9$ mm at $f = 16$ GHz (c) electric field magnitude on conventional patch at $f = 17.6$ GHz, (d) electric field magnitude on present structure with $a_h = 2.9$ mm at $f = 16$ GHz

Therefore, the hexagonal defects efficiently perturb the TM_{02} mode and enhance the bandwidth of the primary dominant TM_{10} mode. In fact, the reflection coefficient profile of the antenna structure is mainly governed by E/H ratio (electric field to magnetic field intensity ratio) near the feed location. In the present configuration,

because of the hexagonal geometry of the defect, the E and H fields beneath the patch are modulated in such a way that it offers a very good matching over wide range of frequencies at its primary dominant TM_{10} mode. Therefore, it may be concluded that, the judicious choice of the geometry of the defect and its dimension plays a vital role for obtaining the optimum performance of the patch antenna.

Now, we may focus into the radiation pattern of such configuration. The peak gain and the front to back radiation isolation (F/B radiation isolation) of RMA with (finite a_h values) and without ($a_h = 0$) hexagonal defect is depicted in **Fig. 3.5**. It is observed from the figure that, as soon as the hexagonal defect with $a_h = 1\text{mm}$ is incorporated in ground plane, the peak gain of the structure increases around 1 dB.

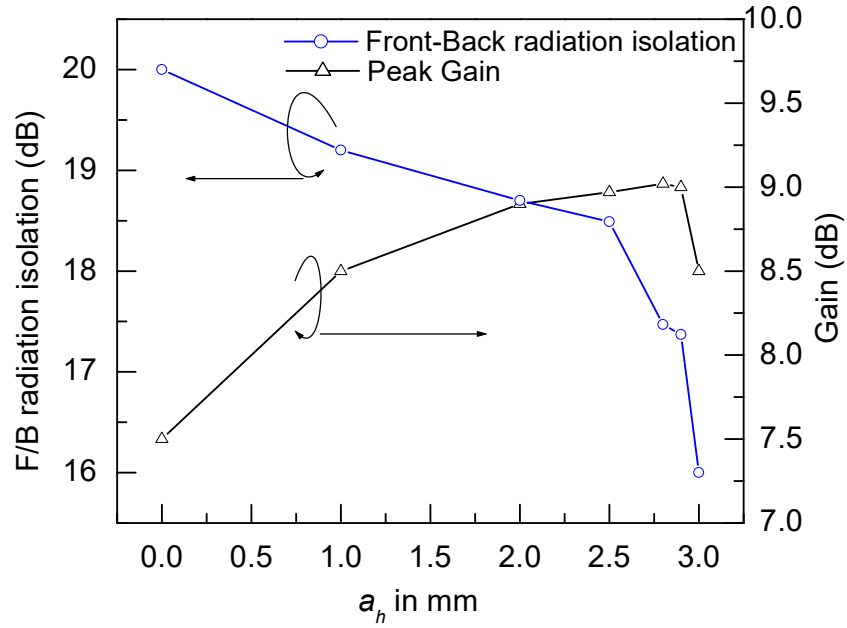


FIGURE 3.5 Gain and F/B radiation isolation of conventional RMA and HDGS integrated RMA for different side length a_h in mm.

The gain of the conventional antenna without HDGS is 7.5 dBi, while the same with HDGS structure is around 8.35 dBi. Then, the value of a_h , increases gain increases up to 9.03 dBi (when $a_h = 2.8\text{mm}$). It may also be noted from **Fig. 3.5** that the rate of increase in gain is higher than rate of degradation of F/B ratio till $a_h = 2.5\text{mm}$. After that point the back radiation increases abruptly and hence the F/B ratio degrades significantly. However, the performance of gain and F/B ratio is still better till $a_h = 2.9\text{mm}$. In fact, the fringing fields near radiating edges follow the defect

periphery and hence, increase the fringing length. Therefore, the effective aperture increases and this may be attributed to higher gain in HDGS integrated RMA. **Fig. 3.6** depicts the electric field distribution over the substrate for conventional and proposed HDGS integrated RMA. It is clear from the figure that, the electric fields are distributed over wider area in HDGS integrated RMA compared to that for conventional RMA.

The effective aperture of the antenna is given by [2]

$$\frac{A_{eff}}{\lambda^2} = \frac{[(L + 2\Delta L)(W + 2\Delta W)]}{\lambda^2} \quad (3.1)$$

Where, ΔL and ΔW is the fringing length and width of the patch of length L and width W . The operating wavelength is λ .

It may also be noted that, as the value of a_h is increased, back radiation also increases. This in turn, degrades the F/B radiation isolation. The F/B radiation isolation for conventional structure is around 20 dB while the same for HDGS integrated RMA with $a_h = 2.8$ mm is 17.5 dB. The further increment of a_h results in the reduction of gain. This may be due to the severe back radiation, as there is significant leakage of radiation field in the back side of the antenna due to its large defect dimension. However, when $a_h = 2.9$ mm; the gain of the structure becomes slightly less than that for $a_h = 2.8$ mm and it is around 9.01 dBi while its F/B radiation isolation is around 17.43 dB. Further increase in a_h ($= 3$ mm) offers the peak gain of 8.5 dBi with F/B radiation isolation of 16 dB. Hence, $a_h = 3$ mm is not justified because of its poor F/B radiation isolation with the peak gain similar to the case of $a_h = 1$ mm.

In order to investigate the versatility of the present structure in other frequency band, similar configuration has been designed with HFSS [11] for X band with $L = 12$ mm, $W = 18$ mm, and $a_h = 5$ mm. It is found that the structure exhibits broad impedance bandwidth of 72.28% (7.14 GHz to 12.65 GHz) with respect to its design frequency (**Fig. 3.7**). The simulated peak gain of the structure in X band varies from 9.55 dBi to 10.5 dBi over the band though not shown in this chapter. The F/B radiation isolation of the structure is observed to be around 16 dB at the design frequency. In order to suppress the back radiation, another metallic plate (designated

as 2nd ground plane) has been employed behind the conventional defected ground plane. It may be noted that, the F/B radiation isolation of the structure with the 2nd ground plane has been improved by 2 dB while it losses both the features of broad impedance band width and high gain.

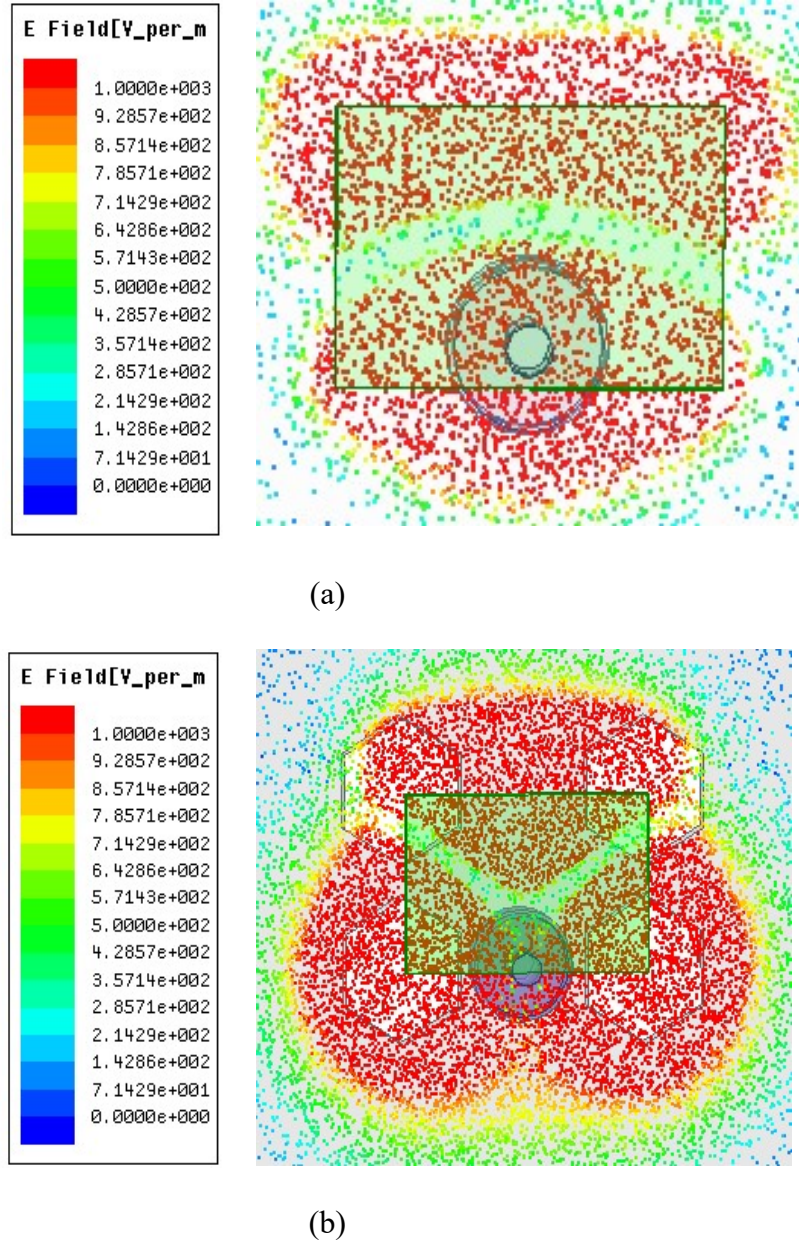


FIGURE 3.6 Magnitude of electric field distribution over the substrate for (a) conventional and (b) HDGS integrated RMA with $a_h = 2.9$ mm.

It is because of the fact that, much of the fringing fields near radiating edges will be terminated at 2nd ground plane rather than being terminated at defect periphery. Therefore fringing length reduces which in turn, decreases the effective aperture and hence the gain of the structure. Furthermore, the loss due to back radiation is minimized due to the presence of 2nd ground plane. This in fact, decreases the Q factor due to radiation loss and consequently reduces the input impedance bandwidth. A similar investigation has been carried out with another dielectric plate (PTFE; $\epsilon_r = 2.33$) behind the conventional defected ground plane. No such specific improvement is noted. Therefore, the idea of employment of 2nd plate (metallic/dielectric) behind the ground plane has not been considered and examination of the structure in X, Ku and Ka band without any back plate for experimental verification is continued with.

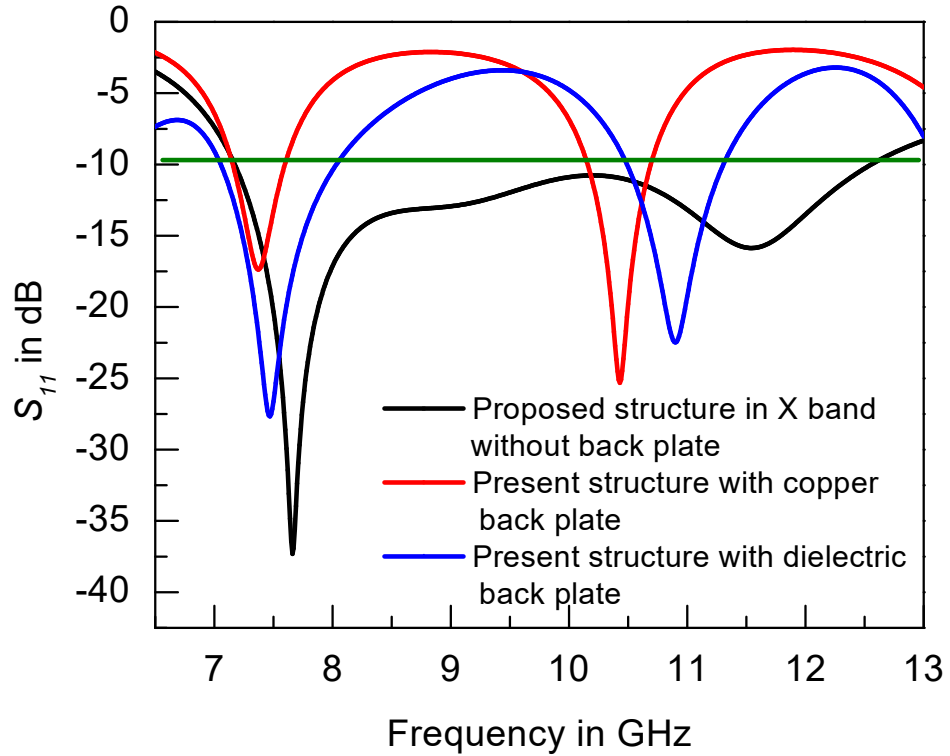


FIGURE 3.7 Simulated reflection coefficient profile of X band HDGS integrated RMA with and without back plate (metallic/dielectric).

3.2.2 Proposed Structure

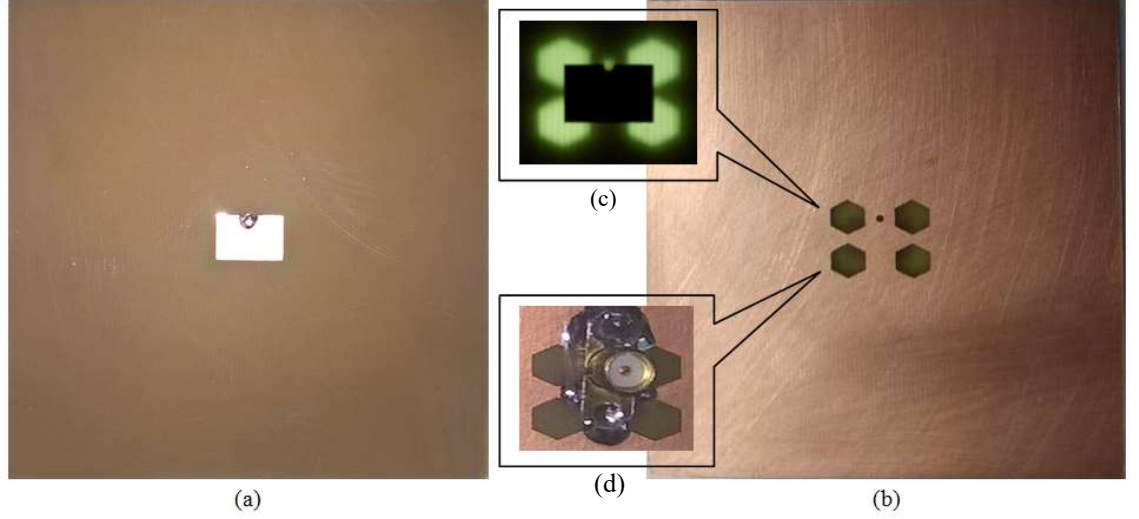


FIGURE 3.8 Fabricated HDGS of patch length $L = 7.1$ mm, width $W = 10.8$ mm on RT Duroid/5870 with dielectric substrate of permittivity $\epsilon_r = 2.33$, height $h = 1.575$ mm (a) patch side, (b) ground plane side, (c) multi layer image with help of neon light and (d) ground plane side with completely integrated with SMA connector.

RMA of length $L = 7.1$ mm, width $W = 10.8$ mm fabricated on RT duroid/5870 dielectric substrate of permittivity $\epsilon_r = 2.33$, height $h = 1.575$ mm for X, Ku and Ka band as shown in **Fig 3.8**. The dimension of the ground plane is $80 \times 80 \text{ mm}^2$. Four defects of hexagonal geometry of side length $a_h = 2.9$ mm is placed at four corners of the patch in such a way that, the centre of hexagon coincides with the patch corner as shown in **Fig. 3.1** and **3.8**.

3.2.3 Experiments and Results

The simulated (HFSS [11]) and measured results for the proposed HDGS integrated RMA are presented in the following section. The patch is fed with a SMA connector at 3.3 mm from the centre of the patch. The radiation pattern has been measured using Agilent network analyzer, Agilent power sensor with Agilent's probe. Agilent single channel power meter is also utilized for the measurement. **Fig. 3.9** shows the measured and simulated reflection coefficient profile for proposed HDGS integrated RMA with $a_h = 2.9$ mm.

The resonant frequency has been obtained from S_{11} minimum and it shows that the structure is resonating near 12.2 GHz at the optimum feed position. It is observed from the figure that, the impedance bandwidth of proposed HDGS integrated RMA with $a_h = 2.9$ mm is around 58% at its design frequency.

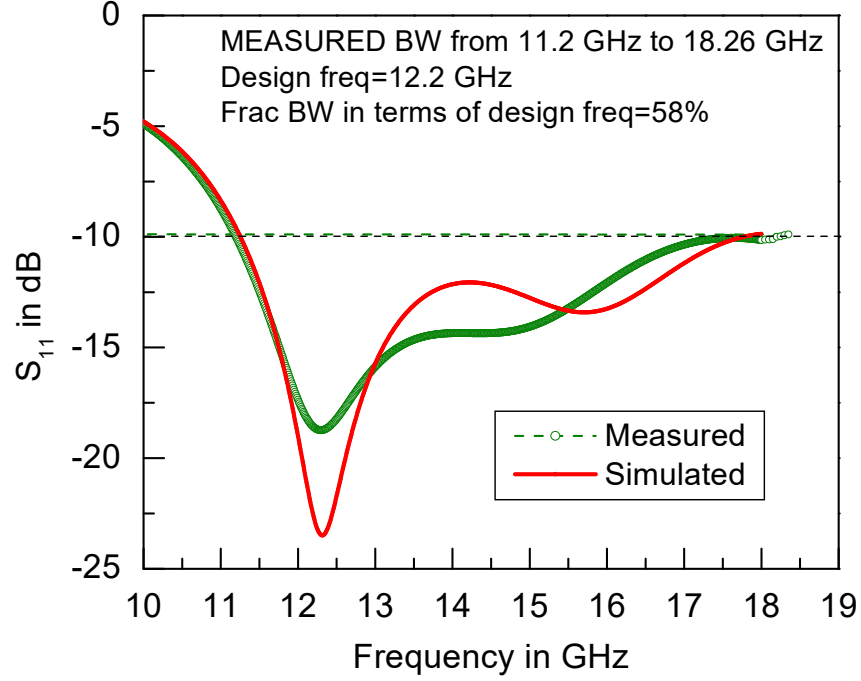


FIGURE 3.9 Measured and simulated reflection coefficient profile of HDGS integrated RMA with $a_h = 2.9$ mm.

The present antenna operates over the frequency range from 11.2 GHz to 18.3 GHz i.e it covers the whole Ku band (12-18 GHz) of frequency.

Therefore,

$$\frac{2(f_H - f_L)}{(f_H + f_L)} = 0.5 > 0.2 \quad (3.2)$$

and following [12], the present HDGS integrated RMA can be designated as UWB patch antenna. **Fig. 3.10** shows the complete radiation characteristics of the present antenna in the entire band of frequencies. Simulation results are also incorporated in the same plot for comparison. Close mutual agreement between the simulation and measured results are revealed in both the planes. Measured gain of the present antenna varies from 8.5 dBi - 9.01 dBi in the entire operating band. It is revealed from **Fig. 3.10** that, the radiation pattern of the present antenna is quite stable in the whole range of frequencies from 11.2 GHz to 18.26 GHz. However, at very high frequency $f = 17.9$ GHz, pattern is little distorted. It is evident from **Fig. 3.10(f)** that, at $f = 17.9$ GHz, there is a sharp null at one side (at around 35°) in the E plane of radiation pattern of proposed HDGS integrated RMA. This is mainly due to the unwanted probe radiation [13].

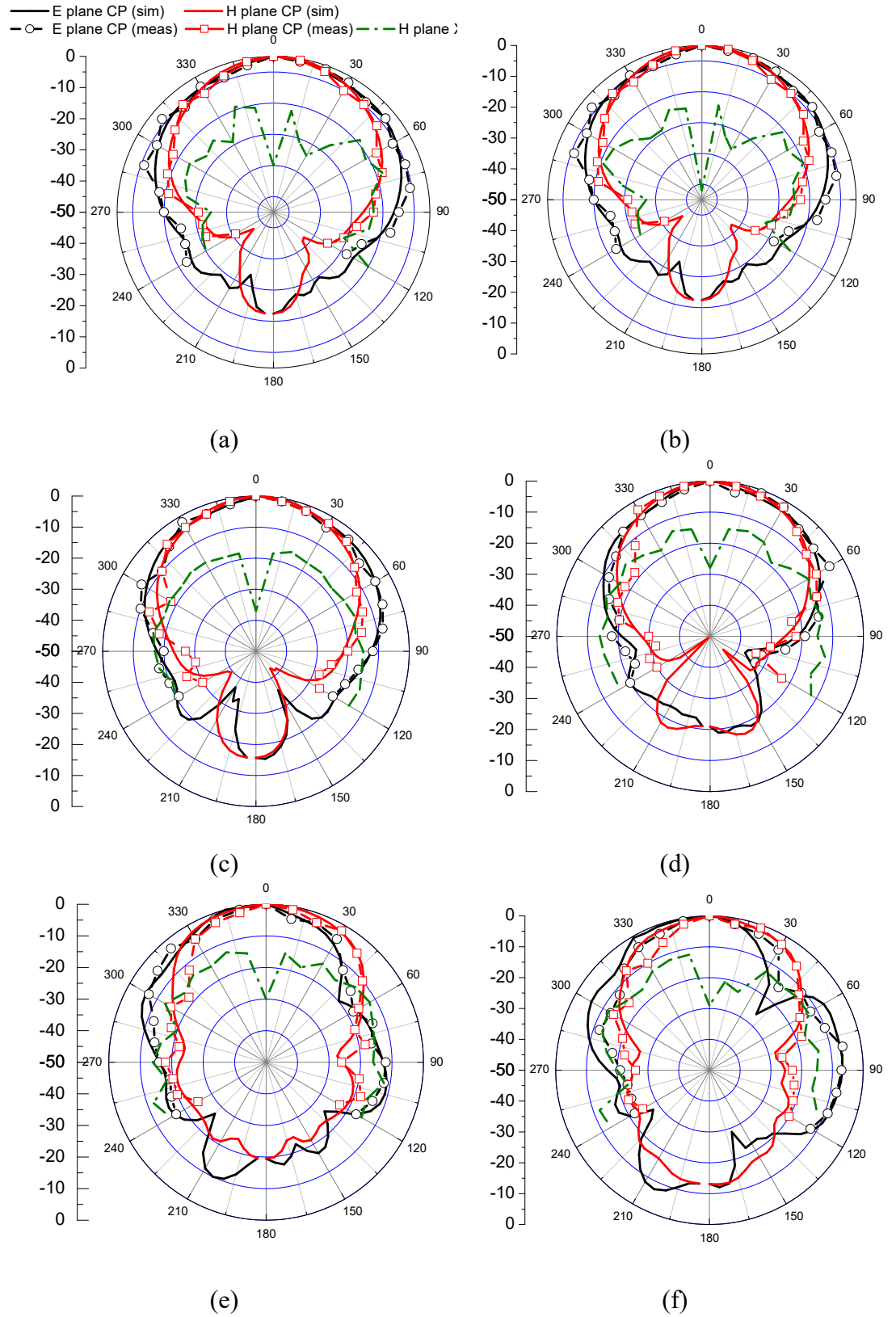


FIGURE 3.10. Measured and simulated radiation pattern for E and H plane with proposed HDGS integrated RMA ($a_h = 2.9$ mm) at different frequencies. (a) $f = 11.8$ GHz, (b) $f = 12.2$ GHz, (c) $f = 13$ GHz, (d) $f = 14.9$ GHz, (e) $f = 16.9$ GHz, (f) $f = 17.9$ GHz

In fact, the probe at such high frequency near 18 GHz, acts like short monopole and radiates some unwanted fields. Therefore, this causes an unexpected null on one side in E plane, leading to an asymmetric pattern. The back radiation of the present antenna near the design frequency is around 18 dB while it degrades as frequency increases. This becomes worse at very high frequency at $f = 18$ GHz and i.e around 10 dB. However, in most of the frequency region the back radiation is below 16 dB from the peak CP gain.

The variation of the measured gain and CP-XP isolation of the present HDGS integrated RMA in the entire operating band of frequency is depicted in **Fig. 3.11**. It is observed that the gain of the antenna varies from 8.5 dBi to 9.35 dBi as the frequency changes from 11.2 GHz to 18.3 GHz. In fact, the electrical effective aperture of any antenna increases with frequency results in an enhancement of gain. However, it may be concluded that, the present antenna exhibits flat gain over the entire frequency range. On the contrary, the measured CP-XP isolation of the present antenna is degraded as the frequency increases in its operating bandwidth as is seen in **Fig 3.11**. It may be noted that the cross polarized radiation (XP) is low for the proposed antenna near the design frequency. Around 22.5 dB to 23 dB of CP-XP radiation isolation is noted near design frequency $f = 11.8$ -12.2 GHz. But, towards the higher side of the spectrum, XP performance becomes poor. Around 14-16 dB of CP-XP isolation is obtained from present antenna up to $f = 17$ GHz; while it becomes 13 dB at $f = 18$ GHz as is evident from **Fig. 3.11**.

However, a convention RMA at such high frequency ($f = 18$ GHz), shows very poor XP performance and in that case CP-XP isolation is around 8 dB (as per the simulation results). In fact, XP radiation usually increases with frequency. This is because, at high frequency, the substrate becomes electrically thick and at the same time, probe contributes unwanted radiation which in turn increases XP radiation. Therefore, compared to conventional RMA, the present antenna shows much better XP performance in the entire operating band.

Nevertheless, the present Ku band HDGS integrated RMA ($a_h = 2.9$ mm) exhibits stable radiation pattern with high gain (around 9 dBi) with better CP-XP isolation in the entire 58% bandwidth. Therefore, this antenna may be utilized in

different satellite applications where, the scientists, researchers and practicing engineers looking for high gain UWB antenna in Ku band.

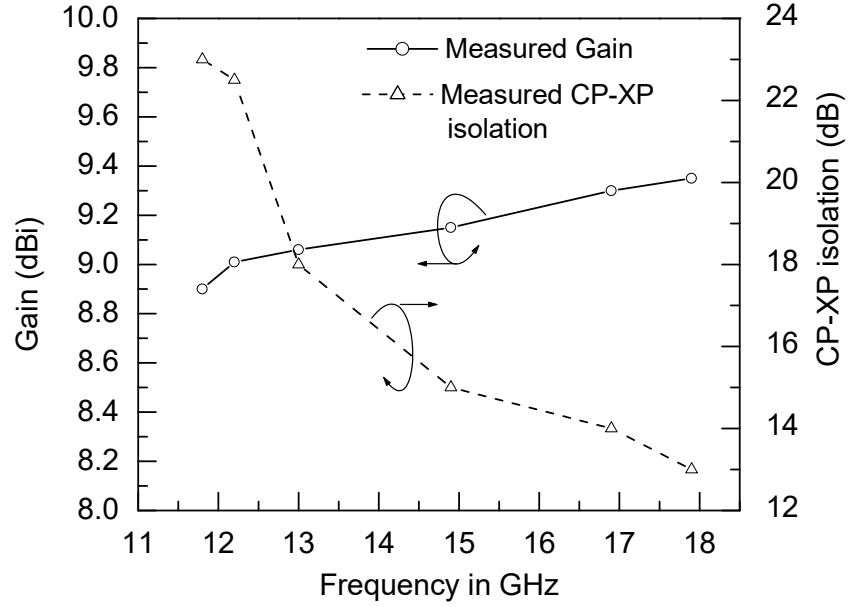


FIGURE 3.11. Variation of measured gain and CP-XP radiation isolation as a function of frequency for proposed HDGS integrated RMA with $a_h = 2.9$ mm.

3.3 Performance Evaluation of Various DGS Integrated RMA (Defects with Increasing Order of Polygons)

This section evaluates various types of optimized DGS integrated RMAs which can be selected for particular applications based on the performance and the concept behind the same can be analyzed.

3.3.1. Requirement of Various Types of DGSs (Polarimetric Radar)

In the fields of not so very exploited polarimetric radars, improvements in antenna parameters with compulsorily maintaining the polarization purity is the key issue. Because of some beautiful characteristics of Microstrip patch antenna (MPA) it is the most suitable candidate for the same. A conventional rectangular microstrip patch antenna (RMA) resonating in its fundamental TM_{10} mode radiates co-polarized (CP) fields in the broadside direction as is discussed in section 2.1. Orthogonal radiation called as cross-polarization (XP) fields are also there as is explained earlier. This XP radiation is the most prominent due to first higher order orthogonal mode i.e. TM_{02} . A broadband system always demands a broadband antenna/ radiator. A

CRMA has impedance bandwidth of around 5% [14] and various reported techniques to increase the same are L-probe feed inverted EE-H shaped slotted MPA [15], E [16] and Ψ [17] shaped patch antenna. Impedance bandwidths reported in those papers are 21.15%, 30%, and 54% respectively.

Out of different techniques as mentioned above, fractal concept are now being applied to antenna designs as being applied to various branches of engineering and science including electrodynamics, propagation and scattering [18]-[22]. However the limitations of all above highlighted structures are that they have poor CP-XP isolation (polarization purity). Some significant research results illustrate the investigation on minimizing the radiation of cross-polarized fields by altering the feed structure [12], [23] and ground plane structure [24], [25]. 10-20 dB CP-XP isolation is reported in those articles without any improvement in impedance bandwidth. Recently, defected ground structure (DGS) and defected patch surface (DPS) based on electronic band gap (EBG) theory have been used to improve the XP radiation purity of 10-15dB is reported in those articles. The use of defected ground structure technique is the most popular and widely acceptable technique to improve polarization purity and other antenna parameters.

In the present comparative study between various existing DGS which are particularly in increasing order of polygon (simple RMA without DGS [26], Triangular DGS integrated RMA [27], Pentagon DGS integrated RMA [28], Hexagon DGS integrated RMA [29] and Circular/ Ring DGS integrated RMA [30]) has been thoroughly studied with the aim to bring out the concept behind the benefits that they present and implication of the increasing order of polygon in particular.

3.3.2. Selection Criteria for Comparison

The selection of polygons is practically adequate and covers an aspect of zero sides to infinite sides of the defects placed on the ground plane. The antennas selected for comparison are operating either in X band and Ku band only. The antennas selected for comparison are primarily having good CP-XP isolation (polarization purity), high impedance bandwidth and gain. However the selections are not random. Selection of antennas is with an aim to recommend the concept behind them as opportunity to the field of polarimetric radars.

Also, the comparison is meaningful if the design concepts are largely similar. All antennas are probe fed and have linear polarization pattern of radiation. All the antennas have incorporated DGS at the non-radiating sides of the rectangular patch which is the primary source of the cross polarization radiation [7], [31], [32], [33].

The important concept of incorporating defect on the ground plane of antenna structure is being compared and the selection of polygons is in the increasing order. Few dominating key parameters like impedance bandwidth, gain, polarization purity has been compared. All the structured have been optimized to get the best performance out of each structure.

The bandwidth of the antenna is directly proportional with the different losses provided by the antenna i.e. as losses increases bandwidth also increases. In each of the structure studies have been initiated with a small defect size at the appropriate position to improve the performance. Then the size of the defect increases gradually to get the optimum antenna structure which produces best performance in terms of impedance bandwidth. The impedance bandwidth may increase with the further increment of the defect size but other parameters like gain, polarization purity may be hampered. Therefore the optimum defect size has been considered for each defect geometries in regard to both the input as well as radiation characteristics.

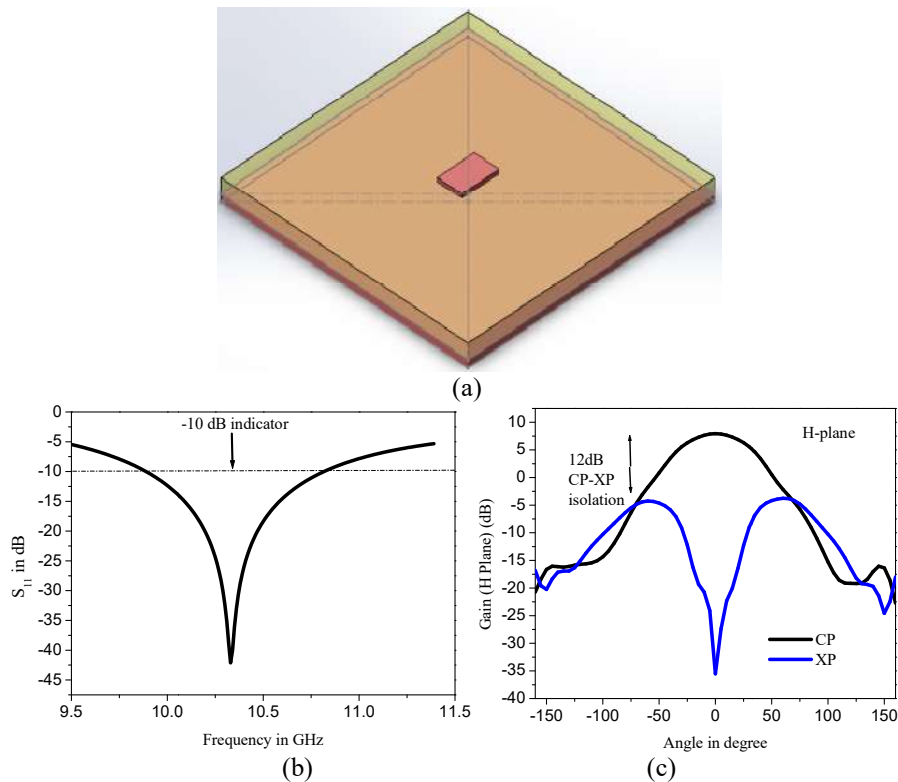
3.3.3. Results of Different Structures

The selection of the DGSs as mentioned above are very specific and more importantly they are in the increasing order of polygon. Investigation has been performed with similar types of DGS integrated RMA with equal electrical dimension for excitation of similar frequency. Also, the selection of the DGSs are located specifically or close to a particular reference locations on the ground plane. The features of these antennas are tabulated in **Table 3.1**.

TABLE 3.1. Parameters of the RMA used for investigations (Substrate thickness $h = 1.575$ mm)

Name	Antenna Structure	L (mm)	W (mm)	Number sides in DGS (N)	Feed position (offset from centre) (mm)
Antenna 1	Conventional RMA	8	12	0	2.4
Antenna 2	RMA with Triangular DGS	8	12	3	3.1
Antenna 3	RMA with Pentagon Dumbelled DGS	8	12	5	4.32
Antenna 4	RMA with Hexagon DGS	7.1	10.8	6	3.3
Antenna 5	RMA with ring DGS	8	12	∞	3.1

The results obtained from each antenna used for comparison is simulated using [11] and documented in the following sections.

**FIGURE 3.12:** Conventional RMA (a) 3D view, (b) reflection coefficient profile (c) H-plane radiation pattern

Antenna 1: In Antenna No 1 that is conventional RMA (without DGS, $N = 0$), the conducting patch and ground plane form perfect electric conducting (PEC) boundary

while edges boundaries provides perfect magnetic conducting (PMC) wall [4], [29], [30]. The reflection coefficient profile and the H plane radiation characteristics are depicted in **Fig. 3.12**. Well known literatures reported that conventional RMA suffers from two common limitations namely narrow bandwidth (typically 5%) and low polarization purity (typically 10-15 dB). These two limitations are confirmed from **Fig. 3.12(b)** and (c).

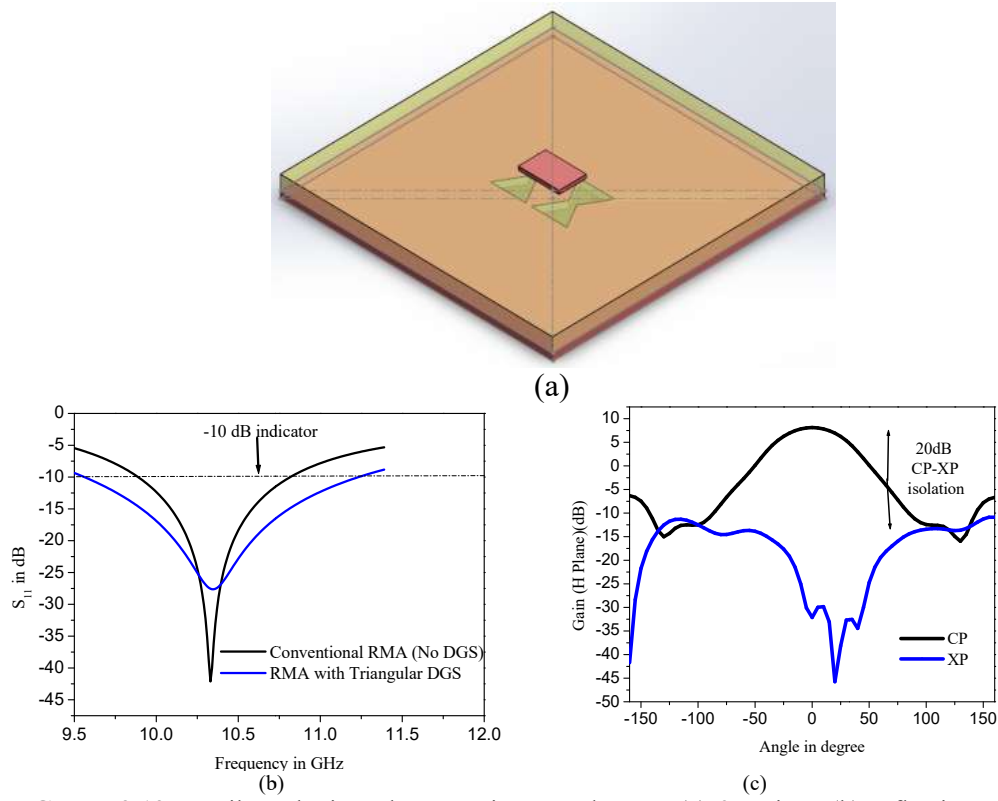


FIGURE 3.13: Equilateral triangular DGS integrated RMA (a) 3D view, (b) reflection coefficient profile (c) H-plane radiation pattern

Antenna 2: In Antenna No 2 a pair of triangular shaped defect (DGS with $N=3$) has been introduced at the non-radiating sides of patch to effect the cross polarization radiation of the antenna [27]. The impedance bandwidth achieved through the proposed equilateral triangular shaped defected ground structure integrated RMA is 17% which is much better as compared to the conventional RMA (**Fig. 3.13(b)**). The polarization purity of 22 dB over a wide angle of $\pm 130^\circ$ [20] has been achieved through the optimum structure where each side of the equilateral triangular shaped DGS is 10.4 mm (**Fig. 3.13(c)**).

Antenna 3: Four regular pentagon shaped defects (DGS with $N=5$) have been laid down just below the corners of the RMA in such a way that the center of pentagon coincides the corners of patch [28]. Two slits of 1 mm width is itched out below the non radiating sides of the patch centrally and these slits connects the pentagon defecting as seen in **Fig 3.14**. The structure fails to improve the impedance bandwidth as compared to conventional RMA but significantly improves the polarization purity up-to 25 dB over a wide angular range of $\pm 180^\circ$ when the arm of the regular pentagon is 5 mm [31].

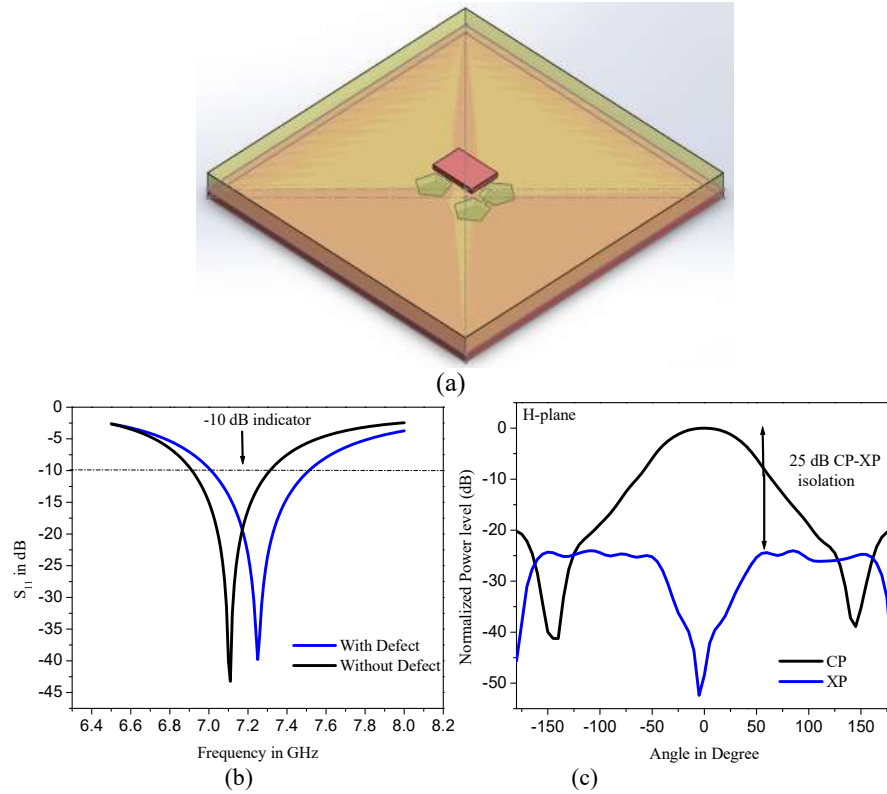


FIGURE 3.14: Regular pentagon dumbelled shaped DGS integrated RMA (a) 3D view, (b) reflection coefficient profile (c) H-plane radiation pattern

Antenna 4: Four hexagonal shaped defects (DGS with $N=6$) are itched out at the ground plane in such a way that, centre of the hexagons matches with the patch corners (**Fig. 3.15(a)**) [29]. The fractional bandwidth of hexagonal shaped DGS integrated RMA with one side of hexagon of 2.9 mm becomes around 58% (**Fig. 3.15(b)**) while the polarization purity varies between 13- 22 dB within the wide operating bandwidth which is quite good for such an UWB antenna [7].

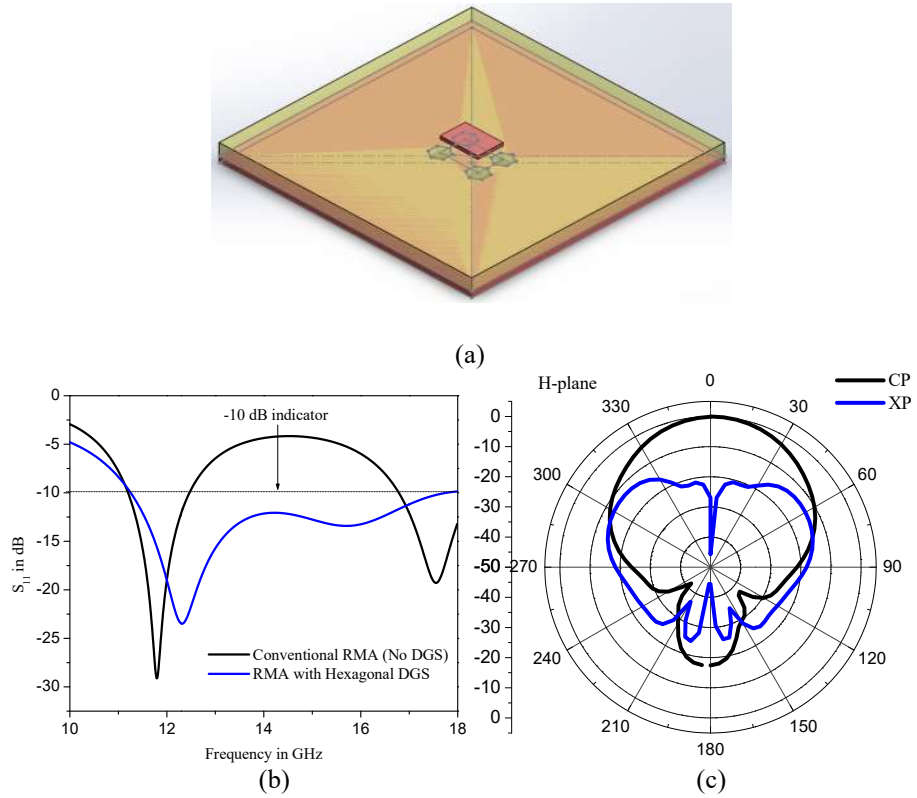


FIGURE 3.15: Hexagon shaped DGS integrated RMA (a) 3D view, (b) reflection coefficient profile (c) H-plane radiation pattern

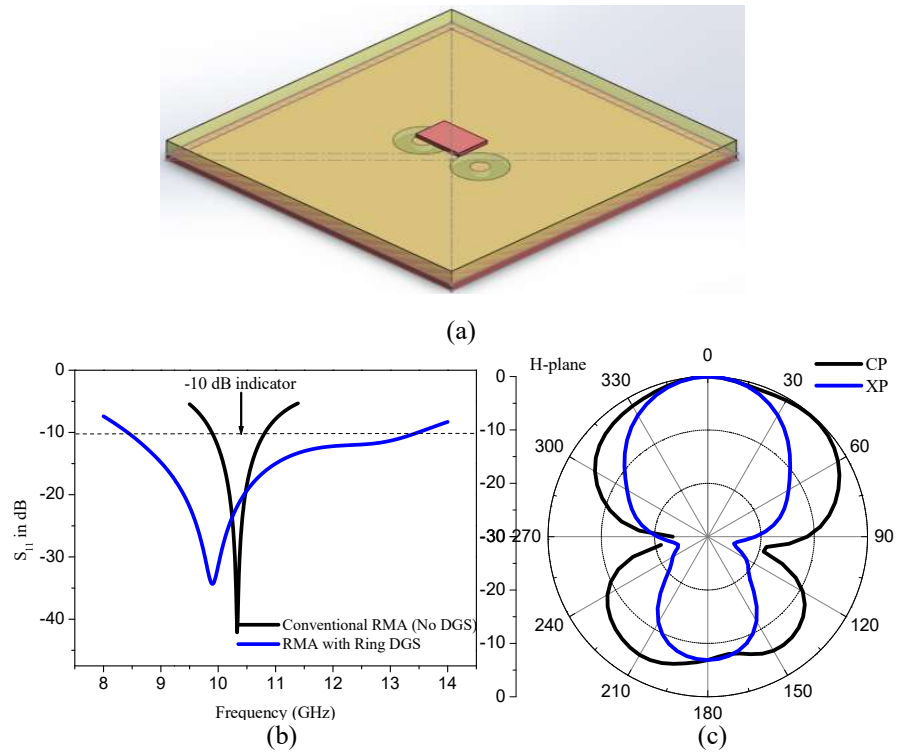


FIGURE 3.16: Ring shaped DGS integrated RMA (a) 3D view, (b) reflection coefficient profile (c) H-plane radiation pattern

Antenna 5: The final structure that has been considered for comparative study is a ring shape DGS integrated RMA with external diameter (S_o) of 6 mm and internal diameter (S_i) of 2 mm (**Fig. 3.16(a)**). Maximum impedance bandwidth of 47% (**Fig. 3.16(b)**) along with comparable polarization purity has been achieved from the structure [30].

The performance of different antenna for the comparative study has been summarized in **Table 3.2**.

TABLE 3.2. Comparison between input and radiation properties of different antenna structure

Type of DGS	Defect Dimension (mm)	Operating Band	Resonating Freq (GHz)	Variation of Gain (dBi)	Impedance BW (%)	Polarization purity (dB)
Conventional RMA	nil	X band	10.33	3-4	3- 4	12
RMA with Triangular DGS	$S = 10.4$	X band	10.35	7 - 8.7	17	22
RMA with Pentagon Dumbelled DGS	$S = 5$	X band	5.6	6.6 – 7.4	15	28
Hexagonal DGS integrated RMA	$S = 2.9$	Ku band	12.2	7.5-9.1	58	22.5
Ring DGS-integrated RMA	$S_o = 6$ $S_i = 2$	X band	9.86	4.5-5.7	47	22

3.4 Conclusion

In this chapter, the employment of DGS has been considered mainly to improve the gain and bandwidth of RMA. As such, the classical report on implementation of defected ground structure (DGS) in microstrip antenna was prominently considered for lowering cross-polarized radiation.

The experimental investigations with hexagonal defected ground structure (HDGS) integrated rectangular microstrip antennas (RMA) has been considered in the present chapter and it shows that the bandwidth and the gain properties of such antenna can also be improved by judicious exploitation of the defect geometry on ground plane. Around 58% input impedance bandwidth (covering Ka and Ku spectrum) with high gain (around 9.1-9.4 dBi) and stable radiation pattern is

obtained from the structure. The XP radiation for the present antenna shows much better results than conventional RMA at Ku band.

Furthering the study, a comparative analysis between various existing DGSs which are particularly in increasing order of polygon has been methodically carried out. The geometry of DGS is a critical factor that governs the input parameters and the radiation characteristics of an antenna. The bandwidth of an antenna enclosed in a given space can be enhanced only if the antenna exploits the space within it proficiently. In view of the above, it can be concluded that, amongst the available polygons, the hexagonal DGS integrated RMA can address all the issues of XP/polarization purity and board banding along with higher gain of around 9 dBi. Further to it, it offers UWB. And, the above mentioned requirements are inescapable being fundamental in nature to the field of polarimetric radars.

The structure (HDGS) is very simple and easy to manufacture. The HDGS integrated RMA will surely be helpful for scientific community looking for broadband, high gain antenna with stable radiation pattern and polarization purity in Ku band operations and applications.

In the next Chapter, unlike the present approaches, no slots or shorts have been implemented on the patch or even in the ground plane respectively to suppress the cross-polar radiation from an antenna. An attempt has been made to achieve better performance from an extremely simple structure.

References

- [1] S. Chattopadhyay, J. Y. Siddiqui, & D. Guha, "Rectangular microstrip patch on a composite dielectric substrate for high gain wide-beam radiation patterns". *IEEE Trans Antennas Propag.* vol. 57, pp. 3324–3327, 2009.
- [2] D. Guha, S. Chattopadhyay and J. Y. Siddiqui, "Estimation of gain enhancement replacing PTFE by air substrate in a microstrip patch antenna", *IEEE Antennas Propag Mag.*, vol. 52, pp. 92–95, 2010.
- [3] Y. T. Liu, C. W. Su, K. L. Wong, & H. T. Chen, "An air substrate narrow patch microstrip antenna with radiation performance for 2.4 GHz WLAN access point", *Microwave Opt. Technol. Lett.*, vol. 43, pp. 189–192, 2004.
- [4] R. Garg, P. Bhartia, I. Bahl and A. Ittipiboon, *Microstrip Antenna Design Handbook*, Norwood, MA, USA: Artech House, 2001.
- [5] D. Guha and Y.M.M. Antar, *Microstrip and printed antennas – new trends techniques and applications*, UK: John Wiley, 2011.
- [6] S. Chakraborty and S. Chattopadhyay, "Substrate fields modulation with defected ground structure: A key to realize high gain wideband microstrip antenna with improved polarization purity in principal and diagonal planes", *Int. J. RF Microw. Comput. Aided Eng.*, vol. 26, no. 2, pp. 174–181, 2016.
- [7] A. Ghosh, D. Ghosh, S. Chattopadhyay, L. L. K. Singh, "Rectangular microstrip antenna on slot type defected ground for reduced cross polarized radiation", *IEEE Antennas Wirel. Propag. Lett.*, vol. 14, pp. 324–328, 2015.
- [8] C. Kumar and D. Guha, "DGS integrated rectangular microstrip patch for improved polarization purity with wide impedance bandwidth", *IET Micro. Ant. Prop.*, vol. 8, pp. 589–596, 2014.
- [9] C. Kumar and D. Guha, "Asymmetric geometry of defected ground structure for rectangular microstrip: a new approach to reduce its cross-polarized fields", *IEEE Trans. Antennas Propag.*, vol. 64, no. 6, pp. 2503–2506, 2016.
- [10] C. Kumar, M.I. Pasha and D. Guha, "Microstrip patch with nonproximal symmetric defected ground structure (DGS) for improved cross-polarization properties over principal radiation planes", *IEEE Antennas Wirel. Propag. Lett.*, vol. 14, pp. 1412–1414, 2015.

- [11] High Frequency Structure Simulator, HFSS v.14, *Ansoft Corporation*
- [12] W. Wiesbeck, G. Adamiuk, & C. Sturm, "Basic Properties and Design Principles of UWB Antennas", *Proceedings of the IEEE*, vol. 97(2), pp. 372-385, 2009.
- [13] A. Petosa, A. Ittipiboon and N. Gagnon, "Suppression of unwanted probe radiation in wide band probe-fed microstrip patches", *Electron. Lett.*, vol. 35, pp. 355-357, 1999.
- [14] G. Kumar and K.P. Ray, *Broadband microstrip antennas*, Boston, London:Artech House, 2003.
- [15] M. T. Islam, M. N. Shakib, N. Misram, "Design Analysis of High Gain Wideband L-Probe fed Microstrip Patch Antenna," *Prog. In Electromagnet. Research*, vol. 95, pp. 397-407, 2009.
- [16] F. Yang, X. Zhang, X. Ye, Y. R. Samii, "Wide-band E-shaped Patch Antennas for Wireless Communications", *IEEE Trans. Ant. and Prop.*, vol. 49(7), pp. 1094-1100, 2001.
- [17] S. K. Sharma, L. Shafai, "Performance of a novel Ψ -shape microstrip patch antenna with wide bandwidth", *IEEE Ant. and Wireless Prop. Lett.*, vol. 8, 468-471, 2009.
- [18] H. N. Kritikos, D.L. Jaggard,(eds.) *On Fractal Electrodynamics*. In *Recent Advances in Electromagnetics Theory*, *Springer-Verlag*, New York, 183-224, 1990.
- [19] H. L. Bertoni, L. B. Felsen, (eds.). *Fractal Electrodynamics and Modeling in Direction in Electromagnetics Wave Modeling*, *Plenum Publishing*, New York, 435-466, 1991.
- [20] D. L. Jaggard, "Fractal Electrodynamics: Wave Interactions with Discretely Self-Similar Structures", C. Baum and H. Kritikos (eds.), in *Electromagnetic Symmetry*, *Taylor & Francis Publishers*, Washington, DC, 231-281, 1995.
- [21] D. H. Werner, "An overview of Fractal Electrodynamics Research", *Proceedings of the 11th Annual Review of Progress in Applied Computational Electromagnetics (ACES)*, vol. 2, pp. 964-969, 1995.

- [22] D.L. Jaggard, “Fractal Electrodynamics: From Super Antennas to Superlattices”, J. L. Vehl, E. Lutton, C. Tricot (eds.). *In Fractal in Engineering*, Springer-Verlag, 204-221, 1997.
- [23] P. Li, H. W. Lai, K. M. Luk, and K. L. Lau, “A Wideband Patch Antenna with Cross-Polarization Suppression,” *IEEE AWPL*, vol. 3, pp. 211-214, 2004
- [24] K. L. Wong, C. L. Tang, and J. Y. Chiou, “Broad-band probe-fed patch antenna with a W-shaped ground plane,” *IEEE Transactions on Antennas and Propagation*, vol. 50, no. 6, pp. 827–831, 2002.
- [25] W. H. Hsu, and K. L. Wong, “Broad-band probe-fed patch antenna with a U-shaped round plane for cross-polarization reduction,” *IEEE Transactions on Antennas and Propagation*, vol. 50, no. 3, pp. 352–355, 2002.
- [26] D. R. Jackson, N. G. Alexopoulos, “Simple approximate formulas for input resistance, bandwidth, and efficiency of a resonant rectangular patch”, *IEEE Transactions on Antennas and Propagation*. vol. 39(3), pp. 407–410, 1991.
- [27] A. Ghosh, B. Basu, “Triangular slotted ground plane: a key to realize high gain, cross- polarization free microstrip antenna with improved bandwidth,” *Turk. J. Electr. Eng. Comput. Sci.*, vol. 27, pp. 1559–1570, 2019.
- [28] A. K. Nath, L. L. K. Singh, S. Chattopadhyay, A. Ghosh, “Study of polarization purity of rectangular microstrip antenna integrated with pentagon dumbelled shaped defected ground structure”, *In Intelligent Techniques and Applications in Science and Technology*, Springer International Publishing, 484–492, 2020.
- [29] U. A. Pawar, S. Chakraborty, L. L. K. Singh, S. Chattopadhyay, “Application of defected ground structure for augmenting high-gain ultra-wide bandwidth from rectangular microstrip antenna,” *Electromagnetics*, vol. 38: pp. 123–133, 2018.
- [30] U. A. Pawar, A. Ghosh, L. L. K. Singh, S. Chattopadhyay, “Application of defected ground structure for stable gain with ultrawide bandwidth,” *Advances in Communication, Devices and Networking*, Lecture Notes in Electrical Engineering, Springer Singapore, vol. 537, pp. 141-149, 2019.

- [31] D. Ghosh et al., “Physical and quantitative analysis of compact rectangular microstrip antenna with shorted non-radiating edges for reduced cross-polarized radiation using modified cavity model,” *IEEE Antennas Propagation Magazine*, vol. 56, no. 4, pp. 61–72, 2014.
- [32] A. Ghosh, S. Chakraborty, S. Chattopadhyay, A. Nandi, B. Basu, “Rectangular Microstrip Antenna with Dumbbell Shaped Defected Ground Structure for Improved Cross Polarized Radiation in Wide Elevation Angle and its Theoretical Analysis,” *IET Microwaves, Antennas & Propagation*, vol. 10, no. 1, pp. 68-78, 2016..
- [33] S. Chattopadhyay, S. Chakraborty, “A physical insight into the influence of dominant mode of rectangular microstrip antenna on its cross-polarization characteristics and its improvement with T-shaped microstrip antenna,” *IEEE Access*, vol. 6, pp. 3594-3602, 2018.

**Bracketed and Stub-loaded
Rectangular Microstrip Antenna:
A Novel Approach to Improve Polarisation Purity**

4.1 Introduction

In present wireless world, rectangular microstrip antenna (RMA) is probably the most functional planar radiator due to its multiple attractive features like light weight, small size and low cost as discussed in Chapter 1. Such a RMA radiates linearly polarized wave at its broadside with some orthogonally polarized wave referred as cross-polarized (XP) radiation [1]. These XP radiations are more prominent in H plane than in E plane as reported in [2]. Therefore, it has certain major restriction for applications such as adaptive antenna arrays for cellular, or other wireless communications, where wide angular coverage is usually required [3].

In the previous chapter, the issue of broad banding and gain while maintaining polarization purity in RMA has been well addressed by means of Defected Ground Structure (DGS). However, there are few marginal shortcomings. The DGS integrated RMAs suffers from significant back radiation. Also in some cases the radiation pattern are not stable with off-boresight nulls which may be due to diffracted radiations in back side due to sharp edges of defects of ground plane. Notably, defecting the ground plane and at the same time proper placement of feed probe at ground plane is a critical fabrication task. Therefore some new techniques other than DGS must be explored to address the issues of XP radiation from RMA.

Although the sources of XP fields are believed to be germinated from higher order orthogonal TM_{02} mode, a recent investigation [4] shows that considerable XP

radiations are generated from its own dominant TM_{10} mode. In fact, the possibility of contribution to the XP fields due to excitation of TM_{02} mode is fewer in the patch with width (W) to length (L) ratio $W/L = 1.5$ as the frequency of TM_{02} mode is situated far away from the dominant mode frequency in the frequency spectrum, and it is more prominent for the cases with $W/L > 1.5$. The elaborate qualitative and quantitative discussions in [4] establishes that, the deviation of magnetic field (H) locus beneath the patch due to the placement of feeding probe is the key reason for high XP in RMAs.

Few investigations, e.g. by modifying the feed structure [5], [6] and ground planes [7], [8] for microstrip antenna were reported to have 15-18 dB of XP suppression. These include the dual feeding with 180° phase difference, meandered line feeding or W and U shaping of ground planes. Nevertheless, these structures suffer from either complex manufacturing process or composite feeding techniques. Beside this, the employment of defected ground structure (DGS) [9]-[13], defected patch surface (DPS) [14], [15] and shorting techniques [16]-[18] have been reported to have successfully achieving improved co-polar to cross polar radiation isolation (CP-XP isolation). In these techniques, polarization purity of RMA can be improved to higher degree than feed or ground plane modification techniques. Around 19 dB-22 dB of CP-XP isolation with no improvement in gain has been achieved with different DGS geometries [9]-[13]. However, in all the cases of DGS integrated RMA, the H plane XP suppression occurs mainly near the bore sight at the cost of enhanced XP radiation near the back side (at around $\pm 150^\circ$ or $\pm 160^\circ$) of the antenna at its H plane [12]. On the contrary, DPS technique can improve the CP-XP isolation in the entire elevation angle and around 24 dB of isolation is achieved [14], [15]. However, this technique suffers from poor impedance matching, because it is difficult to place the feeding probe due to the placement of defect on the patch surface. Consequently, the antennas cannot be fed optimally and hence suffers from poor radiation efficiency and gain. The RMA with shorted edge [16]-[18] give around 20 dB-25 dB of CP-XP isolation. Nevertheless, in [16], the excited mode is TM_{11} and its operating frequency becomes 26% higher than the conventional RMA. It is evidently against the era of miniaturization of the patch and moreover, the structures [16]-[18] have complex manufacturing process. Out of all the DGS

integrated RMA, only in [11], the technology is applied to 2×2 array and around 20 dB of CP-XP isolation is revealed in the report. However, the single DGS integrated RMA reported in [11] has inadequate gain of 6 dB with poor impedance matching.

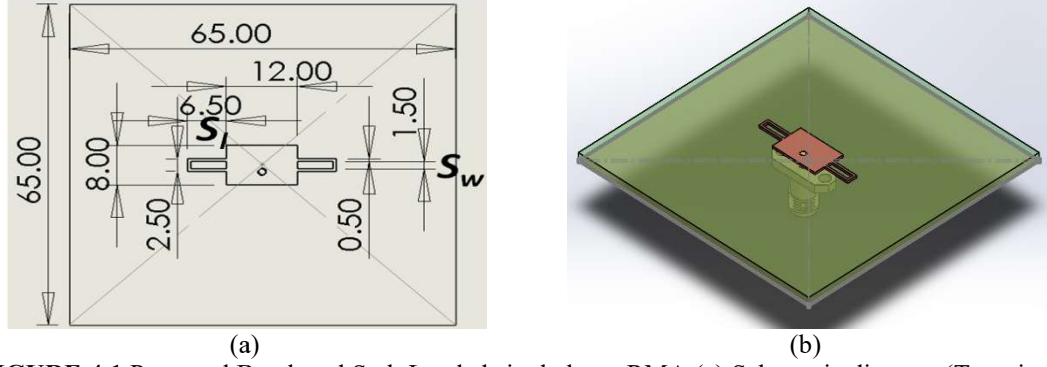


FIGURE 4.1 Proposed Bracketed Stub Loaded single layer RMA (a) Schematic diagram (Top view), (b) 3D CAD image.

Furthermore, the structure is intuitive and suffers from back radiation in terms of H plane XP fields as is expected from DGS structures.

In order to alleviate the lacunae of the earlier techniques, in the present chapter the CP-XP isolation issue has been addressed with a novel approach by employing stub loaded RMA. In the present work, a pair of bracketed stub of length slightly greater than $\lambda_g/4$ has been integrated centrally nears the non radiating edge of a conventional RMA to achieve best impedance matching. It modulates the magnetic (H) field locus in an excellent way. In general, the H field locus beneath a conventional RMA takes arc shape due to placement of feed or probe [4]. Hence, electric field distribution over the lower and upper half section of the patch gets modified, and in turns enhances the XP radiations from RMA. However, the H field locus should be along the central part of the patch following a linear locus from $-W$ to $+W$ as suggested in conventional cavity model [4]. It will create a uniform distribution of electric fields between lower and upper half section of the patch that results in improving the CP-XP isolation. The same phenomena is observed with the proposed bracketed stub loaded single layer RMA with a pair of stub of length slightly greater than $\lambda_g/4$. Also, instead of suppressing higher order orthogonal TM_{02} mode, the effort has been given to restrict spurious radiation from probe that is a major factor of XP radiation. The schematic and 3D CAD design of the proposed bracketed stub loaded single layer RMA is shown in **Fig. 4.1**. The proposed antenna

also exhibits better aperture field distribution than that of a conventional RMA to achieve higher gain. Around 8 dBi peak CP gain with more than 27 dB of CP-XP isolation is achieved with single antenna. Furthermore, to investigate the compatibility of the proposed structure in array, a 2 element array has been examined and 10 dBi peak CP gain with more than 27 dB of CP-XP isolation is obtained from the 2 element array.

The proposed structure is completely planar and simple, and it can exhibit multiple functionalities in single and array configuration. Unlike earlier works, no slot or short have been made on the ground plane and patch surface. Also, the effect of feed inductive reactance is nullified using capacitive reactance produced by a pair of bracketed stubs, which helps to achieve excellent impedance matching. Such excellent impedance matching brings linearity in the H field locus from $-W$ to $+W$ that creates uniform distribution of electric fields between lower and upper half section of the patch, leading to the XP suppression with high gain.

4.2 Parametric Studies and Design Approach

Qualitative and quantitative analysis has been given in succeeding sections for Bracketed Stub Loaded RMA based on simulations and measurements.

4.2.1 Effect of feed position on a bracketed stub loaded RMA for a fixed stub line of length S_l :

First, a pair of bracketed shorted stub line of length $S_l = 6$ mm is connected at the central part of a non radiating edge the patch (length $L = 8$ mm, width $W = 12$ mm designed on PTFE substrate with thickness $h = 1.575$ mm and relative permittivity $\epsilon_r = 2.33$) as shown in **Fig. 4.1**. The simulated [19] electric current vectors and reflection coefficient of a bracketed stub line loaded RMA ($L = 8$ mm, $W = 12$ mm and $S_l = 6$ mm) with different feed positions (fed near edge and fed near centre) are presented in **Fig. 4.2**. From simulation [19], it is apparent that the current from feed or probe will travel through the stub lines and this allows the current to move through a little longer path length that in turn produces lower frequency. However, it is also dependent on the probe positions, for example when the probe is near the centre of the patch (**Fig. 4.2(b)**), much of the currents will follow the longitudinal path towards the radiating edge of the patch as is the case for conventional RMA. On the contrary, while, the patch is fed near the edge (**Fig.**

4.2(a)), a portion of currents will follow the path through stub lines along with the conventional longitudinal current path. Therefore, the probe position may be shifted towards the edge to allow the current to follow the stub lines. On the contrary, if the probe position is near the centre i.e. slightly offset from the centre, much of the currents will follow the conventional path, and the operating frequency will be constant and same as the dominant mode frequency of conventional RMA. The corresponding reflection coefficient profiles for both cases are depicted in Fig. 4.2(c). In both the feed positions, the antenna is matched with feeder.

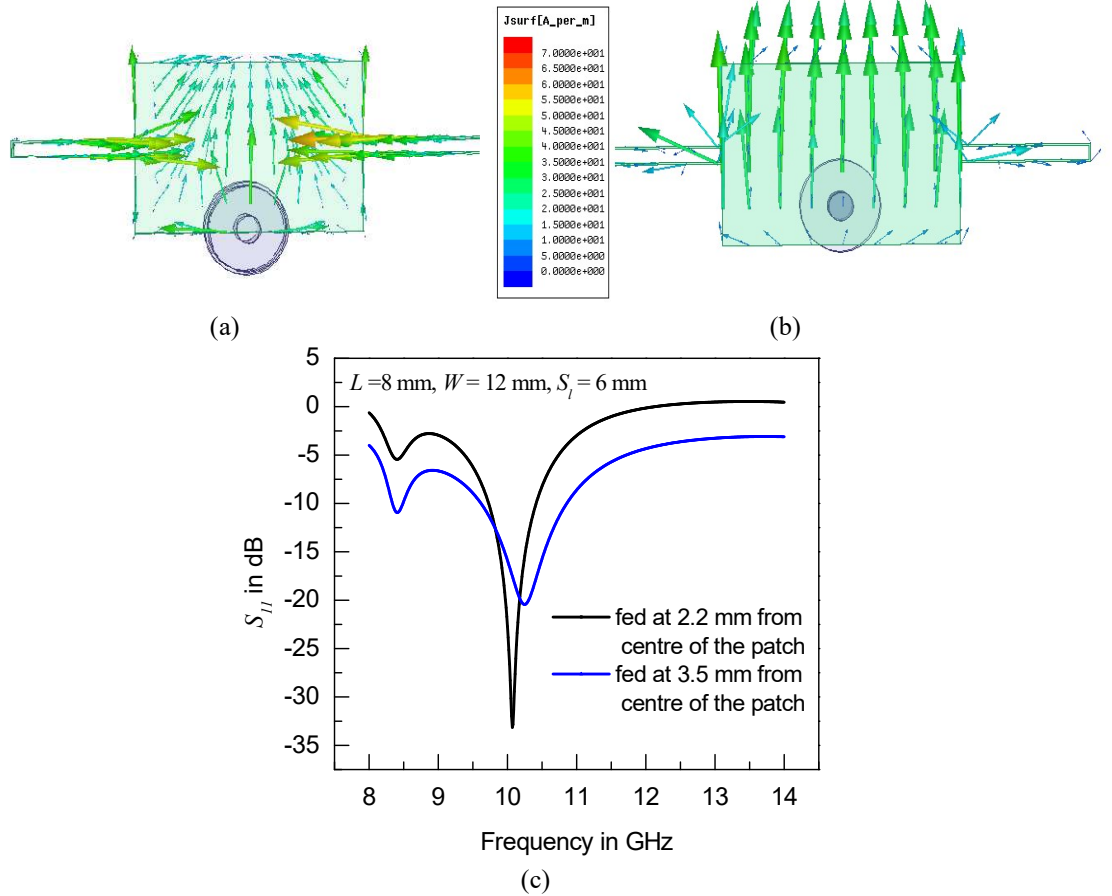


FIGURE 4.2 The simulated [19] electric current vectors and reflection coefficient profiles for a bracketed stub loaded RMA ($L = 8$ mm, $W = 12$ mm and $S_t = 6$ mm) with different feed positions (a) electric current vectors patch fed near edge and (b) electric current vectors patch fed near centre, (c) reflection coefficient profiles for both the cases.

Indeed, the conjecture of the different current paths due to shift in feed position is confirmed from both the figures (Figs. 4.2(a) and (b)). Although, a patch fed near the edge can yield miniaturization, the matching between the feed and antenna is still poor. Furthermore, the currents in the stub line produces y-polarized orthogonal

current that enhances the XP radiation. Therefore, efforts have been given to suppress the lower frequency and to excite the same frequency equivalent to conventional RMA with $L = 8$ mm, $W = 12$ mm by modulating the feed position.

4.2.2 Effect of Stub line length S_l on the impedance matching of a bracketed stub loaded RMA for fixed probe position:

To examine the effect of stub lengths on impedance matching for optimized feed position, the simulated reflection coefficient of the bracketed stub line loaded RMA with different stub length S_l are presented in **Fig. 4.3**. Here, a conventional RMA (with $L = 8$ mm, $W = 12$ mm fabricated on PTFE substrate with $h = 1.575$ mm and $\epsilon_r = 2.33$) produces its lowest order dominant TM_{10} mode at 10.22 GHz. It is noticed from **Fig. 4.3**, that the present bracketed stub line loaded RMA also resonates at the same mode. It may be noted that, when $S_l < 5$ mm; the present bracketed stub line loaded RMA cannot excite any mode. Hence, in **Fig. 4.3**, we refrain from giving the results for the cases when $S_l < 5$ mm. The same reason has been explained in subsequent section.

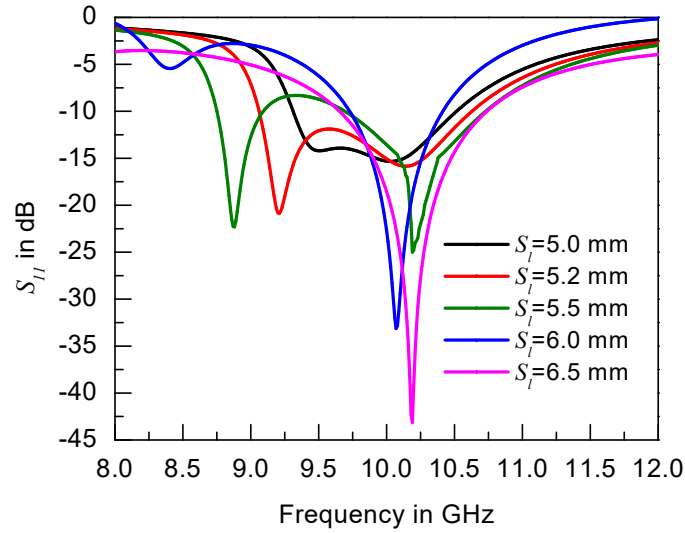


FIGURE. 4.3. The simulated [19] reflection coefficient profiles for the bracketed stub loaded RMA for different stub length S_l

On the contrary, when $S_l \geq 5$ mm; the present antenna will excite near 10 GHz. However, it is interesting to note from **Fig. 4.3** that there is a possibility of excitation of a mode with lower frequency spectrum which is more prominent when $S_l = 5.2$ mm and 5.5 mm. Notably modes with lower frequencies such as $f = 8.88$ GHz ($S_l = 5.5$ mm) and $f = 9.20$ GHz ($S_l = 5.2$ mm) are also excited with the

conventional operating frequency of $f = 10.2$ GHz. It is further observed that as the stub length increases beyond $S_l = 0.25\lambda_g = 5$ mm, the matching becomes gradually better. The best matching is obtained with stub length $S_l = 0.33\lambda_g = 6.5$ mm. This is expected because of the capacitive reactance produced by the stub of length $S_l > 0.25\lambda_g$ balancing the inductive reactance produced by the feed and hence achieving better matching. The simulated impedance locus on the smith chart is depicted in **Fig. 4.4** for conventional as well as present bracketed stub loaded RMA with different stub lengths S_l . Here, this bracketed stub of length S_l may be considered as a short circuited transmission line that produces input reactance of

$$Z_{in} = jZ_0 \tan(kS_l) \quad (4.1)$$

at the patch surface [20] where, $k = 2\pi/\lambda_g$ and Z_0 is the characteristic impedance of the line. This input impedance of short circuited transmission line follows the oscillatory profile with S_l and produces inductive and capacitive reactance for $S_l = 0$ to $0.25\lambda_g$ and $S_l = 0.25\lambda_g$ to $0.5\lambda_g$ respectively.

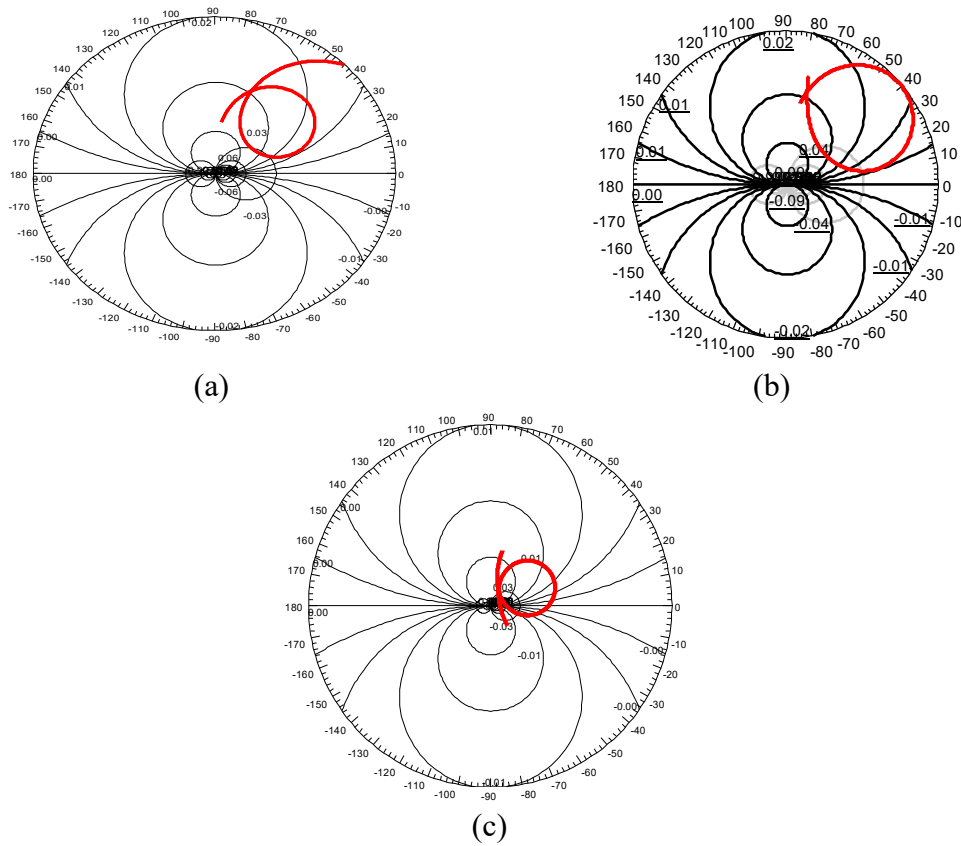


FIGURE 4.4. The simulated impedance locus on the smith chart for (a) conventional RMA, (b) bracketed stub loaded RMA with $S_l = 4.8$ mm ($S_l < 0.25\lambda_g$), (c) bracketed stub loaded RMA with $S_l = 6.5$ mm ($S_l > 0.25\lambda_g$)

This reactance definitely modulates the probe input reactance and hence the probe input reactance of stub loaded patch follow the oscillatory nature as the stub length is increasing in [21]. In general, the probe fed patch has high inductive reactance due to the probe inductance. Because of this high inductive reactance, probe fed microstrip patch often suffers from poor impedance matching.

Therefore, From **Fig. 4.4(a)**, the impedance locus is found to lie on the upper section of the Smith Chart for conventional RMA. if the bracketed stub loaded RMA with $S_l = 4.8$ mm is used ($S_l < 0.25\lambda_g$ which produces inductive reactance at the input of stub), the patch input impedance becomes more inductive and the impedance locus shifts upward compared to conventional RMA as is observed from **Fig. 4.4(b)**. It is well known that, in microstrip patch antennas, the probe is characteristically inductive and it prevents from good matching of the antenna impedance with input connector or probe [22]. Therefore, as the probe is inherently inductive, further increase in the inductive reactance due to the stub is not useful for impedance matching. Hence, the bracketed stub loaded RMA with $S_l = 4.8$ mm ($S_l < 5$ mm $\sim 0.25\lambda_g$) cannot excite proper radiating mode. The simulated input impedance profile of the patch (with $S_l = 4.8$ mm), and compared with the conventional patch has been depicted in Fig. 4.5 The simulated S_{11} profile of the bracketed stub loaded RMA with $S_l = 4.8$ mm is also been shown in the same plot that confirms the observation. It is found that the input reactance of conventional RMA is 40Ω while the same for bracketed stub loaded RMA with $S_l = 4.8$ mm is 70Ω .

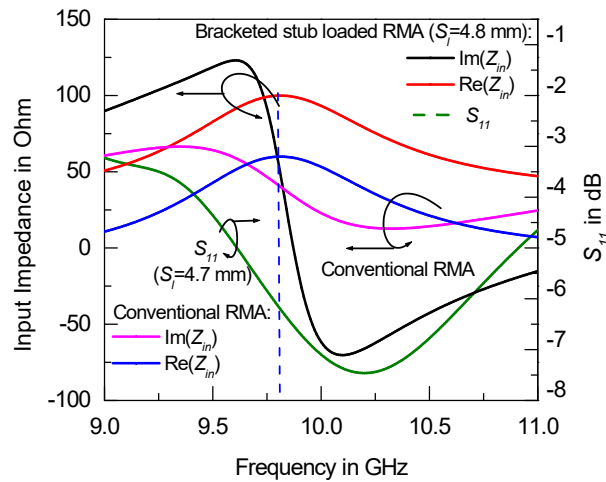


FIGURE 4.5. Reflection coefficient of the bracketed stub loaded RMA with $S_l < 5$ mm i.e $S_l = 4.8$ mm and input impedance of the same and conventional RMA.

Moreover, input resistance has also been increased from 60Ω to 100Ω due to the incorporation of stub ($S_l = 4.8 \text{ mm}$). On the contrary, in the bracketed stub loaded RMA with $S_l = 6.5 \text{ mm}$ ($S_l > 0.25\lambda_g$ that produces capacitive reactance at the input of stub), the inductive reactance is reduced and the patch input impedance locus shifts downward (**Fig. 4.4 (c)**). This confirms the direct influence of the reactance of inductive stub ($S_l = 4.8 \text{ mm} < 0.25\lambda_g$) and capacitive stub ($S_l = 6.5 \text{ mm} > 0.25\lambda_g$) on patch input reactance and reveals more better matching in case of present structure with capacitive stub of length $S_l = 6.5 \text{ mm}$.

For further corroboration of the conjecture, the input impedance of conventional RMA and bracketed stub loaded RMA (with $S_l = 5.5 \text{ mm}$, 6.0 mm and 6.5 mm ($S_l > 0.25\lambda_g$ in all the cases) are studied and presented in **Fig. 4.6**. For the bracketed stub loaded RMA, as stub length increases, the input resistance of the patch decreases as in [21]. By further observing **Fig. 4.6**, it shows that as soon as the stub is connected, the input reactance of the patch decreases drastically from 40Ω (conventional RMA) to 19Ω (bracketed stub loaded RMA with $S_l = 5.5 \text{ mm}$).

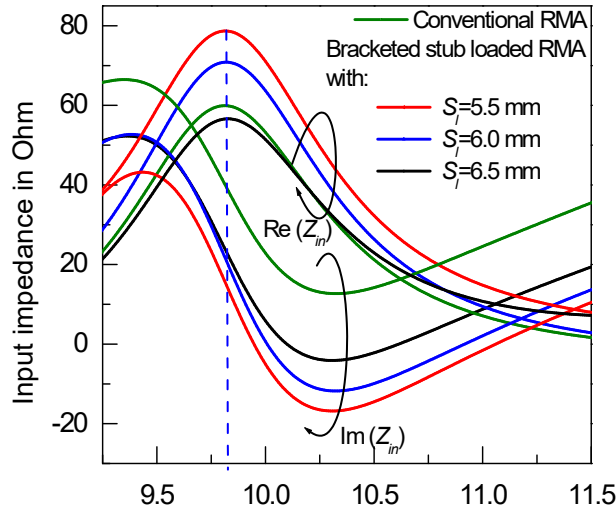


FIGURE. 4.6. Input impedance of conventional RMA and bracketed stub loaded RMA (with $S_l = 5.5 \text{ mm}$, 6.0 mm and 6.5 mm ($S_l > 0.25\lambda_g$ in all the cases))

In fact, the high capacitance produced by the stub of length 5.5 mm (which is greater than $\lambda_g/4 = 5 \text{ mm}$) reduces the patch input reactance and hence the inductive reactance of the feed is mitigated. Next, as S_l increases, the capacitance decreases (following equation (1)) and hence the patch input reactance is slightly increased. In fact, the capacitive reactance produced by stub changes with stub length following

equation (1), which directly influence the probe inductance. Nevertheless, the increment of probe inductive reactance is marginal with $S_l = 5.5$ mm to 6.5 mm and produces no such effect in matching. It is found that the patch input inductive reactance increases from $19\ \Omega$ to $21.5\ \Omega$ when S_l increases from 5.5 mm to 6.5 mm. However, the input resistance of the patch decreases significantly from $78\ \Omega$ to $55.5\ \Omega$ as S_l increases from 5.5 mm to 6.5 mm. This is expected as the effective width of the structure increases due to the incorporation of stubs [2], [23] with larger S_l value. Consequently, the patch input impedance becomes well matched with input probe and hence offers better matching of the proposed antenna.

In conclusion, (i) compensation of the feed reactance can be achieved by tuning the stub, (ii) reduction of input resistance towards $50\ \Omega$ for better matching of bracketed stub loaded RMA can be attained by setting $S_l = 6.5$ mm. Also, the probe inductance compensation by capacitive stub is not effective if the probe is distant from the patch centre because of the reduction of inductive reactance of the probe with distance from the patch centre [24]. Further increase in S_l does not show significant effect on the resonant frequency or the impedance matching of the present bracketed stub line loaded RMA. Hence, we refrain from giving the results for the cases when $S_l > 6.5$ mm.

4.2.3 Influence of Stub line length S_l on the XP characteristics of a bracketed stub loaded RMA for optimized probe position

The influence of the stub line length on the CP-XP isolation of the present bracketed stub line loaded RMA is investigated. The feed location is optimized near the centre of the patch as discussed in section 4.2.1. It has been discussed in section 4.2.2 that there is an excitation of a mode at lower frequency spectrum for $S_l = 5.2$ mm and 5.5 mm along with the conventional dominant mode frequency. The H plane radiation pattern has been examined for both the frequencies in case of $S_l = 5.5$ mm. The resulting plot is presented in **Fig. 4.7(a)**. It is noted that at lower frequency ($f = 8.88$ GHz), the XP radiation is similar to CP radiation, which is expected because of appreciable y polarized orthogonal electric current as discussed in section 4.2.1. Nevertheless, around 21 dB of CP-XP isolation is clearly noticed at $f = 10.2$ GHz.

It may be noted from **Fig. 4.7(a)** that at the lower frequency ($f = 8.88$ GHz), the XP peaks at 45° while the main CP 3dB beam width is 34° . Therefore, XP peak is

far off from 3dB CP beam and will not cause disturbance in the main beam. Nevertheless, within 3dB main beam, CP-XP isolation at 8.88 GHz is not satisfactory and is around 10-20 dB only. Hence, the structure with $S_l = 5.5$ mm may be useful for dual band applications where this 8.88 GHz signal (1st band) can be used for wireless applications in multi path environment [25], where CP-XP isolation is not an issue. Here, the same structure with $S_l = 5.5$ mm may also be used in borehole radar measurements, where both polarizations are required to obtain more precise data [26].

It is noteworthy that the impedance matching is poor in both bands for the structure with $S_l = 5.5$ mm as is revealed from **Fig. 4.3**. Nevertheless, in the present investigation, the main attempt has been given to conceive a completely planar structure with excellent impedance matching and CP-XP isolation. Therefore, the efforts have been given to suppress the lower frequency and to achieve best matching at the conventional $f = 10.2$ GHz frequency by optimizing the stub length. In fact, improved impedance matching produces more efficient feeding mechanism that in turn results in uniform field distribution between the lower and the upper half sections of the patch, which results in exhibiting two fold improvements i.e. the CP-XP isolation becomes much better as well as the gain of the antenna becomes higher due to uniform aperture distribution at $f = 10.2$ GHz. The simulated H plane radiation pattern for different length of S_l is shown in **Fig. 4.7(b)** at $f = 10.2$ GHz.

As the matching becomes better, CP-XP isolation also improves. The bracketed stub line loaded RMA with $S_l = 0.33\lambda_g = 6.5$ mm produces more than 26 dB CP-XP isolation in the entire elevation angular range (**Fig. 4.7(b)**). The simulated gain of the same bracketed stub line loaded RMA is around 8 dBi.

4.2.4 Physical Insight into the XP radiation suppression of bracketed stub loaded RMA for optimized probe position

As shown in **Fig. 4.8(a)**, a conventional RMA develops an asymmetric field distribution beneath the patch resulting in an arc shaped H field locus. Therefore, the horizontal component of the electric field excited from the patch corners will produce XP radiation as they are not uniform between the upper and lower section of the patch, as shown in **Fig. 4.8(b)**. On the contrary, as shown in **Fig. 4.8(c)**, in the

bracketed stub loaded RMA with stub length $S_l = 0.33\lambda_g = 6.5$ mm, symmetrical field distribution is developed between the upper and lower section of the patch and by

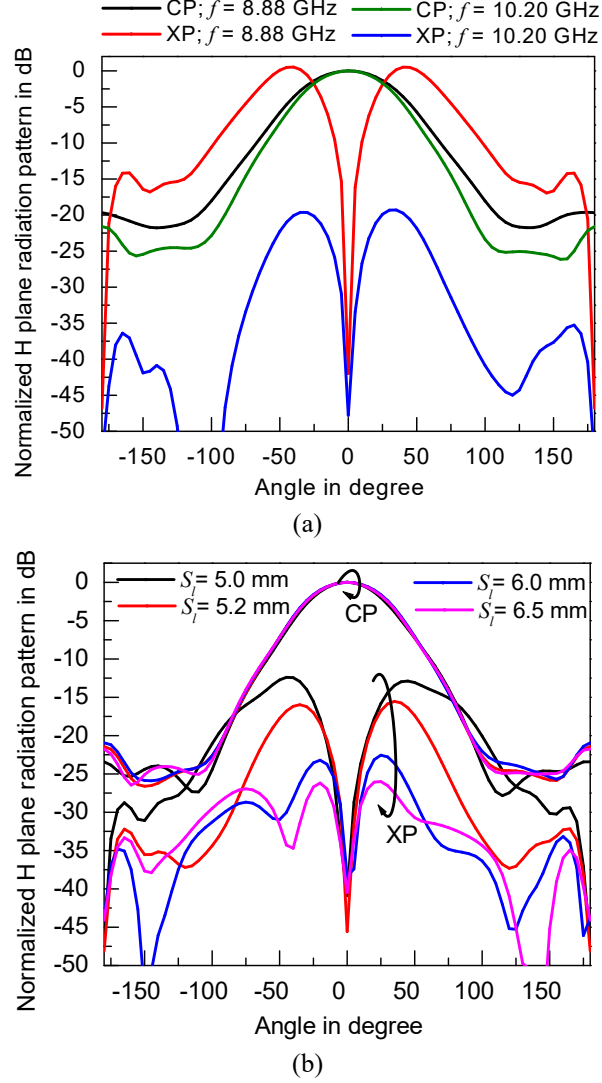


FIGURE 4.7. (a) The simulated H plane radiation pattern of a bracketed stub loaded RMA ($L = 8$ mm, $W = 12$ mm and $S_l = 5.5$ mm) at different frequencies, (b) The simulated H plane radiation pattern of a bracketed stub loaded RMA at different stub length S_l .

this means, the equivalent horizontal component of E field from the upper and lower corners of the patch will cancel each other and hence, reduces the XP radiation, as shown in **Fig. 4.8(d)**. It may be noted that, the stub length is kept a little longer than $0.25\lambda_g$. This is done to create very less (nearly minima) E field (between stub and ground plane) near the central part of non radiating edge of the RMA. It increases the H field at the central part of the non radiating edge of the RMA, and leads to modification of H field locus from arc shape to linear along $-W$ to $+W$. Hence, matching is improved and field distribution becomes symmetric between the upper

and lower section of the patch. Hence, XP radiation is suppressed with higher CP gain.

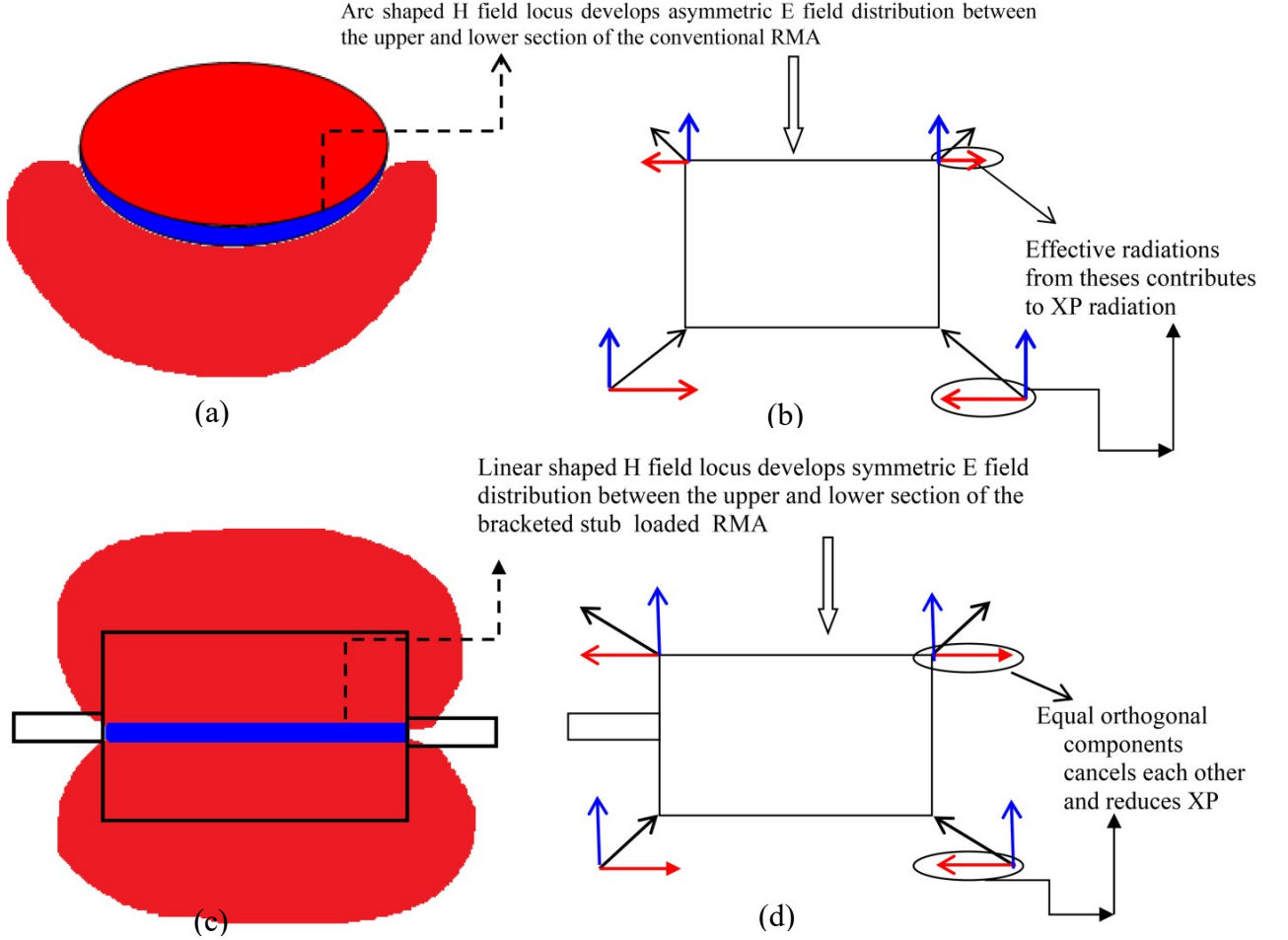


FIGURE 4.8. (a) E (red-max) and H (blue-max) field distribution over the substrate for conventional RMA, (b) corresponding E field component at patch corners for conventional RMA, (c) E and H field distribution over the substrate for single bracketed stub loaded RMA, (d) corresponding E field component at patch corners for single bracketed stub loaded RMA.

4.2.5 The Effect of Stub Width on the Performance of bracketed stub loaded RMA

The effect of stub width S_w on the performance of bracketed stub loaded RMA are investigated and presented in **Fig. 4.9**. In the proposed structure, the stub width S_w is fixed at 1.5 mm. Instead of decreasing S_w (which will make the fabrication process more complex), the effect of increasing S_w on reflection coefficient and input impedance profile are depicted in **Fig. 4.9(a)** and **(b)**, respectively. **Fig. 4.9(a)** indicates that the operating frequency of the proposed structure increases with the width of the stub S_w . In fact, following the literatures

[21], [27], it may be concluded that as width of the stub S_w increases from 1.5 mm to 3 mm, the fringing length ΔL decreases slightly. This may be attributed for slight increase in operating frequency

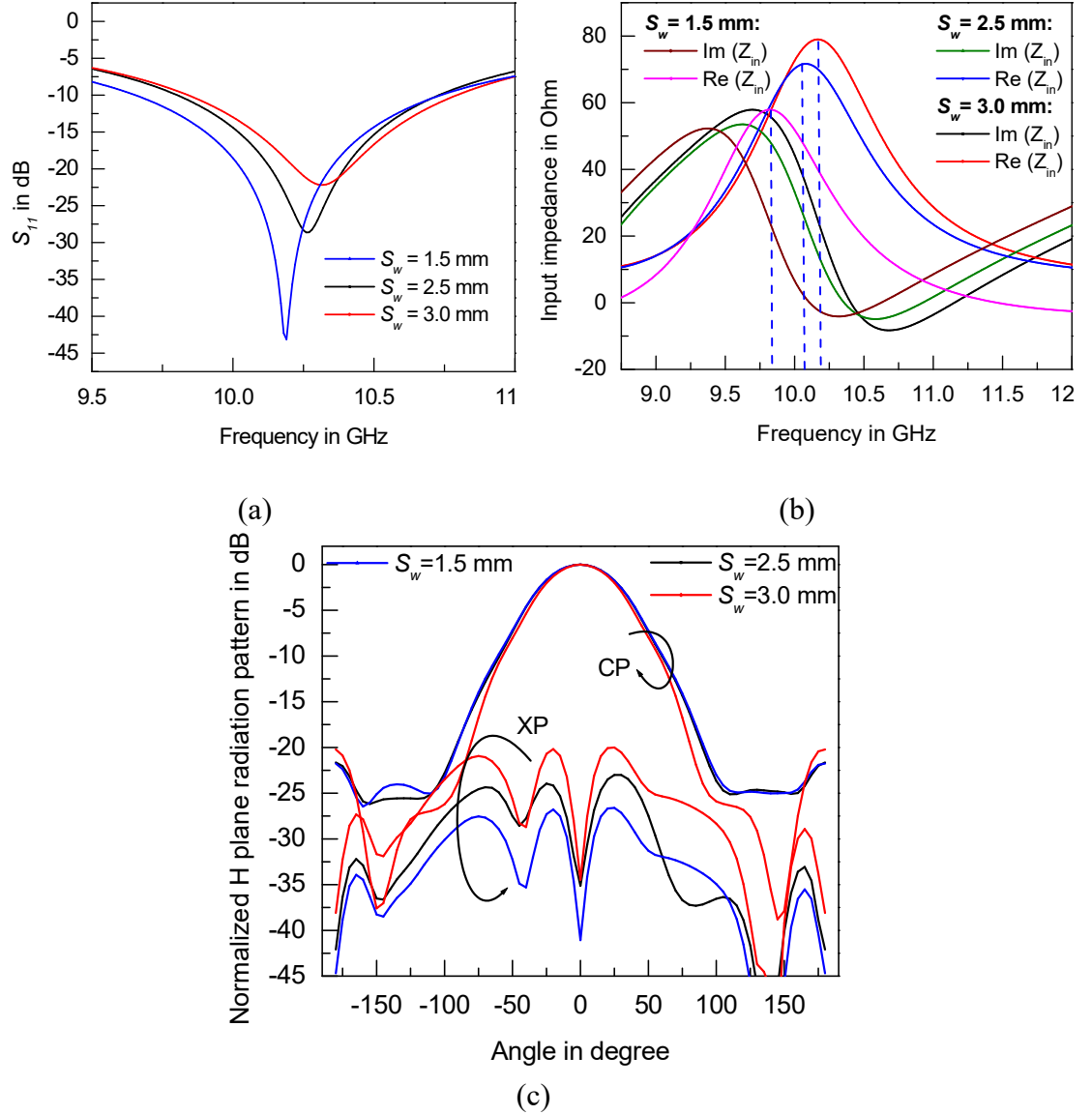


FIGURE 4.9 (a) Reflection coefficients profiles and (b) the input impedance profiles of bracketed stub loaded RMA with different stub widths S_w , (c) Normalized H plane radiation pattern of bracketed stub loaded RMA with different stub widths S_w

with the increment of stub width. Nevertheless, it is noteworthy that as S_w increases from 1.5 mm to 3 mm, the input impedance matching becomes poorer. The input impedance for all three cases is depicted in **Fig. 4.9(b)**. In this figure, the input reactance remains unaffected and maintains between 21.5Ω to 22Ω with the

increment of S_w from 1.5 mm to 3 mm. On the contrary, the input resistance increases from 56Ω to 80Ω as S_w increases from 1.5 mm to 3 mm. In fact, the increment of operating frequency increases the electrical thickness (h/λ_0) of the structure with $S_w > 1.5$ mm. Hence the input resistance increases with S_w values [2],[23] which in turn affect the input impedance matching of the bracket stub loaded RMA for $S_w > 1.5$ mm. Consequently, the polarization purity degrades as is noted from Fig. 4.9(c).

4.3 Proposed Structure

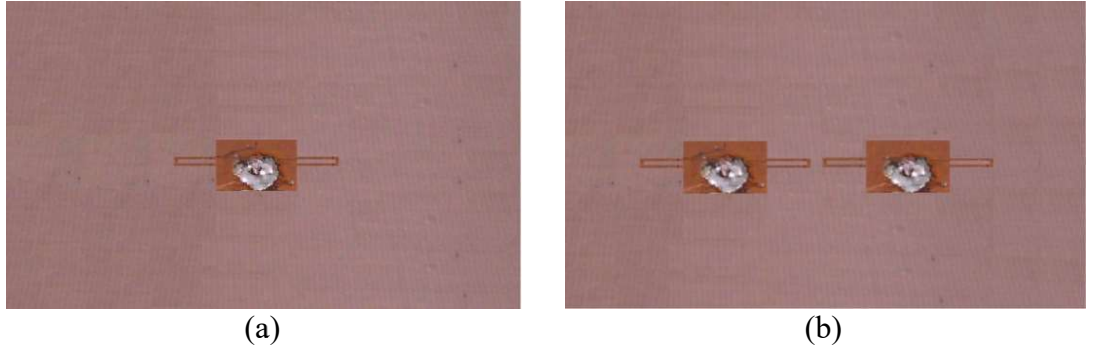
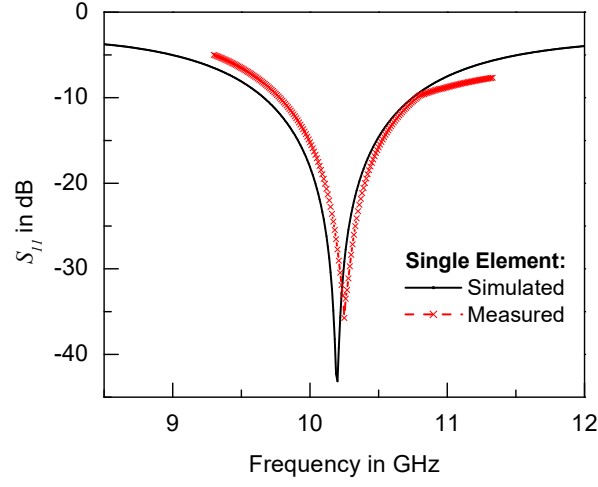


FIGURE 4.10 Image of fabricated BSRMA prototypes (a) Single element, (b) array antenna of two elements

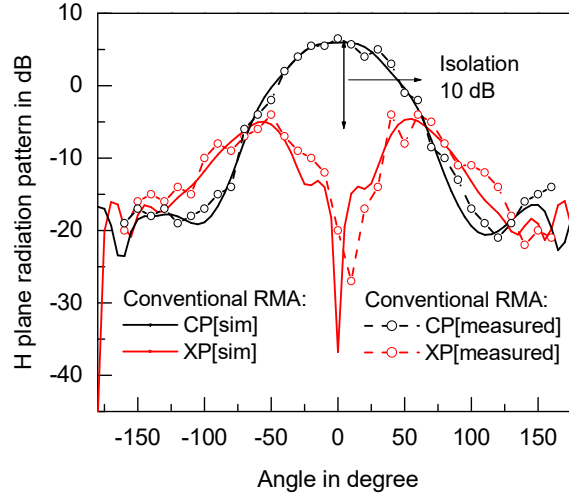
An RMA with $L = 8$ mm, $W = 12$ mm was fabricated on PTFE substrate of thickness $h = 1.575$ mm and relative permittivity $\epsilon_r = 2.33$. A planar shorted stub of length $S_l = 6.5$ mm was incorporated at the central part of non radiating edge as shown in Fig. 4.1. The short circuited stub is created with thin copper strips of 0.5 mm thickness. The width of the stub S_w i.e. the gap between horizontal strips is around 1.5 mm. The antenna is fed at a distance 2.1 mm from the centre of the patch. In addition to that, a two element array (constituted with same structure) was fabricated on a $65 \times 80 \text{ mm}^2$ ground plane. The fabricated prototypes are depicted in Fig. 4.10(b) and (c).

4.4 Results and Analysis

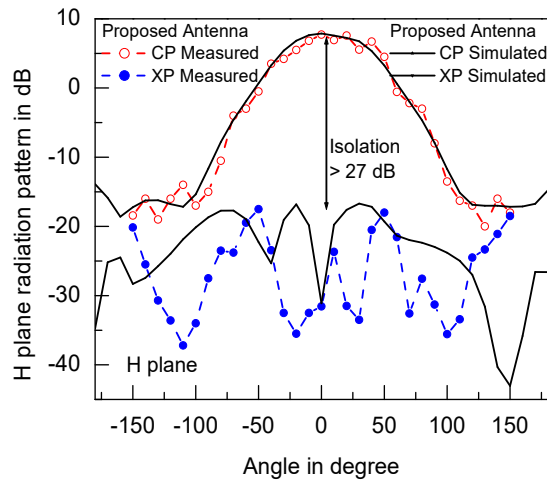
Results and analysis of the design with help of simulation and measurements is enumerated in succeeding sections for single element and also for an array of 2×1 .



(a)



(b)



(c)

FIGURE 4.11. (a) Simulated and measured reflection coefficient profile for the proposed bracketed stub loaded RMA, (b) Measured and simulated H plane radiation pattern for the conventional RMA ($L = 8$ mm, $W = 12$ mm) and (c) Measured and simulated H plane radiation pattern for the proposed bracketed stub loaded RMA ($L = 8$ mm, $W = 12$ mm and $S_l = 6.5$ mm) ($f = 10.2$ GHz).

4.4.1 Single Element Bracketed Stub Loaded RMA

In this section, measured results for single bracketed stub loaded RMA are discussed. **Fig. 4.11(a)** shows the measured reflection coefficient of a single element bracketed stub line loaded RMA. An excellent matching between the bracketed stub line loaded RMA and the feed is clearly shown from the figure for both the simulation and measurement. It is observed that the antenna is resonating at 10.22 GHz. Slight disagreement between measured and simulated results may be due to fabrication error. As shown in **Fig. 4.11(a)**, the proposed structure works in the frequency range from 9.64 GHz to 10.75 GHz, which yields 11% impedance bandwidth. The H plane radiation patterns for conventional RMA and bracketed stub loaded RMA are presented in **Fig. 4.11(b)** and **(c)**. From **Fig. 4.11(c)**, more than 27 dB of CP-XP isolation along with high gain of 8 dBi are observed from the bracketed stub loaded RMA. On the contrary, only around 10 dB of CP-XP isolation with 6 dBi gain are demonstrated by the conventional RMA, as shown in **Fig. 4.11(b)**. Following [16], the field distribution over the aperture is plotted for both the conventional RMA and proposed bracketed stub line loaded RMA, as depicted in **Fig. 4.12**. Indeed, the modulation of H field locus from its arc shape (**Fig. 4.12(a)**; conventional patch) to linear from $-W$ to $+W$ (**Fig. 4.12(b)**; proposed structure) is apparent from the figure that leads to better symmetry in electric fields between the upper and lower sections of the patch as discussed in section 4.2.4. This further confirms the justification developed in relation to **Fig. 4.8**. Therefore, it may be concluded that the aperture field distribution becomes more uniform in proposed structure as compared with conventional patch, and this may be attributed for high gain and improved polarization performance of the proposed structure.

4.4.2 Two Element Array Antenna of Bracketed Stub Loaded Single Layer RMAs

The results of 2 element array constituted by same bracketed stub line loaded RMA are shown in **Fig. 4.12(c)** and **(d)**. To avoid the grating lobes in broadside array, the element spacing should be less than λ [28]. Following the restriction, the inter-radiator spacing is kept 5 mm. Although the present structure is extended along the y direction, this gap can easily be incorporated in between the elements, as the

permissible separation between the radiators is 19.26 mm at 10.2 GHz frequency [28]. The measured and simulated S parameters are depicted in **Fig. 4.12(c)**. Notably, the impedance matching is consistently good for both the antennas and the isolation between them is below 27 dB. However, **Fig. 4.12(c)** shows slight disagreement between the simulation and measurements in terms of S_{12} , and this may be due to fabrication error.

The measured H plane radiation pattern of the antenna array is presented in **Fig. 4.12(d)**. Around 10 dBi of peak gain is achieved with CP-XP isolation of more than 27 dB from the 2 elements array structure. However, the XP isolation in the E plane is always below 35 dB, and hence the E plane pattern is not given, for brevity.

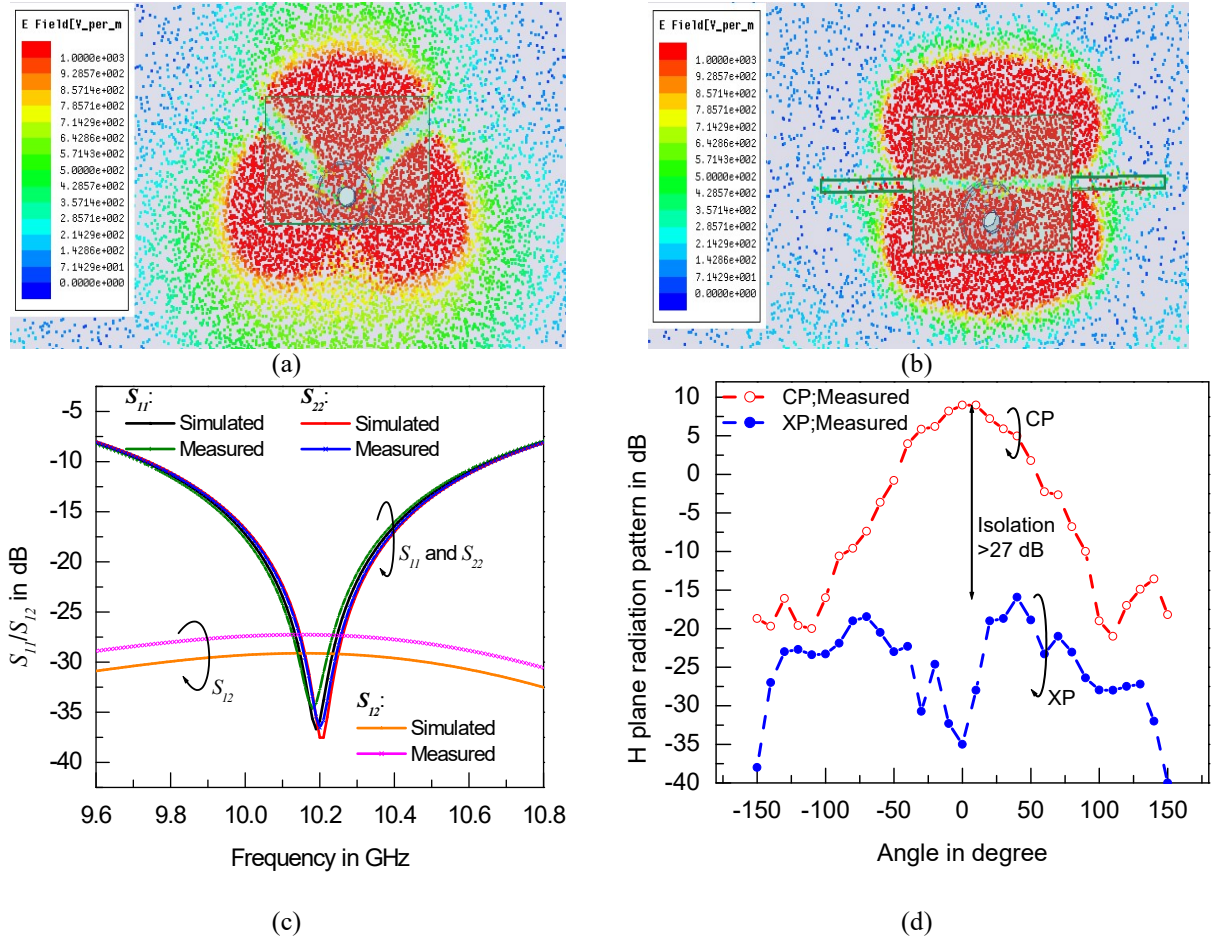


FIGURE 4.12. (a) Simulated electric field distribution over the aperture of single element conventional RMA, (b) Simulated electric field distribution over the aperture proposed single element bracketed stub loaded RMA (c) Simulated and measured S parameters of 2 element array constituted by proposed bracketed stub loaded RMA, (d). Measured H plane radiation pattern of 2 element array constituted by proposed bracketed stub loaded RMA.

TABLE 4.1 : Comparison of present antenna with other recently reported results

Ref. No.	Structural properties /Configuration	Impedance matching (S_{11} (dB) at resonance)	CP-XP isolation (Angular region)	Gain (dBi)	Suitability in array structure	Remarks
[29]	Square patch with symmetric DGS	-37	25dB ($\pm 60^\circ$)	7.5	-	Polarization purity has been achieved over narrow angular range around bore sight, increased back radiation due to DGS
[30]	Shorting pin loaded square patch	-	17.7dB ($\pm 90^\circ$)	< 0	Yes	Gain lower than 0 dB
[11]	Rectangular patch array (2x2) with DGS	-24	20 dB ($\pm 95^\circ$)	12.2	Yes	Complex DGS structure and hence suffers from increased back radiation
[13]	Rectangular patch with asymmetric DGS	-19	19dB ($\pm 110^\circ$)	7	-	Defect geometry is complex and asymmetric, poor matching and suffers from increased back radiation
[31]	Differentially fed dual polarized antenna	-	10dB ($\pm 60^\circ$)	7.9	Yes	Improvement in polarization purity is not apparent, Complex structure
[32]	Air loaded rectangular patch with capacitive fed	-17	19dB ($\pm 50^\circ$)	9	Yes	Improvement in polarization purity over narrow angular range, poor matching
[33]	Rectangular patch with shorting wall and pins	-25	21dB ($\pm 50^\circ$)	8	-	Too many shorting pins and long shorting walls make structure complex
[34]	EH shaped slotted multiple stacked patch antenna	-21	40dB ($\pm 180^\circ$)	11.2	-	High profile, Complex fabrication & feeding mechanism due to multilayer alignment. XP suppression is shown in E plane only
[35]	Graphene based multilayered structure	-27	20dB ($\pm 90^\circ$)	2	-	Multilayered structure, Gain is too low
Present Structure	Bracketed stub loaded RMA	-37	27dB ($\pm 180^\circ$)	10	Yes	Simple single layer structure and low back radiation of 24 dB lower than peak CP radiation.

4.4.3 Comparative Evaluation

The performances of the proposed bracketed stub loaded RMA are compared with recent literatures [29]-[35] and shown in **Table 4.1**. Here, the proposed structure exhibits excellent impedance matching and polarization purity along with high gain. It is also observed that the structure is suitable in array configuration. Therefore, the structure, with high gain and excellent CP-XP isolation in the entire elevation range may be helpful for antenna community to meet the demand of modern wireless communication, as well as different military wireless applications.

4.5 Conclusions

A single layer and planar bracketed stub loaded RMA has been successfully investigated for high gain and low XP radiation in the entire elevation angle. In this concept, the modulation of locus of the magnetic field generated due to feeding by probe has been exploited to evolve a simple and single element with single copper layer structure. This is done with a view to enhance radiation performance by improving impedance matching. Unlike the earlier approaches, the present study optimizes by handling the issue of cross polar radiation in RMA due to its own dominant TM_{10} mode by modulating and ensuring the uniformity in field distribution between upper and the lower half's of a patch to repress the valuable orthogonal radiations (cross polar radiations) from the corners of a radiating patch.

In this approach, unlike the usual style no slots or shorts with the ground plane are made to suppress cross polar radiation, and hence it is a structure which is easy to fabricate. The proposed bracketed stub-loaded single layer RMA structure exhibits good and viable gain of 8 dBi with 27 dB of co-cross polar isolation in the most affected plane i.e H plane. Also, in order to enhance the gain and to study its viability in terms of array, a 2 element array was constituted. Around, 10 dBi gain with 27 dB of co-cross polar isolation was obtained. The structure is quite simple in design and can be easily fabricated. Although the gain issue can be addressed by array implementation, the issues of improved and symmetrical radiation patterns are of significant importance. Hence, some more efforts may be put to improve the co-polarized radiation characteristics.

References

- [1] T. Huynh, K.F. Lee and R.Q. Lee, "Cross-polarization characteristics of rectangular patch antennas", *Electron. Lett.*, vol. 24, no. 8, pp. 463-464, 1988.
- [2] R. Garg, P. Bhartia, I. Bhal et al., *Microstrip antenna design handbook*, Boston, MA, USA:Artech House, 2001.
- [3] Z. Chen and M.Y.W. Chia, "Broad-band suspended probe-fed plate antenna with low cross-polarization levels", *IEEE Trans. Antennas Propag.*, vol. 51, pp. 345-346, 2003.
- [4] S. Chattopadhyay and S. Chakraborty, "A physical insight into the influence of dominant mode of rectangular microstrip antenna on its cross-polarization characteristics and Its improvement with T-shaped microstrip antenna", *IEEE. Access.*, vol. 6, pp. 3594-3602, 2018.
- [5] A. Petosa, A. Ittipiboon and N. Gagnon, "Suppression of unwanted probe radiation in wide band probe-fed microstrip patches", *Electron. Lett.*, vol. 35, pp. 355-357, 1999.
- [6] V. Schejbal and V. A. Kovarik, "A method of cross-polarization reduction", *IEEE Antennas Propag. Mag.*, vol. 48, pp. 108-111, 2006.
- [7] K. L. Wong, C. L. Tang and J. Y. Chiou, "Broad-band probe-fed patch antenna with a W-shaped ground plane", *IEEE Trans. Antennas Propag.*, vol. 50, pp. 827-831, 2002.
- [8] W. H. Hsu and K. L. Wong, "Broad-band probe-fed patch antenna with a U-shaped ground plane for cross-polarization reduction", *IEEE Trans. Antennas Propag.*, vol. 50, pp. 352-355, 2002.
- [9] A. Ghosh, D. Ghosh, S. Chattopadhyay et al., "Rectangular microstrip antenna on slot type defected ground for reduced cross polarized radiation", *IEEE Antennas Wirel. Propag. Lett.*, vol. 14, pp. 324-328, 2015.
- [10] C. Kumar and D. Guha, "DGS integrated rectangular microstrip patch for improved polarization purity with wide impedance bandwidth", *IET Micro. Ant. Prop.*, vol. 8, pp. 589-596, 2014.

- [11] C. Kumar, M.I. Pasha and D. Guha, "Defected ground structure integrated microstrip array antenna for improved radiation properties", *IEEE Antennas Wirel. Propag. Lett.*, vol. 16, pp. 310-312, 2017.
- [12] D. Guha and Y.M.M. Antar, *Microstrip and printed antennas – new trends techniques and applications*, UK:John Wiley, 2011.
- [13] C. Kumar and D. Guha, "Asymmetric geometry of defected ground structure for rectangular microstrip: a new approach to reduce its cross-polarized fields", *IEEE Trans. Antennas Propag.*, vol. 64, no. 6, pp. 2503-2506, 2016.
- [14] S. Chakraborty, A. Ghosh, S. Chattopadhyay et al., "Improved cross-polarized radiation and wide impedance bandwidth from rectangular microstrip antenna with dumbbell-shaped defected patch surface", *IEEE Antennas Wirel. Propag. Lett.*, vol. 15, pp. 84-88, 2016.
- [15] A. Ghosh, S.K. Ghosh, D. Ghosh et al., "Improved polarization purity for circular microstrip antenna with defected patch surface", *Int. J. Microw. Wirel. Technol. Cambridge Univ. Press Eur. Microw. Assoc.*, vol. 8, no. 1, pp. 89-94, 2016.
- [16] D. Ghosh, S.K. Ghosh and S. Chattopadhyay, "Physical and quantitative analysis of compact rectangular microstrip antenna with shorted non-radiating edges for reduced cross-polarized radiation using modified cavity model", *IEEE Antennas Propag. Mag.*, vol. 56, pp. 61-72, 2014.
- [17] R. Poddar, S. Chakraborty and S. Chattopadhyay, "Improved cross polarization and broad impedance bandwidth from simple single element shorted rectangular microstrip patch: theory and experiment", *Frequenz*, vol. 70, no. 1–2, pp. 1-9, 2016.
- [18] N.-W. Liu, L. Zhu, W.-W. Choi et al., "Wideband shorted patch antenna under radiation of dual-resonant modes", *IEEE Trans. Antennas Propag.*, vol. 65, no. 6, pp. 2789-2796, 2017.
- [19] HFSS, High Frequency Structure Simulator, v. 14.
- [20] A.E. Daniel and G. Kumar, "Rectangular microstrip antennas with stub along the non-radiating edge for dual band operation", *IEEE Antennas and Propagation Society Int. Symp.*, pp. 2136-2139, 1995.

- [21] G. Kumar and K.P. Ray, Broadband microstrip antennas, Boston, London:Artech House, 2003.
- [22] P. S. Hall, "Probe compensation in thick microstrip patches", *Electron. Lett.*, vol. 23, no. 11, pp. 606-607, 1987.
- [23] S. Chattopadhyay, M. Biswas, J.Y. Siddiqui et al., "Input impedance of probe-fed rectangular microstrip antennas with variable air-gap and varying aspect ratio", *IET Microw. Antennas Propag.*, vol. 3, no. 8, pp. 1151-1156, 2009.
- [24] D. Guha, M. Biswas and J.Y. Siddiqui, "Harrington's formula extended to determine accurate feed reactance of probe-fed microstrip patches", *IEEE Antennas Wirel. Propag. Lett.*, vol. 6, pp. 33-35, 2007.
- [25] K.F. Lee and K.F. Tong, "Microstrip patch antennas-basic characteristics and some recent advances", *Proc. IEEE*, vol. 100, no. 7, pp. 2169-2180, 2012.
- [26] M. Sato, T. Ohkubo and H. Niitsuma, "Cross polarization borehole radar measurements with a slot antenna", *J. Appl. Geophys.*, vol. 33, pp. 53-61, 1995.
- [27] S. Chattopadhyay, M. Biswas, J.Y. Siddiqui et al., "Rectangular microstrips with variable air-gap varying aspect ratio: improved formulation and experiments", *Microw. Opt. Technol. Lett.*, vol. 51, no. 1, pp. 169-173, 2009.
- [28] R.S. Elliott, Antenna theory and design, Hoboken, NJ, USA:John Wiley, 2006.
- [29] C. Kumar, M.I. Pasha and D. Guha, "Microstrip patch with nonproximal symmetric defected ground structure (DGS) for improved cross-polarization properties over principal radiation planes", *IEEE Antennas Wirel. Propag. Lett.*, vol. 14, pp. 1412-1414, 2015.
- [30] X. Zhang and L. Zhu, "Patch antennas with loading of a pair of shorting pins toward flexible impedance matching and low cross-polarization", *IEEE Trans. Antennas Propag.*, vol. 64, no. 4, pp. 1226-1233, 2016.
- [31] Z. Tang, J. Liu and Y. Yin, "Enhanced cross-polarization discrimination of wideband differentially fed dual-polarized antenna via a shorting loop", *IEEE Antennas Wirel. Propag. Lett.*, vol. 18, no. 8, pp. 1454-1458, 2018.

- [32] C. Sarkar, D. Guha, C. Kumar et al., "New insight and design strategy to optimize cross-polarized radiations of microstrip patch over full bandwidth by probe current control", *IEEE Trans. Antennas Propag.*, vol. 66, no. 8, pp. 3902-3909, 2018.
- [33] N.W. Liu, L. Zhu, G. Fu et al., "A low profile shorted-patch antenna with enhanced bandwidth and reduced H-plane cross-polarization", *IEEE Trans. Antennas Propag.*, vol. 66, no. 10, pp. 5602-5607, 2018.
- [34] M.T. Islam, M.N. Shakib, N. Misran et al., "Low cross polarization broadband microstrip patch antenna", *Proc. of IEEE 2008 6th National Conf. on Telecommunication Technologies and IEEE 2008 2nd Malaysia Conf. on Photonics*, 2008.
- [35] J. Kumar, B. Basu, F.A. Talukdar et al., "Multimode-inspired low cross polarization multiband antenna fabricated using graphene-based conductive Ink", *IEEE Antennas Wirel. Propag. Lett.*, vol. 17, no. 10, pp. 1861-1865, 2018

CHAPTER

5

Quasi Planar Composite Rectangular Microstrip Antenna: An Approach to Achieve High Gain, Flat Top Radiation With Low Cross Polarization

5.1 Introduction

In the present wireless world, with the expeditious growth of modern wireless communication, tiny antennas with wide and symmetrical radiation beam, high gain and low cross-polarization is a crucial challenge to the scientific community. Further, antennas with flat-top radiation pattern are also in great demand for ubiquitous wireless communication services, in base station for mobile communication and as efficient feeds for parabolic reflectors for the sake of uniform aperture illumination [1]–[6]. In fact, antennas with flat-top radiation pattern provide stable maximum gain along boresight to improve signal strength within service coverage area [1]–[6]. The issue of improvement in cross polarization has been discussed with different techniques in the previous chapters. The impedance bandwidth along with wide symmetrical radiation from RMA has also been discussed vividly. However, the concurrent improvement in gain, symmetry in radiation, widening of radiation beam along with low cross-polarization is definitely a vital challenge. Achieving the above mentioned parameters for an RMA is an audacious evocation to antenna research community and this can be attended by composite antenna structures.

Rectangular Microstrip Antenna (RMA) is a very much popular genre of tiny printed antennas for its attractive features as discussed in Chapter 1. In general, linearly polarized (LP) RMA generates asymmetric radiation pattern along its broadside with relatively wider E-plane beam-width than the H-plane beam-width [7]. For instance, the E-plane beam-width of a RMA (fabricated on PTFE substrate with $\epsilon_r=2.33$) is around 80° while the same in H-plane is only 60° [7]. A conventional RMA does not possess a flat-top radiation pattern. Furthermore, RMA suffers from very poor co-polar to cross-polar radiation isolation (CP-XP isolation) particularly in its H-plane; the typical CP-XP isolation in the H-plane is around 8-10 dB at X band [7]. Also, RMA has poor gain (around 4-6 dBi). In wide-angle scanning phased array applications, antenna with wide beamwidth is preferably required [8]. Also, wide and symmetrical radiation pattern is always preferred in a point-to-multipoint wireless communication system. Although, RMA is an attractive contender for such applications, the narrow H-plane beam-width with asymmetrical 3D radiation pattern puts a major drawback in its use. A wide beam composite substrate RMA configuration was reported in [9] with 88° and 64° 3 dB beamwidth in E-plane and H-plane, respectively. However, the structure is complex to fabricate because of composite nature of dielectric which limits practical use. A shorted comb shaped antenna proposed in [10] exhibited around 100° 3 dB beam-width but suffered from the feeding problem and the maximization of the patch size for a resonant frequency. A two-layer stacked patch structure reported in [11] exhibits symmetrical radiation pattern in E and H planes with 60° beam-width in both planes. However, because of the stacking, the structure became bulky with no improvement in XP performance [11]. Earlier, non-planar microstrip-monopole antenna topology was reported in [12], where four finite height metallic rods were integrated with a circular microstrip antenna to achieve only broad 3 dB beam-width (170°) and circular polarization. The antenna structure reported in [12] is basically a composite antenna made up of cylindrical rods (monopole antenna) integrated with circular microstrip antenna. Any improvement in CP-XP isolation is not apparent from [12]. Furthermore, none of the antennas reported in these works [8]-[12] exhibit flat-top radiation pattern.

Recently, a few research results have been reported on flat-top radiation pattern from antennas. Around 60° flat-top radiation pattern with 28 dB CP-XP

isolation with 7.9 dBi gain has been obtained from LP double shell lens antenna in [1]. Four element linear and 8×8 planar array LP antenna have been proposed in [2], [3] to obtain 46° and 20° flat-top radiation pattern with side lobe level -20 dB and -15 dB respectively. The 3 dB beam-width in [2] is 60° in the principal planes. The techniques to develop flat-top radiation pattern and pencil beam have been discussed in [4]. Circular polarized array antenna with flat-top radiation pattern and dual patch with flat gain have been reported in [5], [6]. However, the angular range of flat-top sector is very small, and antenna structures are complex and expensive to fabricate [5], [6]. Additionally, the studies on symmetry in radiation patterns, broadening of beams and CP-XP isolation are not apparent from these works. It is also observed that flat-top radiation was achieved from non-planar antennas, high-profile antennas or volumetric antennas [1]-[6]. More importantly, no effort has been reportedly made to achieve flat-top radiation pattern from a simple, single element RMA. Also, the physics behind achieving flat-top radiation pattern have not explored in all these works.

Improved CP-XP isolation is very much required over wide angular range in numerous applications [7]; for instance, it is an issue of vital relevance in the design of fully polarimetric synthetic aperture radars for convenient polarimetric data calibration and in maritime surveillance applications [13], as well as in dual-polarized hybrid antenna array for 5G communication MIMO operation [14]. The widespread techniques for achieving good CP-XP isolation (around 22-30 dB) in LP antennas are employment of defected ground structures (DGS) [15], defected patch structure (DPS) [16] and shorted patch technique [17]. In recent years, DGS has been widely used in a number of applications for instance in designing RFID tag [18] and band pass filter [19]. However, DGS and DPS integrated RMAs experience complexity in probe feeding in view of the difficulty in placing the slots either on the ground plane or on the patch surface. Enhanced back radiation from such DGS structures is a severe limitation in wireless communication. Shorted patch technique conflicts with the miniaturization as the operating frequency increases thereby making it non-attractive for miniaturized wireless systems. Furthermore, the antennas proposed in these reports emphasizing only on CP-XP isolation [15]-[17] did not exhibit wide, symmetrical, flat-top radiation pattern. The composite and non

planar antennas such as magneto-electric dipole antennas [20], horn antenna integrated microstrip antennas [21], lens integrated microstrip antennas [1], microstrip monopole antenna loaded with metamaterial superstrate [22], 3D printed fractal antenna [23] are very much popular and widely investigated in the recent years. Nevertheless, in some cases such as in surveillance application and satellite communication where, the user defined stringent performance criteria are to be met, antenna of one type is really difficult to meet the requirement. Therefore, two different types of structures with different characteristics may be employed which lead to a composite volumetric antenna structure. For instance, a microstrip antenna integrated with bi-conical antenna can be used in satellite digital multimedia broadcast [24].

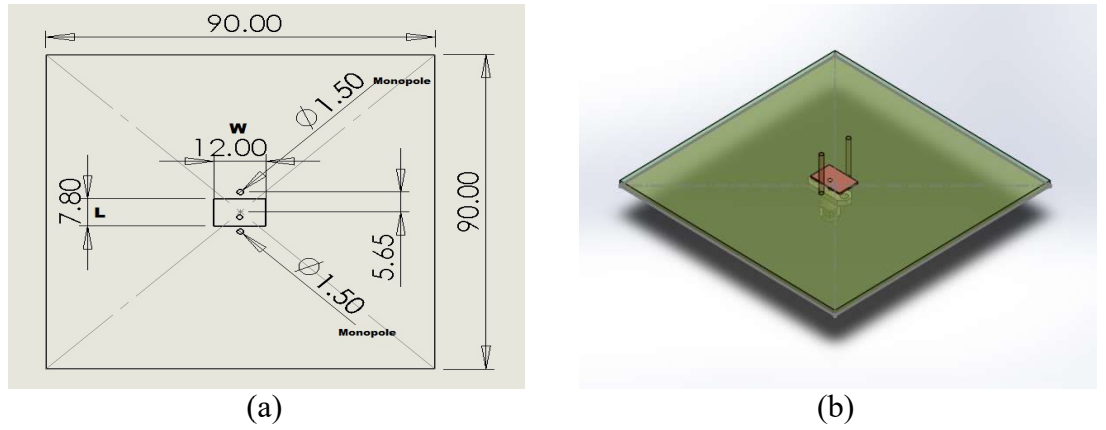


FIGURE 5.1. Proposed QPCMA RMA (a) Schematic Diagram (b) 3D image

In order to alleviate the lacunae of the earlier works and further to take care of the improvement of complete radiation performance, i.e., for improving the symmetry in radiation pattern, achieving flat-top radiation pattern in principal planes, widening 3dB beam-width, and improving gain and CP-XP isolation in both the principal planes; in the present work, a simple, quasi-planar composite microstrip antenna (QPCMA) consisting of a single element RMA along with two metallic posts (monopoles) is proposed (**Fig. 5.1**). Around 90° of 3 dB beamwidth in both the principal planes have been achieved from the proposed QPCMA. The proposed antenna exhibits wide beamwidth with 145° symmetry in radiation pattern in principal planes along with considerably high gain of 8.2 dBi (although using a FR-4 substrate) and around 26-40 dB CP-XP isolation concurrently. Further, the present QPCMA exhibits around 70° of flat-top radiation pattern with almost no ripple. Also,

the physics behind the germination of flat-top radiation pattern from the proposed QPCMA have been explored thoroughly and accurately. Same concept has been investigated for low loss substrate and excellent results have been observed.

The Chapter has been covered in following sections. Section 5.2, gives physical insight of the proposed structure wherein, Subsection 5.2.1. covers effect of monopole height on improving co-polar (CP) radiation pattern of QPCMA. Subsection 5.2.2, effect of monopole length on suppressing cross-polar (XP) radiation from QPCMA. Subsection 5.2.3 covers effect of monopole spacing on CP and XP radiation patterns of QPCMA. Section 5.3 covers the theoretical aspects wherein, Subsection 5.3.1 gives theoretical look into flat-top radiation, Subsection 5.3.2 gives theoretical look into wide angle gain, Subsection 5.3.3 gives performance analysis of QPCMA with low loss substrate. Section 5.4 gives the details of proposed structure. Section 5.5 enumerates the results and analyses it. Section 5.6 compares the proposed design with various established designs for its advantages. And finally, Section 5.7 concludes the chapter.

5.2 Physical Insight

Quantitative and qualitative analysis is carried out in succeeding sections for various optimizations of monopole lengths, spacing, etc. with respect to patch.

5.2.1 Effect of Monopole Height on Improving Co-Polar (CP) Radiation Pattern Of QPCMA

Following the aperture modeling technique [25], it is evident that any perturbation (like metallic post or monopole) placed at the radiating slot apertures, significantly modifies the field distribution which, in turn alters the radiation pattern of RMA. The investigations has been started with simple RMA of dimension $(L \times W) = 7.8 \times 12 \text{ mm}^2$ and has been fabricated on FR-4 dielectric substrate with dimension of $90 \text{ mm} \times 90 \text{ mm}$ ($5\lambda_g \times 5\lambda_g$) ($\epsilon_r = 4.4$, height $h = 1.58 \text{ mm}$) (**Fig. 5.1**). The antenna has been fed at 2.1 mm from the centre of the patch. And then two metallic posts of 1.5 mm diameter acting like monopoles are placed centrally near radiating edges of the patch of a RMA to realize a QPCMA (**Fig. 5.1**). These monopoles are parasitically coupled with the patch and the distance between patch edge and outer surface of the monopole is optimized to 1 mm for achieving best result. This pair of

monopoles forms a linear array along the E-plane ($\phi = 0^\circ$ plane) with inter radiator spacing $\sim \lambda_g/2 \sim 9.5$ mm and are excited with 180° out of phase fields from radiating edges of the patch. Hence, the array factor produces maxima along $\phi = 0^\circ$ and 180° while, it exhibits null radiation along the H-plane ($\phi = 90^\circ$ plane). From simulations [26], it is clear that if the monopoles are of length $\lambda_g/4 = 4.5$ mm; the monopole like radiation pattern dominates the overall CP radiation pattern of the QPCMA at E-plane (**Fig. 5.2(a)**). Hence, the peak gain in E-plane is slightly offset from the bore sight. It rolls off after the peak point (approximately around 60°) due to the composite effect of radiation from RMA with that of monopoles at E-plane.

When, height of the monopole increases to $\lambda_g/2 = 9.3$ mm; E-plane beamwidth of the QPCMA becomes narrower than that of conventional RMA (**Fig. 5.2(b)**). This is expected as the radiation from $\lambda_g/2$ monopole is very less near the bore sight. However, the effect of monopole like radiation is still evident from the creation of one sided null in the CP radiation pattern of the QPCMA at E-plane. Unlike, conventional RMA, the E-plane beamwidth of the QPCMA becomes narrower at the cost of significant radiation near 90° elevation angle ($\theta = 90^\circ$) (**Fig. 5.2b**). Unlike **Fig. 5.2(a)**, the peak gain of the QPCMA at its E-plane occurs along bore sight because of the generation of very thin or pencil beam from $\lambda_g/2$ monopoles along the horizon i.e. along 90° elevations.

Now, if the length of monopoles is increased beyond $\lambda_g/2$; it starts to develop certain lobes along the higher elevation angles. These lobes merge with the original E-plane radiation pattern of the RMA and broadens the overall E-plane beam-width of QPCMA. The radiation pattern of the QPCMA (**Fig. 5.2c**) shows that when each monopole length is $3\lambda_g/4 = 13.7$ mm; it yields wide E-plane beamwidth in comparison to the structure with $\lambda_g/2$ monopoles (**Fig. 5.2b**). It may be noted that the length of monopole does not have an influence on the H-plane beam-width of the QPCMA as the array factor exhibits null radiation along the H-plane ($\phi = 90^\circ$ plane). However, it can be observed that the H-plane beamwidth of QPCMA is wider compared to that of conventional RMA. This H-plane beam-width is consistently wide for all lengths of monopole as seen from **Figs. 5.2(a), (b) and (c)**.

In all the cases, the H-plane CP radiation pattern becomes 40% wider (yielding 85° beamwidth) than that of conventional RMA fabricated on conventional RT-Duroid or PTFE substrate with $\epsilon_r=2.33$.

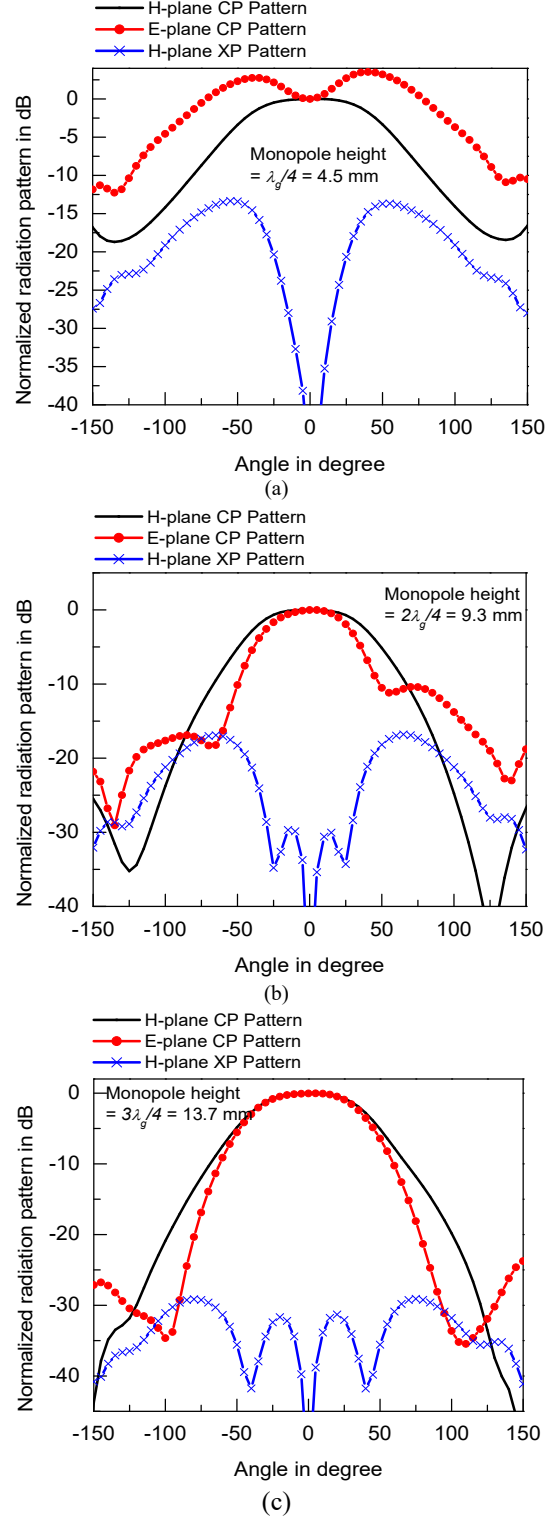


FIGURE 5.2. E and H-plane radiation patterns of QPCMA for different monopole height (a) for $\lambda_g/4$ monopole, (b) for $2\lambda_g/4$ monopole, (c) for $3\lambda_g/4$ monopole.

In general, a RMA fabricated on higher dielectric constant (like FR-4) exhibits wider beamwidth in comparison to the same fabricated on lower dielectric constant substrate (**Fig. 5.3**). Here, QPCMA structure is fabricated on higher dielectric constant substrate (FR-4). Along with the same, as the monopoles are placed near the radiating edges of the patch; it localizes more H-fields at the vicinity of the monopoles. This result into the reduction of E-fields at the vicinity of the monopole causing a non-uniform distribution of E-field along the radiating slot aperture width (contained in H-plane).

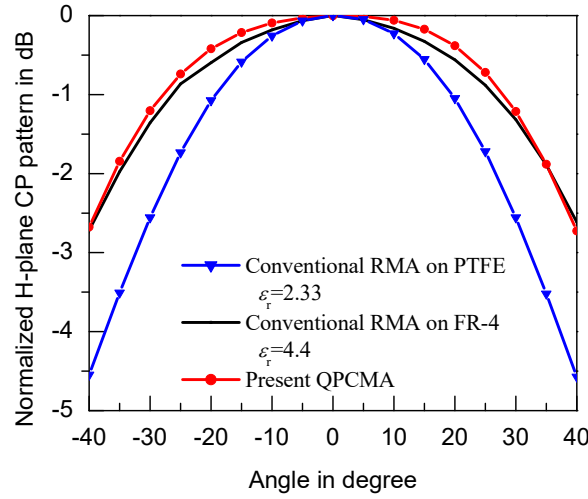


FIGURE 5.3. Normalized H-plane CP profile of conventional RMA with PTFE substrate ($\epsilon_r = 2.33$), conventional RMA with FR-4 substrate ($\epsilon_r = 4.4$) and the present QPCMA with FR-4 substrate ($\epsilon_r = 4.4$).

Therefore, this non-uniform distribution of fields along the radiating slot aperture width (contained in H-plane of QPCMA) widens the beam-width of QPCMA more at its H-plane [9],[25]. In fact, the non-uniform distribution of field at any plane of aperture antennas results in wide beam-width at corresponding plane [27],[28]. The field distribution over the substrate for both the present QPCMA and conventional RMA with FR-4 substrate is presented in **Fig. 5.4**. This confirms the observation of this non-uniform distribution of fields along the radiating slot aperture width (**Fig. 5.4(a)**). From the figure, it may also be noted that the fringing E-fields are extended in both lateral and longitudinal directions as they are mitigated at the central region of radiating edge because of the presence of monopoles there. This effectively increases the H-plane dimension QPCMA (as fringing width ΔW increases). Therefore, the use of FR-4 substrate, the non-uniform distribution of field

along the radiating slot aperture width (H plane) causes wide beam-width at the H-plane of the QPCMA.

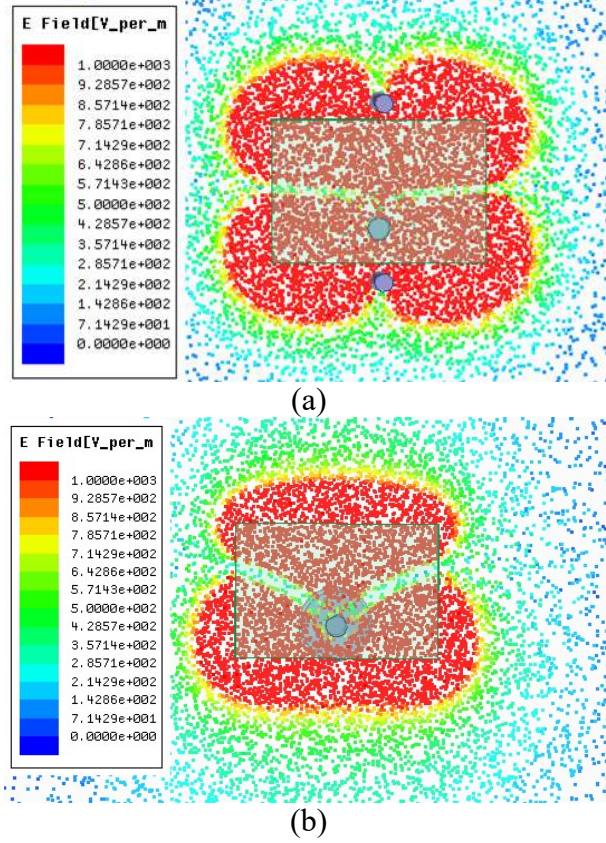


FIGURE 5.4. Field distribution over the substrate for (a) QPCMA with FR-4 substrate, (b) conventional RMA with FR-4 substrate.

Now, if we concentrate on the overall radiation pattern of the QPCMA structure, it is observed from **Fig. 5.2(c)** that in both the principal planes (E and H-plane), beam-widths of the structure with $3\lambda_g/4$ monopoles are symmetrical and significantly wide 3 dB beam-widths of 90° . Around 140° to 150° symmetry in principal E and H-planes are observed from **Fig. 5.2(c)**. It is very motivating to observe that the CP radiation patterns are quite flat about 70° along the bore sight (**Fig. 5.2(c)**). Commonly, the flat-top radiation pattern can be obtained from array configuration by manipulating the amplitude and phase excitation of individual elements.

This in fact increases radiation in the desired front direction while eliminates the side lobes slightly off side from the desired direction. However, in present investigation, the merging of monopole lobes at higher elevation angle with the E-

plane lobe of RMA is exploited to achieve such flat-top radiation patterns. Also, the flat-top region in the radiation patterns is of all most no ripple.

5.2.2 Effect of Monopole Length on Suppressing Cross-Polar (XP) Radiation from QPCMA

It is observed from **Fig. 5.2** that as the monopoles are introduced; CP-XP isolation in the radiation pattern of QPCMA improves. In fact, these monopoles mitigate the electric fields at their vicinity and intensify the magnetic fields in the same region (**Fig. 5.4 (a)**). It results in a uniform field distribution between the lower and upper half sections of the QPCMA at its non-radiating edges (**Fig. 5.4(a)**) whereas, the field distribution is highly non-uniform between the lower and upper half sections of conventional RMA [29] (**Fig 5.4(b)**). Consequently, CP-XP isolation improves [29]. As the monopole length is increased from $\lambda_g/4$ to $3\lambda_g/4$; CP-XP isolation improves from 14 dB to 28 dB (**Fig. 5.2**). Following the current distribution of the monopole, it may be noted that the magnetic field near the base of monopole is maximum for monopole length of odd multiple of $\lambda_g/4$ than monopole length of even multiple of $\lambda_g/4$. Hence, the electric fields are not too less at the vicinity of the monopoles in case of the structure with $\lambda_g/2$ length.

It, in turn, cannot produce a uniform field distribution between the lower and upper half sections of QPCMA at its non-radiating edges [29] and hence, CP-XP isolation does not improves. The effects of increasing the length of monopoles beyond $\lambda_g/2$ on the overall radiation properties (**Table-5.1**); corroborates the observed phenomenon. As the height of monopole increases gradually from $\lambda_g/2$ to $3\lambda_g/4$; base feed current increases and hence the magnetic fields near the base of monopole increases. Therefore, electric field reduces at the vicinity of the monopole at the cost of increased electric fields at the upper patch corners which, improves the CP-XP isolation [29]. Moreover, the excellent symmetry between the E and H-plane radiation patterns for the QPCMA with monopole length $3\lambda_g/4$ is also the reason for improved CP-XP isolation.

5.2.3 Effect of Monopole Spacing on CP and XP Radiation Patterns of QPCMA

In the present QPCMA structure, the monopoles are placed at close proximity of the radiating edges. This is done with a view to couple the fields

efficiently from radiating edges of the patch to the monopole. The distance from the post surface to radiating edge is 1 mm i.e. the distance from each radiating edge to centre of each post is $a = 1.75$ mm. This yields an asymmetric distribution of fields along radiating slot aperture width (**Fig. 5.4(a)**) and uniform field distributions between lower and upper half section of patch which causes wide symmetrical flat-top radiation patterns in conjunction with low XP radiation in the present QPCMA structure with monopole length $3\lambda_g/4$ as discussed elaborately in section 5.2.1 and 5.2.2. Now, if we increase the distance of monopole from the radiating edge of patch i.e. if a increases, initially, the radiation patterns does not degrade much.

Table-5.1 Radiation properties of the QPCMA with different monopole heights: patch length $L = 8$ mm, width $W = 12$ mm, substrate permittivity $\epsilon_r = 4.4$, substrate height $h = 1.58$ mm

Electrical length of monopole	E- plane 3 dB beam-width	H- plane 3 dB beam-width	CP-XP isolation in dB	Symmetry in principal planes	Flat-top range in the radiation pattern
$2\lambda_g/4$	70°	86°	17	30°	45°
$2.3\lambda_g/4$	74°	86°	21	40°	50°
$2.5\lambda_g/4$	78°	88°	25	60°	60°
$2.7\lambda_g/4$	82°	87°	28	95°	68°
$3\lambda_g/4$	90°	90°	26	145°	72°

However, significant distortion is noted in the radiation pattern for higher values of a . The radiation patterns for QPCMA for different a values are depicted in **Fig. 5.5**. It is found that if the monopoles are at a distance $a = 2.5$ mm, there is no significant change in radiation patterns of the QPCMA. Hence, the QPCMA with $a = 2.5$ mm, also exhibits high-gain symmetrical, wide beam-width and flat-top radiation pattern with low XP radiation. This is because of the extension of fringing fields at patch radiating edges which, efficiently couples the fields to the monopoles. Hence, this extended fringing fields interact with the monopoles in a similar manner (like $a = 1.75$ mm) which in turn cause no change in radiation characteristics of QPCMA. The magnitude of electric field distribution is depicted in Fig. 3.6(a) for the QPCMA with $a = 2.5$ mm is to a certain extent similar to that of the QPCMA with $a = 1.75$ mm (**Fig. 5.4(a)**). Next, the separation is increased (increase a values), radiation pattern of QPCMA particularly in the H-plane XP starts to degrade significantly.

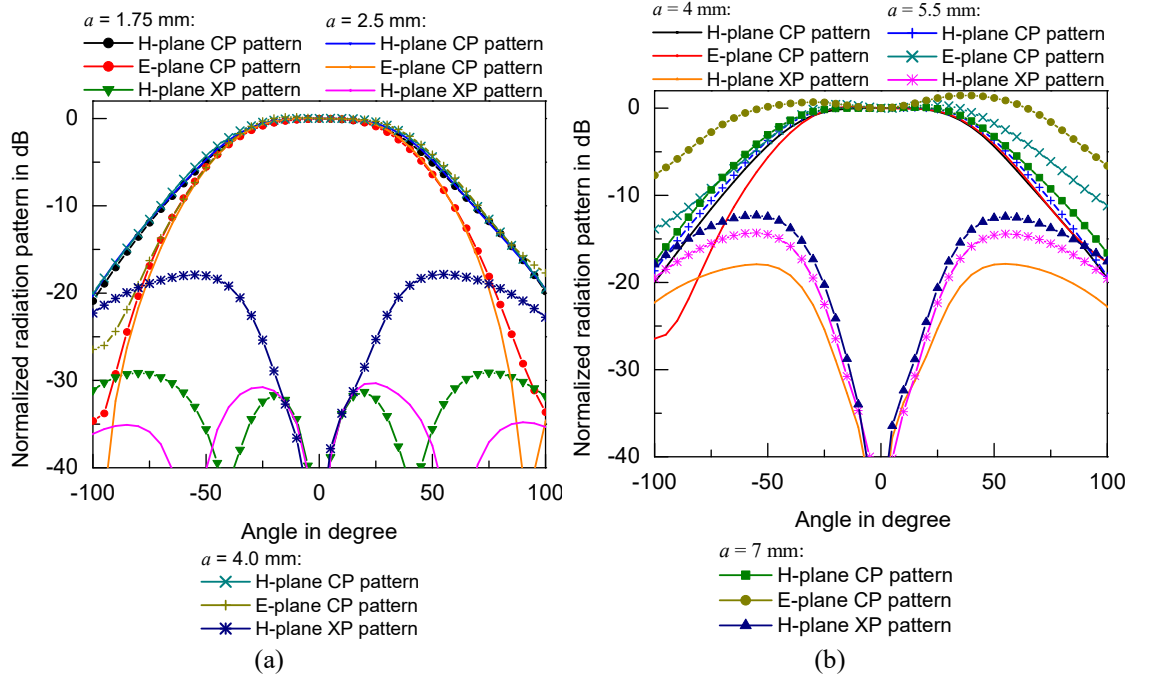


FIGURE 5.5. Normalized radiation pattern of the present QPCMA for different spacing (a values) between monopole and the radiating edges of RMA.

The radiation pattern of QPCMA for $a = 4$ mm, incorporated in the same plot (**Fig. 5.5(a)**) shows noteworthy increase in H-plane XP radiation and hence fails to improve the CP-XP isolation. Close inspection of **Fig. 5.5** also shows some asymmetry between the E and H-plane CP patterns of QPCMA in case of $a = 4$ mm. It is found that the E and H-plane CP patterns of QPCMA are symmetric in right side while the same is not true in the left side of the radiation pattern plot. The magnitude of electric field distribution is depicted in **Fig. 5.6(b)** for the QPCMA with $a = 4$ mm. Although, an asymmetric distribution of fields along radiating slot aperture width is maintained to some extent, still there is an asymmetry in field distribution between lower and upper half section corners of the patch which degrades the CP-XP isolation [29] of the QPCMA with $a = 4$ mm. The radiation patterns for the QPCMA for values $a \geq 4$ mm are illustrated in **Fig. 5.5(b)**. It is found that for higher values of a ($=5.5$ mm or 7 mm), the QPCMA exhibits the radiation pattern like conventional RMA. This is expected because the monopoles are far away from radiating edges and hence the extended fringing fields cannot interact with the monopoles. Therefore, the composite effect on radiation pattern of QPCMA is not apparent.

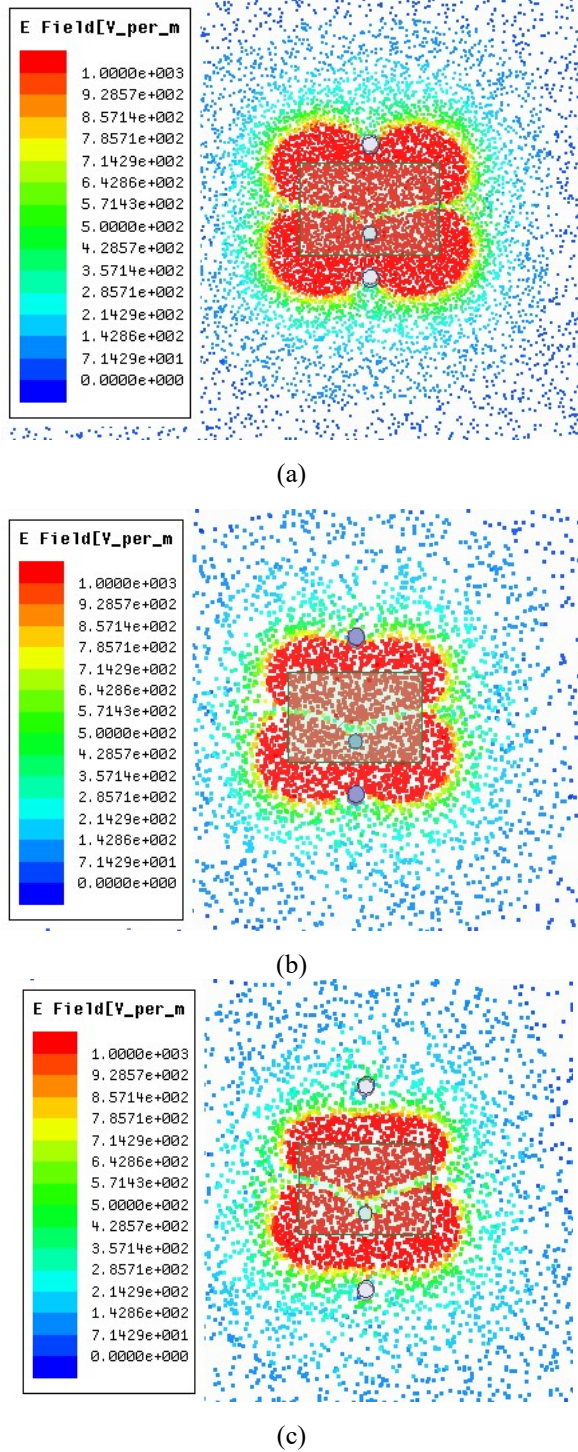


FIGURE 5.6. Field distribution over the substrate for QPCMA with (a) $a = 2.5$ mm, (b) $a = 4$ mm, (c) $a = 5.5$ mm

The E-field magnitudes in case of QPCMA with $a = 5.5$ mm is portrayed in **Fig. 5.6(c)** which is similar to conventional RMA (**Fig. 5.4(b)**) and confirms the observations. Hence, the monopoles of length $3\lambda g / 4$ are placed at close proximity

($a = 1.75$ mm) to the radiating edge of the patch for obtaining best performance for further investigations.

5.3 Theory

Theoretical analysis for flat top, wide angle gain to include performance analysis of QPCMA with low loss substrate is given in succeeding sections.

5.3.1 Theoretical Look into Flat-Top Radiation

It is clear from Section 5.2.1 that the $3\lambda_g/4$ monopole has a critical influence in the overall E-plane radiation pattern of QPCMA. On the contrary, the H-plane beam-width of QPCMA is already wide due to non-uniform electric field variation at slot aperture as discussed in same section 5.2.1. Therefore, it is necessary to look into the physics behind the beam-width widening of QPCMA in its E-plane.

For a conventional RMA, E_θ and E_ϕ components of the far-field radiation pattern can be expressed as [7]

$$[E_\theta]_{RMA} = 2 \cos \phi \frac{\sin\left(\frac{k_0 W \sin \theta \sin \phi}{2}\right)}{\left(\frac{k_0 W \sin \theta \sin \phi}{2}\right)} \cos\left(\frac{k_0 L \sin \theta \cos \phi}{2}\right) \quad (5.1)$$

and

$$[E_\phi]_{RMA} = 2 \cos \theta \sin \phi \frac{\sin\left(\frac{k_0 W \sin \theta \sin \phi}{2}\right)}{\left(\frac{k_0 W \sin \theta \sin \phi}{2}\right)} \cos\left(\frac{k_0 L \sin \theta \cos \phi}{2}\right) \quad (5.2)$$

Where $W = 1.5 L$; $L = \lambda_g/2$ and $k_0 = 2\pi/\lambda_g$

For a simple metallic post or monopole antenna of length l , E_θ component of the far-field radiation pattern is

$$[E_\theta]_{\sin gle_monopole} = \frac{\cos(kl \cos \theta) - \cos(kl)}{\sin \theta} \quad (5.3)$$

Two monopoles constitute a linear array along $\phi=0^\circ$ and the array factor will be

$$\begin{aligned}
 F &= \frac{\sin(k_0 d \sin \theta \cos \phi + \delta)}{\sin \left[\frac{1}{2} (k_0 d \sin \theta \cos \phi + \delta) \right]} \text{ where } \delta = \pi \text{ and } d \cong \lambda_g / 2 \\
 &= 2 \sin \left(\frac{\pi}{2} \sin \theta \cos \phi \right)
 \end{aligned} \tag{5.4}$$

Hence, contribution from monopoles can be computed as

$$[E_\theta]_{monopole} = \left[\frac{\cos(kl \cos \theta) - \cos(kl)}{\sin \theta} \right] \left[2 \sin \left(\frac{\pi}{2} \sin \theta \cos \phi \right) \right] \tag{5.5}$$

In E-plane, $\phi = 0^\circ$ and in H-plane, $\phi = \pi/2$

In case of array of two dissimilar sources, the total field pattern factor may be written as [30] for E-plane,

$$[E_\theta]_{TOTAL} = [E_\theta]_{monopole} + [E_\theta]_{RMA} \tag{5.6}$$

and for H plane,

$$[E_\theta]_{TOTAL} = [E_\theta]_{monopole} + [E_\phi]_{RMA} \tag{5.7}$$

The computed field components radiation patterns in E and H-plane show wide and flat-top radiation pattern in both planes. This is clearly due to the effect of monopole as clear from equation (5.5). Also, a close inspection of equation (5.3) reveals that when the length of monopole is greater than $3\lambda_g/4$, it develops higher elevation lobes which is superposed with the radiation pattern of conventional RMA and hence, the proposed QPCMA develops wide flat-top radiation pattern.

The computed E-plane pattern for conventional RMA and the present QPCMA using above equations is depicted in **Fig. 5.7**. The above analysis can also be done with the simple pattern multiplication method. However, it is not shown in this chapter.

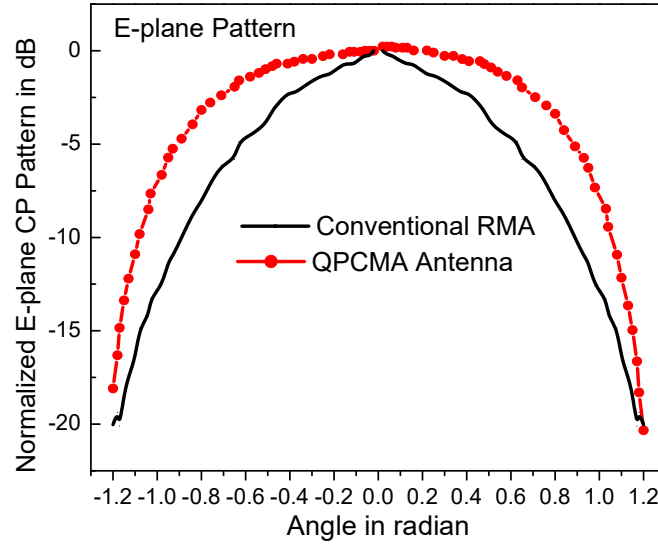


FIGURE 5.7. Computed E-plane pattern for conventional and present QPCMA

5.3.2 Theoretical Look into Wide Angle Gain

The modulation of near field distribution to obtain enhanced radiation performance is a useful technique which has been currently adopted in some very recent investigations [31], [34]. In general, a RMA produces non-uniform aperture field distribution over the substrate (**Fig. 5.4(b)**). This leads to poor aperture efficiency and poor gain of such antenna [33], [34]. Unlike conventional RMA, the presence of two monopoles in case of QPCMA modulate the field distribution in such away (as discussed above) that the E-fields extend in both lateral and longitudinal directions near the corners of the patch as shown in **Fig. 5.4(a)**. This in turn, results in a uniform aperture distribution over the substrate and hence the gain of the QPCMA is much improved [33], [34]. On the contrary, the field distribution of conventional RMA shown in **Fig. 5.4(b)** reveals non-uniform field distribution over the aperture and hence the aperture efficiency decreases and reveals low gain. [33], [34].

Furthermore, in QPCMA, due to the tapering of fringing fields at the central part of the radiating edges (**Fig 5.4(a)**), the fields are extended in both lateral and longitudinal directions which increase the effective fringing length ΔL and fringing width ΔW which increases the effective aperture $(L+2\Delta L)(W+2\Delta W)$.

Therefore the gain of the QPCMA antenna [33], [34] increases due to the increments of ΔL , ΔW and also the aperture efficiency ε_{ap}

$$G = \varepsilon_{ap} \frac{4\pi(L + 2\Delta L)(W + 2\Delta W)}{\lambda^2} \quad (5.8)$$

Therefore, the gain of the present QPCMA configuration is high. It is also found that the present QPCMA with $2\lambda_g/4$ monopole exhibits wide beam-width in H-plane and narrow beam-width in the E-plane.

The close look of **Fig. 5.8** for the CP profile of the structure in both E and H-planes corroborate the observation. It is important to note that though their peak gain is high (around 8.3 dBi) and is maintained in the H-plane over wide elevation angle $\theta = -34^\circ$ to $+34^\circ$, E-plane gain rolls off within a few degrees (around $\sim 22^\circ$). Hence, it is a challenging work to widen the E-plane beam-width of the antenna with stable high gain in wide angular range. As discussed earlier, the lobes of $3\lambda_g/4$ monopole at high elevation angle ($\theta = 15^\circ$ - 45°) merges with the E-plane radiation pattern of the RMA and this results in wide E-plane beam-width in the QPCMA. However, to obtain the stable peak gain over wide elevation angle (within $\theta = \pm 35^\circ$) at E-plane, the portion of high elevation lobe (within $\theta = 22^\circ$ - 35°) of monopole array (which merges with the E-plane radiation pattern of the RMA) should have sufficient gain of around 8-9 dBi.

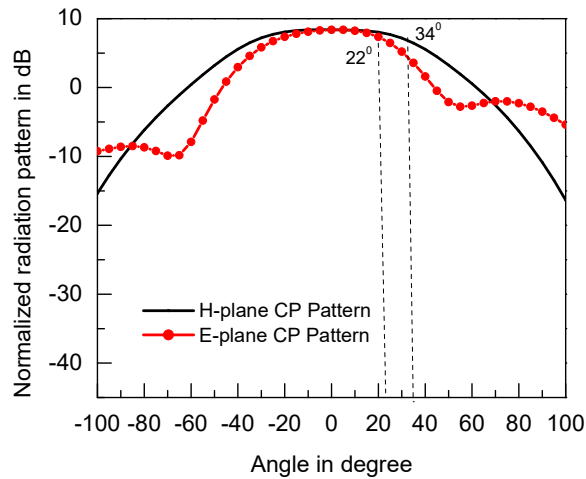


FIGURE 5.8. Radiation pattern of QPCMA with $a = 1.75$ mm and monopole length $l = 2\lambda_g/4$.

Now, the directive gain of a monopole at specified direction can be obtained from [28] as

$$D_{m\theta} = \frac{2f(\theta)}{\int_0^{\pi/2} f(\theta) \sin \theta d\theta} \quad (5.9)$$

Where, $f(\theta)$ is the pattern factor and can be calculated from (2) as

$$f(\theta) = \left[\frac{\cos\left(\frac{3\pi}{2} \cos \theta\right)}{\sin \theta} \right]^2 \quad (5.10)$$

Now,

$$\begin{aligned} \int_0^{\pi/2} f(\theta) \sin \theta d\theta &= \frac{1}{2} \int_0^{\pi} f(\theta) \sin \theta d\theta \\ &= \frac{1}{2} \left\{ 0.5772 + \ln(kl') - C_i(kl') + \frac{1}{2} \sin(kl') [S_i(2kl') - 2S_i(kl')] \right\} \\ &\quad + \frac{1}{2} \cos(kl') \left[0.5772 + \ln\left(\frac{kl'}{2}\right) + C_i(2kl') - 2C_i(kl') \right] \\ &= 0.883 \end{aligned} \quad (5.11)$$

Where, $l' = 2l$

Therefore,

$$D_{m\theta} = 2.27 \left[\frac{\cos\left(\frac{3\pi}{2} \cos \theta\right)}{\sin \theta} \right]^2 \quad (5.12)$$

Now, in E-plane, the normalized array factor of $N = 2$ elements $3\lambda_g/4$ monopole array can be written from (3) as

$$F_n = \frac{F}{N} = \sin\left(\frac{\pi}{2} \sin \theta\right) \quad (5.13)$$

Therefore, from (11), the radiation intensity can be written as

$$U = F_n^2 = \left[\sin\left(\frac{\pi}{2} \sin \theta\right) \right]^2 \quad (5.14)$$

In the upper hemisphere, the average radiation intensity of array of monopoles separated by a distance $d = \lambda_g/2$ is given by [28]

$$U_0 = \frac{\pi}{4Nkd} = \frac{1}{4N \frac{2}{\lambda_g} \frac{\lambda_g}{2}} = \frac{1}{4N} = \frac{1}{8} \quad (5.15)$$

Directive gain of the array as a function of elevation angle θ

$$D_\theta = \frac{U}{1/4N} = \frac{\left[\sin\left(\frac{\pi}{2} \sin \theta\right) \right]^2}{1/4N} = 8 \left[\sin\left(\frac{\pi}{2} \sin \theta\right) \right]^2 \quad (5.16)$$

Therefore, overall directive gain at a particular direction (θ) in case of array of monopoles can be written as

$$D = D_{m\theta} D_\theta = 18.16 \left[\frac{\cos\left(3\pi/2 \cos \theta\right)}{\sin \theta} \right]^2 \left[\sin\left(\frac{\pi}{2} \sin \theta\right) \right]^2 \quad (5.17)$$

Hence, using above equation (5.17), the overall gain of the monopole array in the angular region $\theta = 22^\circ$ to 34° varies from 8 dBi to 11 dBi. Therefore, the monopole array has sufficient gain in the angular region 22° to 34° where, the E-plane gain of the RMA rolls off. This merges with the E-plane radiation pattern of RMA resulting in stable wide angle gain in case of present QPCMA.

5.3.3 Performance Analysis of QPCMA with Low Loss Substrate

Conventional RMA at high frequency is significantly vulnerable to losses and hence, the use of a substrate with high loss tangent is usually not preferred. Consequently, to examine the validity of the present QPCMA in low loss substrate, the antenna has been designed on RT-5870 at X band and the radiation pattern is illustrated in **Fig. 5.9**. It is found that the gain of the QPCMA with RT-5870 increases by 1.2 dB compared to the same with FR4 substrate. In fact, the antenna gain enhances with lower dielectric constant substrate [34] because the E-fields are loosely bound to the substrate which contributes in CP radiation. This may be attributed for higher gain of QPCMA with low loss substrate. On the contrary, as the E-fields are loosely bound to the substrate, it contributes in XP radiation also and hence XP radiation increases. However, around 25 dB of CP-XP isolation is revealed for QPCMA with RT-5870 substrate. It may also be noted from **Fig. 5.9** that the QPCMA exhibits symmetry in radiation patterns of around 110° in principle planes with 69° flat-top regions. The QPCMA with RT- 5870 at X-band also exhibits wide

3 dB beam-width of 89° which is similar to the same with FR-4 substrate. Therefore, it may be concluded that the QPCMA works well with both the low loss and high loss substrate except some degradation in peak gain for high loss substrate.

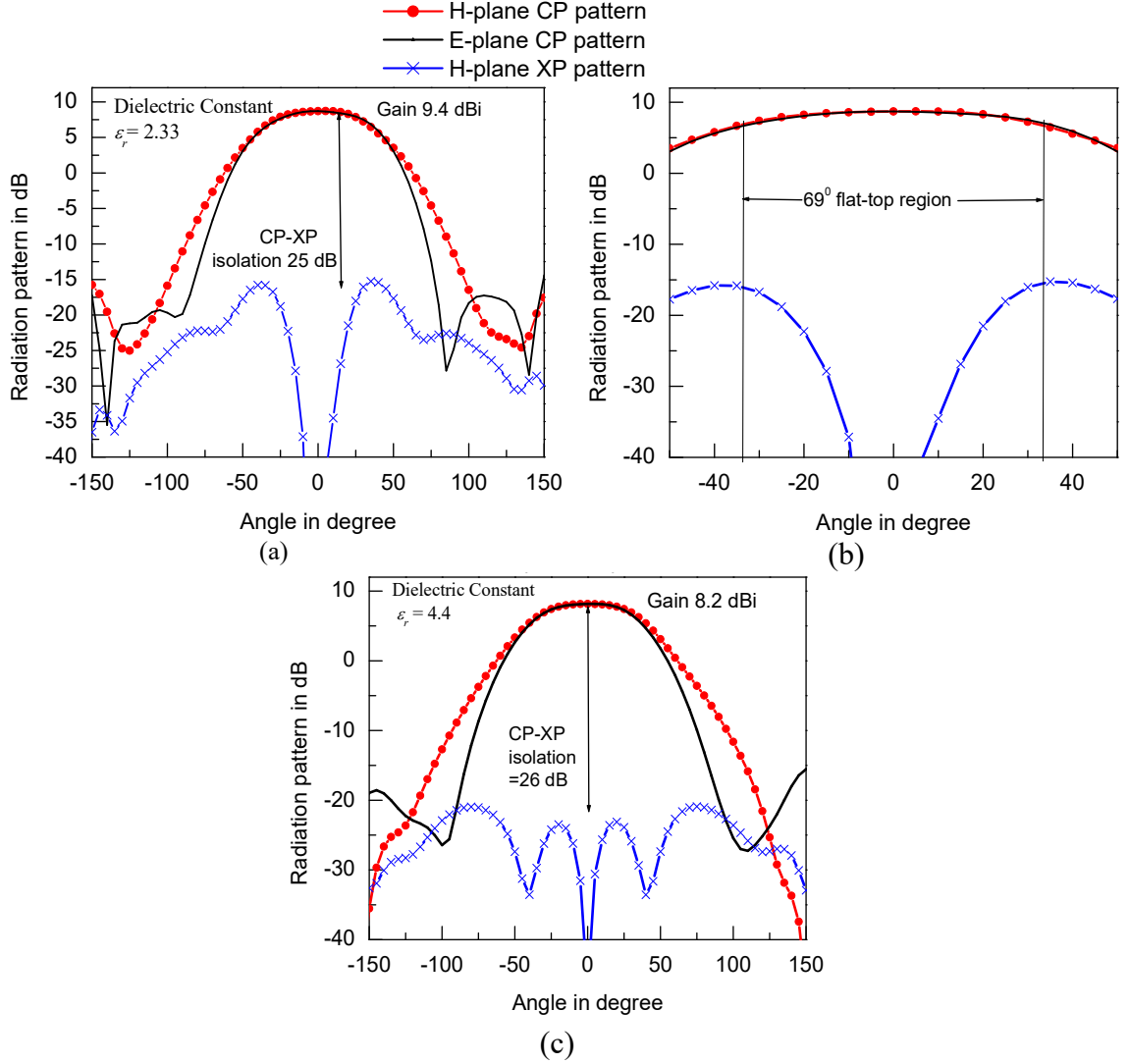


FIGURE 5.9. Simulated radiation pattern of QPCMA with different substrate (a) low loss substrate (RT-Duroid, $\epsilon_r = 2.33$), (b) same as (a) to depict the flat-top region, (c) low loss substrate (FR-4, $\epsilon_r = 4.4$).

In general, the FR-4 substrates are used up to 1-2 GHz. In fact, the dielectric loss tangent increases with frequency in most of the cases. However, the loss tangent of FR-4 is typically constant from 1 to 10 GHz [35]. Therefore, to manufacture low cost antenna, FR-4 may be used by sacrificing gain of the antenna. Furthermore, it may be noted that for such substrate, the gain may be low, but it has lower XP radiation and definitely the wide beam-width.

5.4 Proposed Structure

First, a RMA with dimension $(L \times W) = 7.8 \times 12 \text{ mm}^2$ has been fabricated on grounded FR-4 dielectric substrate with dimension is $90 \text{ mm} \times 90 \text{ mm}$ ($5\lambda_g \times 5\lambda_g$) ($\epsilon_r = 4.4$, height $h = 1.58 \text{ mm}$) (**Fig. 5.1**). The antenna has been fed at 2.1 mm from the centre of the patch. Then, two grooves of diameter 1.5 mm have been cut in the substrate at the central part of radiating edges at a distance of 1 mm from the respective edges. Two conducting copper sticks of length $3\lambda_g/4=13.5 \text{ mm}$ and diameter 1.5 mm are inserted through grooves resulting in proposed QPCMA (**Fig. 5.10(a)** and **5.10(b)**).

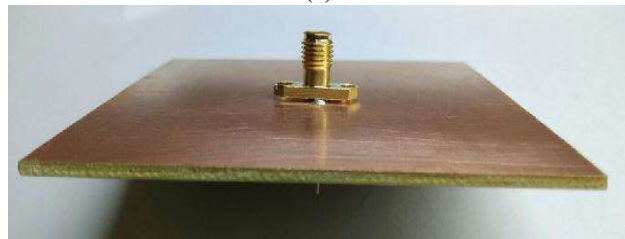
5.5 Results and Analysis

The measured results obtained for the proposed QPCMA prototype have been documented in this section. The resonant frequency of the proposed QPCMA is 8.04 GHz with around 7% impedance bandwidth (from 7.8 GHz to 8.3 GHz) (**Fig. 5.11**). **Fig. 5.12** shows the H and E-plane radiation patterns of the proposed QPCMA along the boresight at two frequencies within its operating band. The H-plane XP radiation pattern is plotted in the same figure. There is no significant change in E-plane XP radiation. Therefore, we refrain from giving E-plane XP radiation pattern in the manuscript for brevity. The measured 3-dB and 10-dB beam-width of the QPCMA are around 90° and 125° , respectively in both the principal planes at centre frequency $f=8.04 \text{ GHz}$. The H-plane beam -width has been broadened by 50% while the same for E- plane is 13% compared to that of a conventional RMA. Around 145° symmetry in measured E and H-plane radiation patterns is clearly found from **Figs. 5.12 (a)** and **(c)** at two frequencies in its operating band.

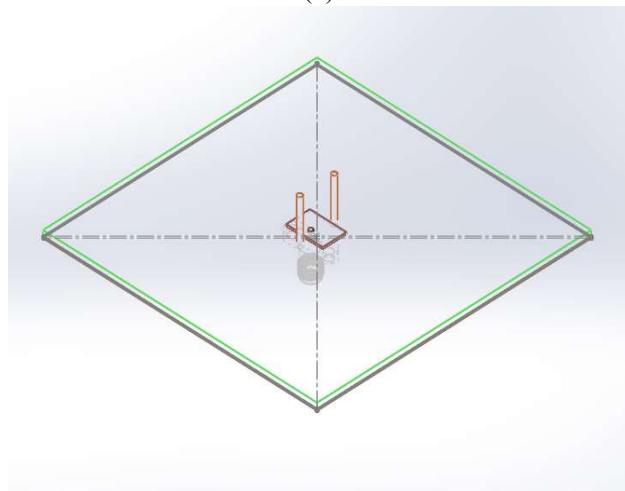
The proposed QPCMA exhibits flat-top radiation in the entire bore sight region. At each frequency, the close view of the flat- top portion in the radiation patterns in the E and H planes is portrayed in **Figs. 5.12 (b)** and **(d)**. Around 70° flat-top in the radiation pattern is revealed from the QPCMA in all the frequencies of operation with almost no ripple.



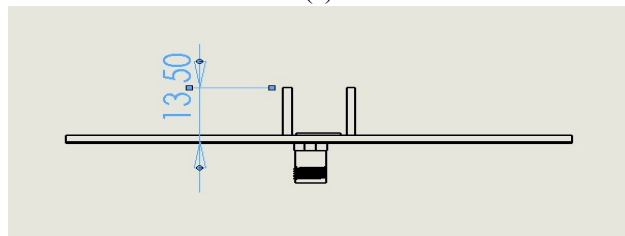
(a)



(b)



(c)



(d)

FIGURE 5.10. Fabricated prototype (a) Top view, (b) Back-view, CAD based (c) isometric view and (d) side view depicting monopoles.

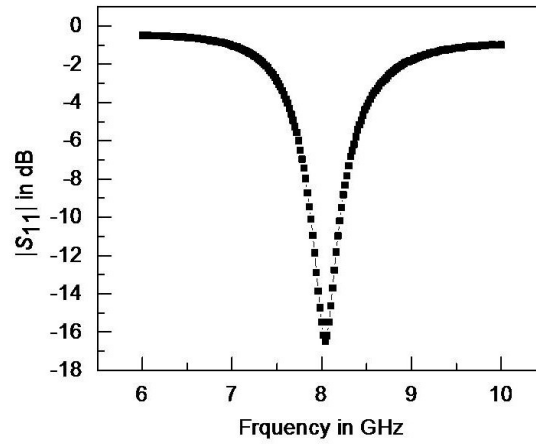


FIGURE 5.11. Measured reflection coefficient profile of the proposed QPCMA.

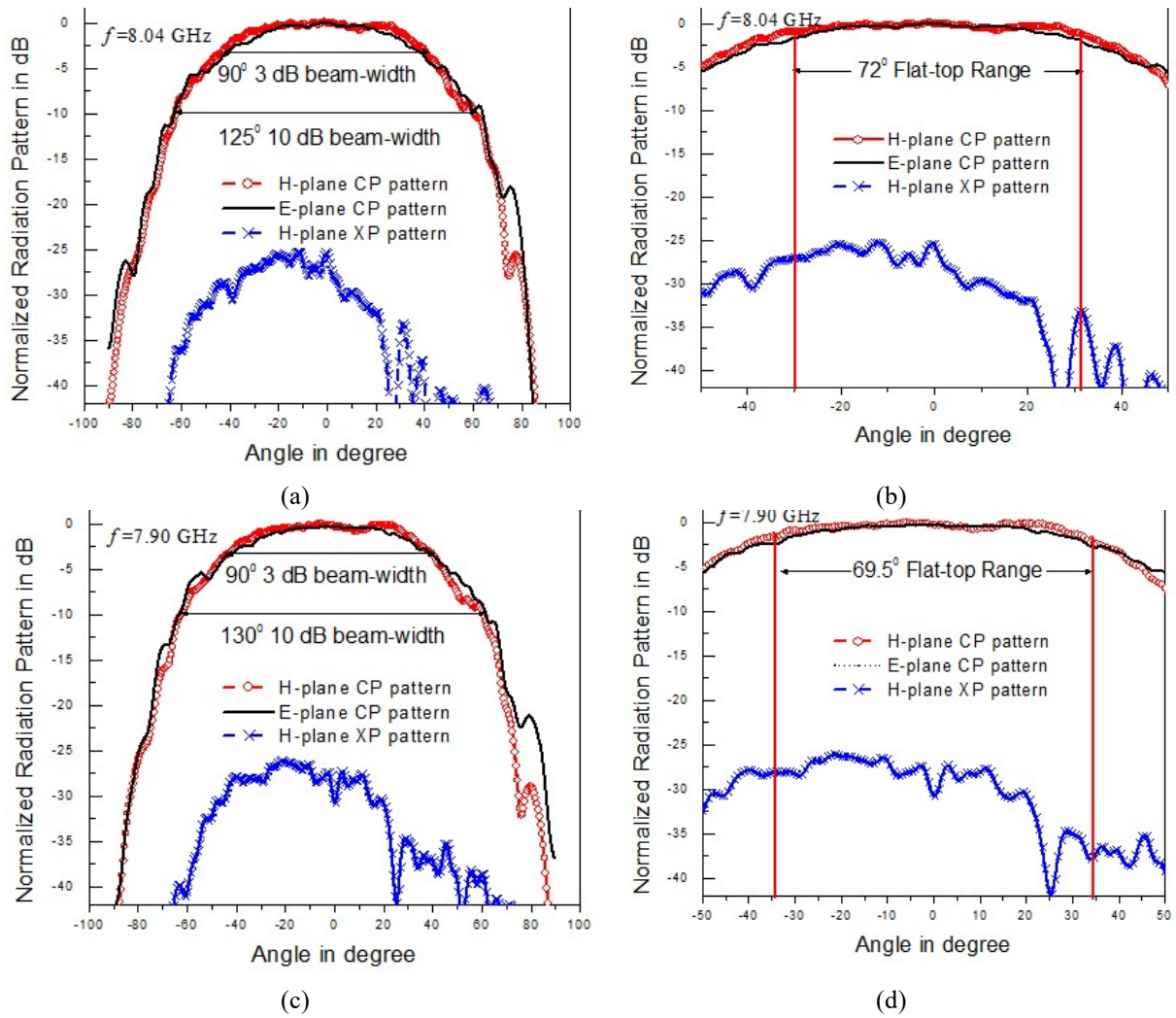


FIGURE 5.12. Measured E and H-plane radiation patterns for QPCMA at different frequency. (a) Complete pattern at $f=8.04$ GHz, (b) flat-top region at $f=8.04$ GHz, (c) complete pattern at $f=7.9$ GHz, (d) flat-top region at $f=7.9$ GHz.

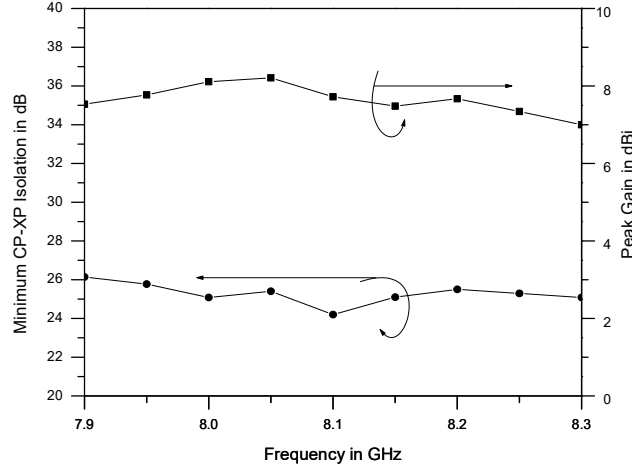


FIGURE 5.13. Measured gain and minimum CP-XP isolation as a function of frequency for QPCMA.

The simulated and measured gain of the proposed QPCMA (fabricated on a grounded FR-4 substrate with $\epsilon_r = 4.4$, height $h = 1.58$ mm) are 8.7 dBi and 8.2 dBi, respectively whereas, the measured gain of a conventional RMA is 4.5 dBi. The measured gain of the proposed QPCMA is reasonably stable and varies from 7.95 dBi to 8.2 dBi in the whole band and the peak CP-XP isolation is in the range of 26-40 dBi the whole operating band. Therefore, around 14-18 dB improvement in suppression of XP radiation is revealed from the proposed QPCMA than that of a conventional RMA. In order to examine the stability of peak gain and the polarization purity of the proposed QPCMA as a function of frequency, the measured values of these are presented in **Fig. 5.13**. It shows that the gain of the QPCMA is quite stable and varies from 7.95 dBi to 8.3 dBi in the whole band. On the contrary, minimum CP-XP isolation is in the range of 26-27 dB in the whole operating band.

Therefore, the proposed QPCMA shows 7% impedance band width, wide-beam flat-top radiation pattern with 145° symmetry in principle planes with high gain (8.2 dBi) and improved CP-XP isolation (26-40 dB along wide elevation angle).

5.6 Comparison between Radiation Properties of the QPCMA with Various Established Designs of RMAS

The performance of QPCMA is compared with conventional RMA designed on FR-4 substrate ($\epsilon_r = 4.4$) and earlier reported works in **Table 5.2**. It is apparent

that the proposed QPCMA exhibits wide beam-width with 145° symmetry in radiation pattern in principal planes along with considerably high gain of 8.2 dBi (although using a FR-4 substrate) and around 26-40 dB CP-XP isolation concurrently. Additionally, the present QPCMA exhibits around 70° of flat-top radiation pattern with almost no ripple.

TABLE-5.2: Comparison between radiation properties of the QPCMA with conventional RMA and earlier reported works

Ref	Antenna type	Gain (dBi)	E-plane 3 dB beam width	H-plane 3 dB beam width	Symmetry between radiation patterns in principal planes	Peak CP-XP isolation in dB	Flat-top range in the radiation patterns	Remarks
-	Conventional RMA ($\epsilon_r = 4.4$)	4.5	65°	70°	-	16	-	Planar structure
[1]	Double shell lens antenna fed by aperture coupled microstrip antenna		80		-	28	80° in H-plane, 60° in E-plane,	Volumetric antenna, ripple in flat-top region
[2]	Switched beam microstrip antenna array	16.6	56°	5°		25	46°	Quasi planar antenna array
[5]	Circularly polarised bow tie array	>11.8	60°	30°		25	30° in E-plane	Quasi planar antenna array
[9]	Composite dielectric loaded RMA	7	64°	88°	-	17	-	Quasi planar structure
[12]	Circularly polarised microstrip monopole antenna	3.5	137°	156°	130°	-	-	Quasi planar structure
[15]	Slot type DGS integrated RMA	-	55°	60°	-	25	-	Planar structure
[17]	Shorted RMA	7.5	60°	70°	-	27	-	Planar structure
[29]	T-shaped microstrip antenna	6.11	56°	-	-	21	-	Planar structure
-	Present QPCMA	8.2	90°	90°	145°	26	72° in both E and H-plane	Quasi planar structure

5.7 Conclusion

A compact QPCMA is proposed for high gain, flat-top, wide beam-width, symmetrical radiation pattern with excellent CP-XP isolation. The concurrent improvement of all the radiation properties with such low profile structure is absolutely new in the field of microstrip radiator till date. The reasons for the improvement in each parameter are thoroughly investigated, analyzed and documented in the present chapter for insightful exploration of the structure. The proposed structure is extremely simple and trouble-free to construct. The proposed antenna structure will surely be helpful for antenna community and find potential applications in the fields of modern wireless communications as it addresses majority of the primary lacunae of an RMA.

References

- [1] N. T. Nguyen, R. Sauleau and L. Le Coq, "Reduced-size double-shell lens antenna with flat-top radiation pattern for indoor communications at millimeter waves", *IEEE Trans. Antennas Propag.*, vol. 59, pp. 2424-2429, 2011.
- [2] H. Wang, Z. Zhang, Y. Li and M. Iskander, "A switched beam antenna with shaped radiation pattern and interleaving array architecture", *IEEE Trans. Antennas Propag.*, vol. 63, no. 7, pp. 2914-2921, 2015.
- [3] H.-J. Zhou, B.-H. Sun, J.-F. Li and Q.-Z. Liu, "Efficient optimization and realization of a shaped-beam planar array for very large array application", *Prog. Electromagn. Res.*, vol. 89, pp. 1-10, 2009.
- [4] R. Eirey-Pérez, A. A. Salas-Sánchez, J. A. Rodríguez-González, and F. J. Ares-Pena, "Pencil beams and flat-topped beams with asymmetric sidelobes from circular arrays," *IEEE Trans Antennas Propag.*, vol. 56, no. 6, pp. 153–161, 2014.
- [5] Z.-Y. Zhang, N.-W. Liu, S. Zuo, Y. Li and G. Fu, "Wideband circularly polarised array antenna with flat-top beam pattern", *Microw. Antennas Propag.*, vol. 9, no. 8, pp. 755-761, 2015.
- [6] C. Meng, J. Shi and J.-X. Chen, "Flat-gain dual-patch antenna with multi-radiation nulls and low cross-polarisation", *Electron. Lett.*, vol. 54, no. 3, pp. 114-116, 2018.
- [7] R. Garg, P. Bhartia, I. Bahl and A. Ittipiboon, *Microstrip Antenna Design Handbook*, Norwood, MA, USA:Artech House, 2001.
- [8] Y.-Y. Bai, S. Xiao, M.-C. Tang, Z.-F. Ding and B.-Z. Wang, "Wide-angle scanning phased array with pattern reconfigurable elements", *IEEE Trans. Antennas Propag.*, vol. 59, no. 11, pp. 4071-4076, 2011.
- [9] S. Chattopadhyay, J. Y. Siddiqui, & D. Guha, "Rectangular microstrip patch on a composite dielectric substrate for high gain wide-beam radiation patterns," *IEEE Trans Antennas Propag.* Vol. 57, pp. 3324–3327, 2009.
- [10] U. A. Pawar, S. Chakraborty, S. Chattopadhyay, "A Compact and Grounded Comb Shaped Microstrip Antenna: A Key to Realize Enhanced Radiation

- Performance,” *International Journal of RF and Microwave Computer Aided Engineering*, Vol. 27, No.6, pp. 1-11, 2017
- [11] C.-W. Su, S.-K. Huang and C.-H. Lee, "CP microstrip antenna with wide beamwidth for GPS band application", *Electron. Lett.*, vol. 43, no. 20, pp. 1062-1063, 2007.
 - [12] C. Wu, L. Han, F. Yang, L. Wang and P. Yang, "Broad beamwidth circular polarisation antenna: Microstrip-monopole antenna", *Electron. Lett.*, vol. 48, no. 19, pp. 1176-1178, 2012.
 - [13] R. Touzi, P. W. Vachon, J. Wolfe, "Requirement on Antenna Cross-Polarization Isolation for the Operational Use of C-Band SAR Constellations in Maritime Surveillance,” *IEEE Geoscience and Remote Sensing Letters*, Vol. 7, Issue. 4, pp. 861-865, 2010.
 - [14] M.-Y. Li, Y. L. Ban, Z. Q. Xu, G. Wu, C. Y. D. Sim, K. Kai, et al., "Eight-port orthogonally dual-polarized antenna array for 5G smartphone applications", *IEEE Trans. Antennas Propag.*, vol. 64, no. 9, pp. 3820-3830, 2016.
 - [15] A. Ghosh, D. Ghosh, S. Chattopadhyay, L. L. K. Singh, "Rectangular Microstrip Antenna on Slot Type Defected Ground for Reduced Cross Polarized Radiation,” *IEEE Ant. Wireless Prop. Lett.*, 2014
 - [16] A. Ghosh, S. K. Ghosh, D. Ghosh and S. Chattopadhyay. "Improved Polarization Purity for circular microstrip antenna with defected patch surface,” *Int. J. of Microwave and Wireless Technologies*, Vol.8, No.1, pp.89-94, 2016.
 - [17] D. Ghosh, S. Kr. Ghosh, S. Chattopadhyay, S. Nand, D. Chakraborty, R. Anand, R. Rajt, and A. Ghosh "Physical and Quantitative Analysis of Compact Rectangular Microstrip Antenna with Shorted Non-Radiating Edges for Reduced Cross-Polarized Radiation Using Modified Cavity Model,” *IEEE Ant. and Prop. Mag.*, Vol. 56, No. 4, pp. 61-72, 2014.
 - [18] M. Veysi, A. Ahmadi, G. Karimi and A. Lalbakhsh, "RFID tag design using spiral resonators and defected ground structure", *Radioengineering*, vol. 26, no. 4, pp. 1019-1024, 2017.

- [19] A. Ahmadi, S. V. Makki, A. Lalbakhsh and S. Majidifar, "A novel dual-mode wideband band pass filter", *Appl. Comput. Electromagn. Soc. J.*, vol. 29, no. 9, pp. 735-742, 2014.
- [20] K.-M. Luk and B. Wu, "The magnetoelectric dipole—A wideband antenna for base stations in mobile communications", *Proc. IEEE*, vol. 100, no. 7, pp. 2297-2307, 2012.
- [21] W. T. Sethi, H. Vettikalladi and M. A. Alkanhal, "Millimeter wave antenna with mounted horn integrated on FR 4 for 60 GHz Gbps communication systems", *Int. J. Antennas Propag.*, vol. 2013, 2013.
- [22] A. H. Abdelgwad and T. M. Said, "High performance microstrip monopole antenna with loaded metamaterial wire medium superstrate", *Int. J. RF Microw. Comput. Aided Eng.*, vol. 29, no. 5, 2018.
- [23] S. Y. Jun, B. Sanz-Izquierdo, E. A. Parker, D. Bird and A. McClelland, "Manufacturing considerations in the 3-D printing of fractal antennas", *IEEE Trans. Compon. Packag. Manuf. Technol.*, vol. 7, no. 11, pp. 1891-1898, 2017.
- [24] L. Shi, H.-J. Sun, W.-W. Dong and X. Lv, "A dual-band multifunction carborne hybrid antenna for satellite communication relay system", *Prog. Electromagn. Res.*, vol. 95, pp. 329-340, 2009.
- [25] P. Hammer, D. Vanbouchaute, D. Verschraeven and A. Van De Capelle, "A Model for Calculating the Radiation Field of Microstrip Antennas," *IEEE Trans Antennas Propag*, Vol. 27, No.2, pp. 267-270, 1979.
- [26] HFSS, "High Frequency Structure Simulator, Version 14," Ansoft Corp.
- [27] D. Kozakoff, *Aperture Antennas*, Hoboken, NJ, USA:Wiley, 2016.
- [28] C. A. Balanis, *Antenna Theory: Analysis and Design*, New York, NY, USA:Wiley, 2001.
- [29] S. Chattopadhyay and S. Chakraborty, "A physical insight into the influence of dominant mode of rectangular microstrip antenna on its cross-polarization characteristics and its improvement with t-shaped microstrip antenna", *IEEE Access*, vol. 6, pp. 3594-3602, 2018.
- [30] W. L. Stutzman and G. A. Thiele, *Antenna Theory and Design*, Hoboken, NJ, USA:Wiley, 2003.

- [31] A. Lalbakhsh, M. U. Afzal, K. P. Esselle and S. L. Smith, "Wideband near-field correction of a Fabry–Perot resonator antenna", *IEEE Trans Antennas Propag.*, vol. 67, no. 3, pp. 1975-1980, 2019.
- [32] A. Lalbakhsh, M. U. Afzal, K. P. Esselle, S. L. Smith and B. A. Zeb, "Single-dielectric wideband partially reflecting surface with variable reflection components for realization of a compact high-gain resonant cavity antenna", *IEEE Trans Antennas Propag.*, vol. 67, no. 3, pp. 1916-1921, 2019.
- [33] S. Chakraborty and S. Chattopadhyay, "Substrate fields modulation with defected ground structure: A key to realize high gain wideband microstrip antenna with improved polarization purity in principal and diagonal planes", *Int. J. RF Microw. Comput. Aided Eng.*, vol. 26, no. 2, pp. 174-181, 2016.
- [34] D. Guha, S. Chattopadhyay, and J. Y. Siddiqui, "Estimation of gain enhancement replacing PTFE by air substrate in a microstrip patch antenna," *IEEE Antennas Propag Mag.* Vol. 52, pp. 92–95, 2010.
- [35] A. R. Djordjevic, R. M. Biljie, V. D. Likar-Smiljanic and T. K. Sarkar, "Wideband frequency-domain characterization of FR-4 and time-domain causality", *IEEE Trans. Electromagn. Compat.*, vol. 43, no. 4, pp. 662-667, 2001.

CHAPTER

6

Conclusion and Scope for Future Studies

In this dissertation we have investigated the most useful and versatile patch antenna geometry i.e. Rectangular Microstrip Antenna (RMA), theoretically and experimentally for the improvement of bandwidth and radiation characteristics.

Rectangular microstrip antenna (RMA) is the most useful antenna structure for its wide variety of applications, due to its simple design, ease of implementation, manufacturing and even production. Modification of and RMA due to its basic structure of just copper clad and dielectrics is very easy and hence tweaking it as per requirement is relatively easy. Because of these features, RMA is a best choice to address all the requirements of latest personal or handheld wireless communication equipment. Noth withstand the above, the RMA is also suitable for certain aerial applications like satellite and missiles due to its conformability and lightweight. Nevertheless, the parameters of an RMA viz-z-viz its versatility are not so promising and its performance without and with modifications are discussed in Chapter 1.

Hence, investigation to enhance some characteristics of rectangular microstrip antennas is imperative for above mentioned applications. As always, an antenna needs to be having high gain, wide bandwidth, low cross polarization, symmetric radiation pattern, stable gain profile over wide angle, etc. However, the physics of an antenna does not permit the concurrent improvement in the characteristics. Hence, it is important to design the antenna judiciously which can improve the needful parameters for a particular application while keeping other parameters well maintained. Notably, complexity of design and manufacturing is a

very important constraint. With that in key sight some designs along with theoretical and parametric analysis have been provided in the preceding chapters. The summary and conclusion is as enumerated below.

In **Chapter 2**, has been investigated the Microstrip patch antenna with defected patch surface (DPS). The chapter has been mainly divided in two parts wherein detailed investigations have been shown in antennas having DPS at radiating and non-radiating side.

In the first part of chapter 2, DPS integrated RMA with defects on non-radiating side have been thoroughly investigated. This germinates a simple and compact grounded comb-shaped microstrip patch antenna with significantly improved radiation performance. The structure shows consistently improved radiation performances such as wide symmetrical radiation beam with very low XP radiation. Around 105^0 - 110^0 of 3 dB beam width is evident with more than 35 dB CP-XP isolation from the structure while the same for a conventional patch is only 15 dB. Around 15 dB of front-to-back radiation isolation is found from the proposed patch. Most importantly, the proposed antenna produces 65% and 35% broader beam in H and E-planes respectively than that of a classical microstrip antenna. The antenna may be useful for polarimetric radars or as feed to parabolic reflector antennas.

In the second part of chapter 2, similar investigations have been carried out by making corrugation like defects on radiating side of RMA. Good Polarization purity along with dual resonance has been obtained from the structure. However, placing defects on radiating edges are not reliable as it may hamper radiating edge fields of TM_{10} mode specifically for smaller patches.

The selection of above mentioned DPS structures for particular applications to be based mainly on the level of requirement of polarization purity and the scope of implementation of array. The employment of array is must since the individual antenna gain is limited here as observed. The bandwidths of the structures are limited too to meet the requirement of high speed data transmission in some specific applications.

With the above discussed facets and limited short coming of marginal gain

and restriction of bandwidth, some other techniques were explored to enhance the gain and bandwidth of RMA in Chapter 3.

In **Chapter 3**, the employment of defected ground structure (DGS) of hexagonal geometry has been methodically investigated. Here, the employment of DGS has been considered mainly to improve the gain and bandwidth of RMA. As such, the classical report on implementation of DGS in RMA is prominently considered for lowering cross-polarized radiation. The experimental investigations with hexagonal DGS (HDGS) integrated RMA shows that the bandwidth and the gain properties can also be improved by judicious exploitation of the defect geometry on ground plane. Around 58% input impedance bandwidth (covering X and Ku spectrum) with high gain (around 9.1-9.4 dBi) and stable radiation pattern is obtained from the structure. The XP radiation for the proposed design shows much better results than conventional RMA at Ku band.

Furthering the study, a comparative analysis between various existing DGSs which are particularly in increasing order of polygon has been methodically carried out. With the results, amongst the available polygons, the hexagonal DGS integrated RMA can address all the issues of polarization purity and board banding along with higher gain of around 9 dBi. Further to it, it offers UWB too. And, the above mentioned requirements are inescapable being fundamental in nature to the field of communications and polarimetric radars. However the cross polar radiation at back side of this structure is relatively higher as is expected from DGS integrated structures.

In the next Chapter, unlike the DPS or DGS approach, no slots or shorts were incorporated on patch surface or anywhere in ground plane to repress cross-polar radiation. A completely novel and easy technique has been employed to address the issue of cross and co-polarization. In **Chapter 4** a single layer and planar bracketed stub loaded RMA has been investigated for high gain and low XP radiation in the entire elevation angle. In this concept, the magnetic field locus due to attachment of coaxial probe feed has been modulated and the same is exploited to evolve a simple, single element with single layer patch.

The proposed bracketed stub-loaded single layer RMA structure exhibits good and viable gain of 8 dBi with 27 dB of co-cross polar isolation in the most

affected plane i.e H plane. Also, in order to enhance the gain and to study its viability in terms of array, a 2 element array was constituted. Around, 10 dBi of gain with 27 dB of co-cross polar isolation was obtained.

TABLE 6.1 Tabulated form of all the investigated structures for objective assessment and selection.

Ser no	Antenna	Opera-ting Band	Resona-ting Freque-ncy	Gain	Band width	Polari-ation Purity	Symmetry between radiation patterns in principal planes	Flat-top range in the radiation patterns	Remarks
			(GHz)	(dBi)	(%)	(dB)	(Degree)		
1(a)	DPS at non-radiating Side	X	8.05	4.89	4.5	35	125°	-	Comb shaped grounded
1(b)	DPS at radiating Side	C	6.6 / 7.7	5	4.2 / 6	30-40	-	-	Dual Frequency
2	HDGS	X and Ku	12.2	7.5 to 9.1	58	22.5	-	-	UWB and High Gain
3	BSRMA	X	10.22	8	11	27	-	-	Without any kind of defecting, excellent impedance matching.
4	QPCMA	X	8.04	8.2	-	26	145°	72°	Quasi planar structure

Although the gain issue can be addressed by array implementation, the issues of improved and symmetrical radiation patterns with low cross polarization are of significant importance. Along with these, achieving the flat top radiation beam from such antennas is very much laudable. Hence, investigations to improve the complete radiation characteristics with an different approach has been covered in next chapter.

In **Chapter 5**, a compact Quasi-planar Composite Microstrip Antenna (QPCMA) has been investigated thoroughly and proposed for high gain, flat-top, wide beam-width, symmetrical radiation pattern with excellent CP-XP isolation. The concurrent improvement of all the radiation properties with such low profile

structure is absolutely new in the field of microstrip radiator. The reasons for the improvement in each parameter are thoroughly investigated, analyzed and documented in this chapter for insightful exploration of the structure. The proposed structure is extremely simple and has potential applications in the fields of modern wireless communications.

The performance comparison for all the investigated structures is tabulated in **Table 6.1**. This may be helpful for practicing engineers to choose the antenna structure for their specific applications.

It may be noted that there is plenty of scope available to exploit different kinds of composite structures. Further, different geometries of patches may be investigated employing the designs documented in this dissertation.

The theoretical and experimental analysis of the investigations, presented in this dissertation, are very much important for scientific and research community. The investigated techniques are most up to date with cutting edge technologies and complete in all aspects and hence should be very much useful for efficient rectangular microstrip antenna design.

LIST OF PUBLICATIONS

Referred Journals (SCI)

1. U. A. Pawar, A. Ghosh, S. Chakraborty, L. L. K Singh, S. Chattopadhyay, C. Y. D. Sim, "Bracketed stub loaded single layer rectangular microstrip antenna: A novel approach for modulation of magnetic field locus to achieve improved matching, and low cross polarisation," *IET Microwaves, Antennas & Propagation*, vol. 13, no. 11, pp. 1866-1875, 2019. doi: 10.1049/iet-map.2018.5720
2. U. A. Pawar, S. Chakraborty, T. Sarkar, A. Ghosh, L. L. K Singh, S. Chattopadhyay, "Quasi-Planar Composite Microstrip Antenna: Symmetrical Flat-Top Radiation With High Gain and Low Cross Polarization," *IEEE Access*, vol. 7, pp. 68917-68929, 2019. doi:10.1109/ACCESS.2019.2918580
3. U. A. Pawar, S. Chakraborty, L. L. K Singh, S. Chattopadhyay, "Application of Defected Ground Structure for Augmenting High-Gain Ultra-Wide Bandwidth from Rectangular Microstrip Antenna," *Electromagnetics*, vol. 38, no. 2, pp. 123-133, 2018. doi:10.1080/02726343.2018.1437108
4. U. A. Pawar, S. Chakraborty, S. Chattopadhyay "A Compact and Grounded Comb Shaped Microstrip Antenna: A Key to Realize Enhanced Radiation Performa," *International Journal of RF and Microwave CAD*, vol. 27, issue 6, 2017. doi:10.1002/mmce.21101

International Conferences

1. U. A. Pawar, D. Mondal, A. Nagaraju, S. Chakraborty, L. L. K Singh, S. Chattopadhyay, "Rectangular microstrip antenna with corrugation like defects at radiating edge: A new approach to reduce cross polarization radiation" *IOP Conf. Ser.: Mater. Sci. Eng.*, vol. 331 012029, 2018. doi:10.1088/1757-899X/331/1/012029
2. U. A. Pawar, A. Ghosh, L. L. K Singh, S. Chattopadhyay, "Performance Evaluation of Rectangular Microstrip Patch Antenna based on Defected Ground Structures ," *Proceedings of 3rd International Conference on Computing Informatics and Networks*, Lecture Notes in Networks and Systems, ICCIN 2020, Springer vol 167, pp. 485-495, 2020. doi:10.1007/978-981-15-9712-1_41

BIO-DATA OF THE CANDIDATE

Name of Candidate	:	Pawar Umesh Ankush
Date of Birth	:	29 Mar 1982
Contact	:	7588905403 upawar@gmail.com
Permanent Address	:	202, Rane Millennium, Saraswati Baugh, Sadbhakti Mandir, Jogeshawari (East), Mumbai 400060, Maharashtra
Married	:	Yes
Educational Details	:	
(a) B.E	:	Electronics Engineering from Mumbai University with First Class (62.71%)
(b) M.Tech	:	Electronics Engineering from JNU with Distinction (88.50 %)
(c) Ph.D Course work:	:	SGPA of 9.00.
Present Occupation Details	:	Government Employee
Organization	:	Indian Army
Rank	:	Lt Col
Job Profile	:	A regular officer of Indian Army serving in Corps of Electronics and Mechanical Engineers and with specialization in Radars. Extensive exposure to various equipments and its maintenance including Radars for long time. Had headed workshops as main commanding appointment for considerable period.

PARTICULARS OF THE CANDIDATE

Name of Candidate	:	Pawar Umesh Ankush
Degree	:	Ph.D
Department	:	Electronics and Communication Engineering
Title of Thesis	:	Investigation to Enhance Some Characteristics of Rectangular Microstrip Antennas
Date of Admission	:	01.08. 2017
Approval of Research Proposal:		
1. BOS	:	17.04. 2018
2. School Board	:	23.04. 2018
MZU Regn No	:	1702111
Ph. D Regn No	:	MZU/Ph.d/1180 of 23.04.2018
Extension	:	NO

(Dr NP Maity)

Head

Dept of Electronics and Communication
Engineering

ABSTRACT

INVESTIGATION TO ENHANCE SOME CHARACTERISTICS OF RECTANGULAR MICROSTRIP ANTENNAS

PAWAR UMESH ANKUSH

MZU REGN NO : 1702111

PH. D REGN NO : MZU/PH.D/1180 OF 23.04.2018



**DEPT. ELECTRONICS & COMMUNICATION ENGINEERING
SCHOOL OF ENGINEERING AND TECHNOLOGY**

MARCH 2021

**INVESTIGATION TO ENHANCE SOME CHARACTERISTICS
OF RECTANGULAR MICROSTRIP ANTENNAS**

BY

PAWAR UMESH ANKUSH

Department of Electronics & Communication Engineering

Name of Supervisor : Dr. Sudipta Chattopadhyay

Name of Co-Supervisor : Prof. (Dr.) L. Lolit Kumar Singh

Submitted

In partial fulfillment of the requirement of the Degree of Doctor of
Philosophy in Electronics & Communication Engineering of Mizoram
University, Aizawl

Introduction

In the dissertation, we have reported the investigations on the useful, versatile and easy to implement patch antenna geometry i.e. Rectangular Microstrip Antenna (RMA), theoretically and experimentally for the improvement of bandwidth and radiation characteristics optimally.

Rectangular microstrip antenna (RMA) is the most useful antenna structure for its wide variety of applications, due to its simple design, ease of implementation, manufacturing and even production. Modification of and RMA due to its basic structure of just copper clad and dielectrics is very easy and hence tweaking it as per requirement is relatively easy. Because of these features, RMA is a best choice to address all the requirements of latest personal or handheld wireless communication equipment. At the same time, the RMA is also suitable for certain aerial applications like satellite and missiles due to its conformability and lightweight. However, the performance of an RMA viz-z-viz its versatility are not so promising. Without modifications, RMA has poor gain and is around 3 to 4 dBi. Also, bandwidth is limited and is up to 5% for conventional microstrip antenna. The efficiency of the antenna too is limited, where in the radiation efficiency is around -3.8 db and total efficiency of is upto -8.8 db. One of the important parameter i.e polarization purity of RMA, is around 10 to 15 dB which is not so promising too. From industrial and military application point of view, the power handling capacity of RMA is limited to mW or few W which is just suitable for home applications. Also, like few other antennas, the RMA too suffers with surface waves which reduces radiation efficiency and directivity.

Objective

Hence, investigations to enhance some characteristics of rectangular microstrip antennas are imperative for effective use of RMA in above mentioned applications.

Specifically, an antenna needs to be having high gain along with stable gain profile over wide angle, wide bandwidth, low on cross polarization, symmetric radiation pattern, etc. But the physics of an antenna does not permits concurrent improvement in these characteristics. Hence, it is essential to design the antenna

optimally, which can improve the requisite parameters for a particular application while maintaining other parameters to a desired level. With that in key sight, some designs supported with theoretical and parametric analysis have been provided in the thesis. The highlights have been summarized and conclusion is enumerated as below.

Summary of Results

In Chapter 1 of the thesis, introduction of the RMA along with its technical aspects have been covered. The chapter also includes radiation characteristics, limitations, and extensive literature survey on improving the radiation parameters of RMA. In order to enhance some characteristics of RMA, initially the application of defecting patch structure was exploited. Hence, in **Chapter 2**, we have investigated the Microstrip patch antenna with defected patch surface (DPS). The chapter has been primarily divided in two parts, wherein detailed investigations have been carried out in antennas having DPS at radiating and non-radiating side.

In first part of chapter 2, DPS integrated RMA having defects on non-radiating side has been investigated. This design form is a simple and a compact grounded comb-shaped microstrip patch antenna with improved radiation performance was designed. The structure exhibited improved radiation performances wherein wide symmetrical radiation beam pattern with very low XP radiation has been observed. Around 105^0 - 110^0 of 3 dB beam width is with more than 35 dB CP-XP isolation has been achieved. Whereas, the same for a conventional patch is only 15 dB. Also, front-to-back radiation isolation has been found to be around 15 dB from the proposed patch modification. Most significantly, the proposed antenna produces 65% and 35% broader beam in H and E-planes respectively than a classical microstrip antenna. The antenna may be useful as feed to parabolic reflector antennas or as a polarimetric radars antenna.

In the second part of chapter 2, corrugation like defects is made on radiating side of RMA and similar investigations have been carried out. Good Polarization purity along with dual resonance has been obtained from the structure. However, it was studied that placing defects on radiating edges are not reliable as it may hamper radiating edge fields of TM_{10} mode specifically for smaller patches.

The above discussed DPS structures were selected for particular applications

to be based mainly on the level of requirement of polarization purity and for implementation of array. The employment of array is must, as the individual antenna gain is limited as observed. The bandwidths of the structures are also limited.

With the above discussed facets and marginal short coming of limited gain and restriction of bandwidth, some other techniques were further explored in Chapter 3 to enhance the gain and bandwidth of RMA.

In **Chapter 3**, a different approach by employing defected ground structure (DGS) of hexagonal geometry has been investigated for RMA. The employment of DGS has been considered in this chapter, mainly to improve the gain and bandwidth of RMA. The experimental investigations of hexagonal DGS (HDGS) integrated RMA shows, the bandwidth and the gain properties can also be improved. However, that requires judicious exploitation of the defect geometry on ground plane. Around 58% input impedance bandwidth of X and Ku spectrum with high gain of around 9.1-9.4 dBi with stable radiation pattern was obtained. The XP radiation for the proposed structure exhibits much better results than conventional RMA in Ku band.

Furthering the study, a comparative analysis of various existing DGSs which are particularly in the increasing order of polygon was carried out. The hexagonal DGS integrated RMA had parameters better than available polygons, which can address the issues of polarization purity, higher gain of around 9 dBi and board banding simultaneously. Further to it, DGS integrated RMA offers UWB. These requirements are imperative being fundamental to the field of communications and polarimetric radars. However, the cross polar radiation on the back side of this structure is relatively higher which is expected from a DGS.

In the next Chapter, a completely novel and easy technique has been employed to address the issue of radiation characteristics (cross and co-polarization). Unlike the DPS or DGS, in this design no slot or short were incorporated. In **Chapter 4**, a planar bracketed stub loading of RMA has been designed and developed and investigated for high gain and low XP radiation for the entire elevation angle. In this concept, the modulation of locus of the magnetic field generated due to feeding by probe has been exploited to evolve a simple and single element with single copper lad structure. This is done with a view to enhance radiation performance by improving impedance matching. The proposed bracketed

stub-loaded single layer RMA structure exhibits good and viable gain of 8 dBi with 27 dB of co-cross polar isolation in the most affected plane i.e H plane. Also, in order to enhance the gain and to study its viability in terms of array, a 2 element array was constituted. Around, 10 dBi gain with 27 dB of co-cross polar isolation was obtained. The structure is quite simple and easy to manufacture.

Although the gain issue can be addressed by array implementation, the issues of improved and symmetrical radiation patterns with low cross polarization are of significant importance. Along with these, achieving the flat top radiation beam from such antennas is very much laudable. Hence, investigations to improve the complete radiation characteristics with a different approach have been attempted in next chapter. In **Chapter 5**, a Quasi-planar Composite Microstrip Antenna (QPCMA) has been investigated thoroughly for overall improvement in radiation parameters like high gain, flat-top, wide beam-width, symmetrical radiation pattern with excellent CP-XP isolation. The concurrent improvement as discussed above of all the radiation properties with such low profile structure is absolutely new in the domain of microstrip radiators. The reasons for improvement in each parameter are systematically investigated, analyzed and documented in the chapter for insightful exploration of the proposed structure. The proposed structure is extremely simple and promising for the fields of modern wireless communications.

The performance comparison for all the investigated structures has been tabulated and provided in the last chapter. This may be helpful for practicing engineers to choose the antenna structure for their specific applications.

Also, there is plenty of scope available to exploit different kinds of composite structures. Further, different geometries of patches may be investigated employing the designs recommended and documented in the dissertation.

The theoretical and experimental analysis of the investigations, presented in this dissertation, are very much important for scientific and research community. The investigated techniques are most up to date with cutting edge technologies and complete in all aspects and hence should be very much useful for efficient rectangular microstrip antenna design.